A THEORETICAL AND EXPERIMENTAL INVESTIGATION INTO THE SPECTRA OF SELECTED RESONATORS

by

JOHN CLIFFORD KELD SHARP

Submitted for the Degree of Doctor of Philosophy

at

The University of Aston in Birmingham

MAY 1974

SUMMARY

An acoustic transmission line system in which the echo returned from a resonator, having an arbitary spectrum of resonances has been analysed. The results show that the system, which is of practical importance because of the separation of the signal transducer and the resonator being studied, can be used for a variety of material measurements. The special case of a line resonator, which has an harmonic spectrum has been examined using Laplace transform technique, and the rigour of the solution is established by specific experimental tests. The approximations of classical accoustical theory which assumes a lumped rather than a distributed resonator and expresses material loss as a 'Q' factor have been reconciled to this exact theory.

Contour vibrations of disk resonators were investigated and the results are compared with recent numerical solutions from theory. A variety of specimens in disk form were used to determine elastic constants and their temperature coefficients with high precision. The extension of the disk theory to cover anisotropic materials has been considered.

The disk theory has been extended to include a second boundary - a concentric hole - and numerical solutions obtained. Results are in agreement with the well-established thin ring spectrum for large holes and disk theory for small holes. Experiments on the full range of hole sizes verify the results to the limit of experimental error.

The theory for the line resonator was extended to show that it is a convenient resonator form for Internal Friction measurement. The material Q of a pure copper rod was measured over a wide temperature

range and the results are in agreement with those of other workers.

The electronic equipment developed for the various measurements is described briefly and the possible methods of automation are discussed.

ACKNOWLEDGEMENT

I wish to thank my project supervisor, Dr.J.F.W. Bell for fruitful discussions throughout the course of the work, and without whose enthusiasm the project would not have been started; Mr. A.E. Sutton of the University Mathematics Department for helpful suggestions on mathematical techniques.

Thanks are also due to Professor J.E. Flood, head of the Electrical Engineering Department, and the Science Research Council for their studentship.

CONTENTS

		Page No.
1.	GENERAL INTRODUCTION	1
2.	THE ECHO TECHNIQUE	2
	2.1 Introduction	2
	2.2 Mathematical Analysis	2
	2.3 Dominant Pole Approximation	7
	2.4 Comparison with Experiment	10
	2.5 The Line Resonator	11
	2.6 Resonators with Anharmonic Spectra	12
	2.7 Experimental Apparatus and Magnetostrictive Transducer	12
	2.8 Applications	13
3.	DISK RESONATORS	28
	3.1 Introduction	28
	3.2 Comparison with Experiment	30
	3.3 Multiple Resonances	31
	3.4 Measurement of Elastic Constants	31
	3.5 Discussion of results	34
	3.6 Possible extension to Anisotropic Disks	34
4.	DISK/RING RESONATORS	52
	4.1 Introduction	52
	4.2 Existing Theory	52
	4.3 Analysis of Disk with Central Hole	53
	4.4 Comparison with Experiment	58
	4.5 Discussion	58
5.	INTERNAL FRICTION	68
	5.1 Introduction	68

Page No.

5.2 Multimode Method of measuring Q_C and Q_M 69

5.3 Experimental work 73

5.4 Discussion of Result 74

6. THE ELECTRONIC SYSTEMS 84

6.1 Introduction 84

6.2 Oscillators 84

6.3 Burst Generators 84

6.4 Automatic Systems 84

List of Symbols 98

References 100

APPENDICES

A.2.2 Mathematical Analysis of Transmission line and Line Resonator 104

A.3.1 Derivation of Frequency Equations for Disks 113

A.3.4 Curve fitting. 122

A.4.3 Tables of K values for Rings. 123

1. GENERAL INTRODUCTION

In radar and sonar systems the characteristics of an echo returned from an object depend on the transmitted signal and the object parameters, such as size, shape, and natural resonances near the transmitted frequency. A resonant object known as an echo box, is often used for tuning and performance checks on these systems. An equivalent mechanical or acoustic system could consist of a wire line carrying a burst of longitudinal plane waves of strain. This signal would echo up and down the line with diminishing amplitude due to attenuation.

The case of such a line terminated by a resonator (Bell 1968) has been analysed and compared with experiment. The general solution obtained can be used to give the transient response of a resonator, having internal energy losses, and an arbitary spectrum of resonances, for any transmitted frequency.

The feature which gives the system its practical importance is the separation of the active electrical parts of the system from the resonator. Thus, for example, the launcher can be in the cool region of a high-temperature furnace, while the resonator being studied is inside it.

2. THE ECHO TECHNIQUE

2.1 Introduction

Fig. 2.1.1 shows the experimental arrangement for this investigation. The short length of magnetostrictive line acts as a launcher and receiver of the mechanical oscillations. It is matched to the line which must be sufficiently long to avoid overlap between the forward signal and the echo return. The resonator shown takes the form of a length of large diameter line, which will resonate giving antinodes at the ends. In all applications only the first reflection of the transmitted signal is looked at in detail. This will be called the "echo".

A typical echo, shown in Fig. 2.1.2 consists essentially of two components; the echo-signal, and the echo-decrement. The echo signal is the direct return of the waves incident on the object, and is at the transmitted frequency. The echo decrement which follows, is the exponential re-radiation of the energy stored, and is always at the natural frequency or frequencies of the resonator.

The mathematical analysis is given here in the form in which it was published. A more explanatory account is contained in Appendix A.2.2 of this thesis.

2.2 Mathematical analysis

Fig. 2.2.1 shows the transmission line and line resonator in diagrammatic form. The fact that the first reflection is of primary interest has been used to simplify this analysis and a solution for the echo alone is obtained.

The impedance z is defined

z = Force (F)/Displacement Velocity (U)

This is convenient as both F and U are continuous at the boundary between line and resonator.

The characteristic equation of motion for plane longitudinal vibrations in a rod is,

$$\frac{\partial^2 U}{\partial \tau^2} = C^2 \frac{\partial^2 U}{\partial x^2} + H \frac{\partial^3 U}{\partial x^2 \partial \tau} \qquad 2.2.1$$

This is the one dimensional form of Stokes' (Stokes 1845) general equation ($U=U(x,\tau)$) and is valid for small values of strain. The term involving H allows for losses due to Internal Friction in the material. The general solution of equation 2.2.1 in its Laplacean Transformation is,

$$\overline{U}(x,p) = A(p)\exp(-\gamma x)+B(p)\exp(\gamma x) \qquad 2.2.2$$

where $\gamma^2=p^2/(Hp+C^2)$ and A(p) and B(p) are functions of p dependent on boundary conditions.

In the resonator region ($l_1 < x < l_1+l_2$) equation 2.2.1 is valid. This can be expressed in the form of two coupled partial-differential equations.

$$\overline{F}_2(x,p) = -\rho_2 A_2 \frac{(H_2 p+C_2^2)}{p} \frac{\partial \overline{U}_2(x,p)}{\partial x} \qquad 2.2.3$$

$$\overline{U}_2(x,p) = -\frac{1}{\rho_2 A_2} \frac{1}{p} \frac{\partial \overline{F}_2(x,p)}{\partial x} \qquad 2.2.4$$

The characteristic impedance is,

$$Z_2(p) = \rho_2 A_2 (H_2 p + C_2^2)^{\frac{1}{2}} \qquad 2.2.5$$

The boundary conditions for the region $(l_1 < x < l_1 + l_2)$ are,

$\overline{F}_2(l_1+l_2,p)=0$; $\overline{F}_2(l_1,p)=\overline{F}_1(l_1,p)$; $\overline{U}_2(l_1,p)=\overline{U}_1(l_1,p)$

These boundary conditions and equations 2.2.2/3/4 can be combined, eliminating $A_2(p)$ and $B_2(p)$, to give,

$$\overline{F}_1(l_1,p)/\overline{U}_1(l_1,p) = Z_2(p)\tanh(\gamma_2 l_2) \qquad 2.2.6$$

where $$\gamma_2^2 = p^2/(H_2 p + C_2^2) \qquad 2.2.7$$

In the line region the general solution equation 2.2.2 becomes,

$$\overline{U}_1(x,p) = A_1(p)\exp(-\gamma_1 x) + B_1(p)\exp(\gamma_1 x) \qquad 2.2.8$$

Suppose that at time $\tau = 0$ a forcing function $U_1(0, \tau) = a \sin \omega_s \tau$ is applied at point x=0, and so,

$$\overline{U}_1(0,p) = a\,\omega_s/(p^2+\omega_s^2) \qquad 2.2.9$$

Equations 2.2.6 and 2.2.9 are used as boundary conditions for equation 2.2.8. The expression for the first reflection obtained in this way is,

$$\overline{R}(x,p) = \frac{Z_1(p)-Z_2(p)\tanh(\gamma_2 l_2)}{Z_1(p)+Z_2(p)\tanh(\gamma_2 l_2)} \cdot \frac{a\omega_s}{p^2+\omega_s^2} \exp\gamma_1(x-2l_1) \qquad 2.2.10$$

γ_1 and Z_1 have expressions of similar form to those for γ_2 and Z_2.

In equation 2.2.10 the term $\exp\gamma_1(x-2l_1)$ contributes a branch point at point $p = -C_1^2/H_1$. In general C_1^2/H_1 is a very large number,

and thus the branch point gives two significant effects when the Laplacean Inversion of $\bar{R}(x,p)$ is undertaken. (For more detail see Appendix A.2.2). First, an attenuation of the whole echo. Secondly, a time delay of $-(x-2l_1)/C_1$ for the whole echo. The time delay can be seen simply in the case of a lossless line by putting $H_1=0$ into equation 2.2.10. Neither of these effects are relevant in the practical case, and a new function $\bar{R}'$ is therefore defined,

$$\bar{R}'(0,s) = \frac{Z_1(s)-Z_2(s)\tanh(\gamma_2 l_2)}{Z_1(s)+Z_2(s)\tanh(\gamma_2 l_2)} \frac{a\omega_s}{s^2+\omega_s^2} \qquad 2.2.11$$

s is the new Laplacean operator for t and $\tau - t = 2l_1/C_1$. The echo signal begins at t=0. This completely general expression can be reduced to that obtained by the conventional analysis of a line terminated by a lumped-parameter resonator, if only one dominant pole is considered. It will be noted that in equation 2.2.11 the observation point for the echo has been taken at x=0

The positions of the poles and zeros of $\bar{R}'(s)$ will be found enabling it to be represented in the s-plane. The function $\bar{R}'(0,s)$ splits conveniently into two parts; the transfer function of the system, and the forcing function applied to it. The transfer function $\left[Z_1(s)-Z_2(s)\tanh(\gamma_2 l_2)\right] / \left[Z_1(s)+Z_2(s)\tanh(\gamma_2 l_2)\right]$ has poles at points where $Z_1(s)+Z_2(s)\tanh(\gamma_2 l_2)=0$. This condition leads to the result,

$$2\gamma_2 l_2 = l_n(r) \qquad 2.2.12$$

where $r=(Z_2(s)-Z_1(s))/(Z_2(s)+Z_1(s))$

r is the reflection coefficient due to the junction mismatch at $x=l_1$.

However, $H_1 << C_1^2$; $H_2 << C_2^2$, and in general,

$$r=(\rho_2 C_2 A_2-\rho_1 C_1 A_1)/(\rho_2 C_2 A_2+\rho_1 C_1 A_1) \qquad 2.2.13$$

So letting $\ln(r)= -k+j\theta$ gives,

$\theta=2n\pi$ where n=0, ± 1, ± 2, etc. and $k=\ln(1/r)$.

The subsequent solutions for poles in the s-plane resulting from equation 2.2.12 are

$$s= -n^2\alpha-\beta+jn\omega_1 \qquad 2.2.14$$

where $\alpha=(H_2\pi^2)/(2l_2^2)$; $\beta=(kC_2)/(2l_2)$; $\omega_1=(C_2\pi)/l_2$

Similarly, solutions for the zeros are given by,

$$s= -n^2\alpha+\beta+jn\omega_1 \qquad 2.2.15$$

A typical s-plane diagram is shown in Fig. 2.2.2.

The imaginary (or frequency) ordinates of s, $n\omega_1$, give the resonant mode frequencies of the resonator. The real ordinates are combinations of α and β. It will be shown later that, β is related to the Q value for coupling between line and resonator, and α is related to the Q of the resonator material.

The Laplacean inversion of equation 2.2.11 can now be undertaken by contour integration in the s-plane, to give a function R'(0,t). However in practice a short burst of oscillations is transmitted and so the forcing function becomes

$$\left[a\omega_s/(s^2+\omega_s^2)\right]\left[1-\exp(-sT)\right] \qquad 2.2.16$$

where $T=2\pi P_N/\omega_s$ and P_N is the number of oscillations in the

burst. In this case the solution of equation 2.2.11 gives the Echo,

$$E=R'(0,t) - h(t-T)R'(0,t-T) \qquad 2.2.17$$

A typical echo, where the transmitted frequency is a resonant frequency is shown in Fig. 2.4.1(a).

Some approximations have been made to obtain this solution. However the present practical applications lie within the following limits:

(1) Oscillations to crossover, P_m, greater than 5.

(2) Natural resonant frequency, f_m, greater than 1kHz.
The experimental techniques below this value have not yet been developed.

(3) Material losses within the condition $5\beta > m^2 \alpha$

These restrictions can be used to examine the approximations made so far. The worst possible error would occur with the resonator tightly coupled at a low resonant frequency with high material losses. In this case the error would effect vectors in the s-plane diagram by approximately $1:10^8$ in their modulus and 0.005 degrees of arc in their angle. For any practical system these approximations are entirely negligible. The dominant pole approximation referred to in section 2.3 has an effect which is a factor of 10^5 greater.

2.3 Dominant pole approximation

An approximation of this kind is possible because of the distribution of poles along the imaginary axis. Consider the s-plane diagram shown in Fig. 2.3.1. m will be used to indicate a general resonant mode (e.g. for fundamental m=1). In this case equation 2.2.11 becomes

$$\bar{R}'(0,s) = \frac{a\omega_s}{(s+j\omega_s)(s-j\omega_s)} \frac{(s-\beta+m^2\alpha+j\omega_m)(s-\beta+m^2\alpha-j\omega_m)}{(s+\beta+m^2\alpha+j\omega_m)(s+\beta+m^2\alpha-j\omega_m)} \qquad 2.3.1.$$

This expression is inverted by summing the residues from the poles. For example, the residue from the pole at $s = -\beta-m^2\alpha+j\omega_m$ is,

$$\frac{2a\,\beta\omega_s(\beta-j\omega_m)(\exp(-\beta-m^2\alpha)t)(\exp j\omega_m t)}{j\omega_m(\beta+m^2\alpha-j(\omega_m+\omega_s))(\beta+m^2\alpha-j(\omega_m-\omega_s))} \qquad 2.3.2$$

The residues from the four poles are summed to give,

$$R'(0,t) = a\left[\frac{V_4V_5}{V_2V_3}\sin(\omega_s t+\theta_6) + 2\frac{\omega_s}{\omega_m}\frac{2\beta V_1}{V_2V_3}\sin(\omega_m t+\theta_7)\exp(-\beta-m^2\alpha)t\right] \qquad 2.3.3$$

where $\theta_6 = \theta_3 + \theta_5 - \theta_2 - \theta_4$; $\theta_7 = \theta_2 + \theta_3 - \theta_1$

$V_1=(\beta^2+\omega_m^2)^{\frac{1}{2}}$; $\theta_1=\tan^{-1}(\omega_m/\beta)$

$V_2=\left[(\beta+m^2\alpha)^2+(\omega_m+\omega_s)^2\right]^{\frac{1}{2}}$; $\theta_2=\tan^{-1}\left[(\omega_m+\omega_s)/(\beta+m^2\alpha)\right]$

$V_3=\left[(\beta+m^2\alpha)^2+(\omega_m-\omega_s)^2\right]^{\frac{1}{2}}$; $\theta_3=\tan^{-1}\left[(\omega_m-\omega_s)/(\beta+m^2\alpha)\right]$

$V_4=\left[(\beta-m^2\alpha)^2+(\omega_m+\omega_s)^2\right]^{\frac{1}{2}}$; $\theta_4=\tan^{-1}\left[(\omega_m+\omega_s)/(\beta-m^2\alpha)\right]$

$V_5=\left[(\beta-m^2\alpha)^2+(\omega_m-\omega_s)^2\right]^{\frac{1}{2}}$; $\theta_5=\tan^{-1}\left[(\omega_m-\omega_s)/(\beta-m^2\alpha)\right]$

The function has been expressed in this form because aspects of its structure can be visualised by examination of individual terms. However, the combined effect is illustrated here by computer plots of the echo traces. Useful expressions can be derived for oscillations to crossover, and steady state echo signal amplitude, at resonance (i.e. $\omega_m=\omega_s$).

The crossover point is defined when the amplitude=0. Let this occur at $t=t_c$.

Then $t_c = [1/(\beta+m^2\alpha)]\ \ln(2\beta/(\beta-m^2\alpha))$ 2.3.4

by neglecting $\beta+m^2\alpha$ compared with $2\omega_s$. So oscillations to crossover=frequency x t_c.

Therefore $P_m = [\omega_m/2\pi(\beta+m^2\alpha)]\ln(2\beta/(\beta-m^2\alpha))$ 2.3.5

Also at resonance ($\omega_m=\omega_s$) the amplitude of the envelope of the echo-signal is given by,

$E = [a/(\beta+m^2\alpha)][-\beta+m^2\alpha+2\beta\exp(-\beta-m^2\alpha)t]$ 2.3.6

The initial amplitude at t=0 is, E_0=a. This checks with the physical situation, because the resonator initially represents a clamped termination (high impedance).

As t approaches infinity the echo-signal approaches its steady-state amplitude $E_\infty = -a(\beta-m^2\alpha)/(\beta+m^2\alpha)$, the minus sign indicating the reverse phase occurring at the crossover.

Hence $E_\infty/E_0 = -(\beta-m^2\alpha)/(\beta+m^2\alpha)$ 2.3.7

It is convenient to relate the Q notation of simple theory to the terms α and β. In most textbooks (Kolsky,1963) the following definition is observed

Q = (Energy Stored)/(Energy lost per radian) 2.3.8

Three Q values are related to the resonator.

Q_{Cm} is coupling Q for mode m

Q_{Mm} is material Q for mode m

Q_{Tm} is total Q for mode m

Using equation 2.3.8., the following expression results, with the normal approximation implicit in the use of Q.

$Q_{Tm} = \omega_m/2(\beta+m^2\alpha)$ 2 3.9

In the lossless case when $\alpha = 0$, Q_{Tm} is due only to reradiation back down the line, so $Q_{Tm} = Q_{Cm}$.

Therefore, $Q_{Cm} = \omega_m / 2\beta$ 2.3.10

$$Q_{Mm} = \omega_m / 2m^2\alpha \qquad 2.3.11$$

2.4 Comparison with experiment

Fig.2.4.1(b) shows an oscilloscope trace for the fundamental mode of an aluminium line resonator. The standard techniques of the magnetostrictive delay line were used. The transmission line was 10 metres of 18 gauge piano-wire. The magnetostrictive material used was permandure which was brazed onto the end of the line. The short coil was 500 turns of thin copper wire, wound on a thin former. Table 2.4.2 shows the calculation of data for the plot of Fig.2.4.1(a).

The envelope of the echo-signal component is exponential having the same time constant as the envelope of the echo-decrement. The phase of the echo-signal component reverses as it goes through the null value and the amplitude rises to steady-state unity, when all the incident signal is reflected, and the junction of resonator and line is an antinode. The initial amplitude is determined by the reflection coefficient, r. The effect of detuning (see Fig. 2.4.3) is an initial loss of the null and a subsequent fall in the energy stored, resulting in a decrease of the echo-decrement amplitude. With still further detuning the echo-decrement disappears, and the echo becomes an image of the incident signal.

2.5 The line resonator

The line resonator has a harmonic spectrum of resonances, so that $\omega_m = m\omega_1$. For a higher order mode (say m=3) a stepped envelope to the echo is observed as predicted by the theory of section 2.2. An oscilloscope trace for the aluminium resonator is shown in Fig. 2.5.1. The amplitude steps at every third oscillation, as this is the transit time for a return signal in the resonator, which is now $3(\lambda/2)$ long.

However the dominant pole approximation of section 2.3 removes this feature from the theory, as does normal acoustic analysis, making the envelope a pure exponential. This has little significance for most applications, but it illustrates the precision of the theory derived in section 2.2.

A computer program was written to compute the echo-signal for mode m=3 but to include residues from poles up to $n = \pm 10$; that is to include poles up to $\pm 10\omega_1$ on the j-axis of the s-plane. The resultant computed echo-signal was an exact replica, showing the stepped form obtained in practice.

The fundamental, of course, is also stepped having a step each cycle. For the first cycle the amplitude is constant being ra. The dominant pole approximation gives an amplitude starting at, a, and dropping to ra over the first cycle.

The computer program referred to above is a good critical test of the general validity of the theory. However, for many applications the dominant pole approximation is adequate.

The line resonator is frequently used in experiments. When establishing an experiment, parameters such as line diameter

and frequency are chosen to give the desired coupling.

Fig. 2.5.2 gives a graph relating these paramters for easy reference. Bell, Noble, Seth 1973 also published a chart of acoustic data to be used for selecting suitable materials for particular applications.

2.6 Resonators with anharmonic spectra

In general, an arbitarily shaped resonator will have an anharmonic spectrum of resonances. For some modes the dominant pole approximation may not be applicable if these modes occur close to each other in frequency. Any number of interacting modes can be analysed by considering the appropriate s-plane diagram. However for practical applications a knowledge of the result of two interacting lossless resonances is sufficient. The s-plane diagram of Fig. 2.6.1 represents this situation. Again a computer was used to evaluate the residues so that for particular input data the echo could be plotted. A typical result is shown in Fig. 2.6.2. See also section 3.3.

If the relation between stored energy in the resonator and amplitude of vibration at the coupling point is known, the coupling Q's can be calculated. Successive computer plots of a particular situation allows the exact resonant frequencies to be determined.

2.7 Experimental apparatus

A schematic diagram of the experimental apparatus is shown in Fig. 2.1.1. In general the coil is positioned so that the backwards travelling signal is reflected to reinforce the signal travelling towards the resonator.

The acoustic bandwidth is determined by considering the situation in Fig. 2.7.1(a). There is a phase reversal at the free end, so the reflected wave will lag the forward wave by an angle $(\pi+2\theta)$ where $\theta=2\pi l/\lambda=2\pi lf/c$. The waves reinforce when this angle is $2n\pi$; (n=1,2,3,etc) i.e.$\theta=\pi/2$, $3\pi/2$, $5\pi/2$ etc. Fig. 2.7.1(b) shows a phase angle diagram. The 3db points for the first reinforcement (n=1) are at $\theta=\pi/4$ and $\theta=3\pi/4$, giving a bandwidth of frequency ratio 3. Similarly the second reinforcement (n=2) gives a frequency ratio of only 1.4. Reinforcements with higher values of n give correspondingly narrower bandwidths. In practice the coil is positioned for the first reinforcement to take advantage of the high bandwidth. In many experiments subsequent re-adjustment of the coil is unnecessary.

The electrical pick-up system is of high bandwidth (low Q) and is tuned by means of the decade capacitor. Johnson 1971 investigated the response, showing that there is negligible effect on the phase and frequency properties of the echo.

Permandure was found to be a most efficient magnetostrictive material. For further information on this topic see Bozorth 1951.

Figs. 2.7.2/3 show photographs of the experimental apparatus used by the author.

2.8 Application

This echo technique was initially applied to temperature measurement (Bell 1968). Probes have been designed and used to measure temperatures in nuclear reactors, liquid metals, and gas flames (Seth 1974).

More recently the method has been applied to:

(1) the measurement of elastic constants (Section 3.4 of this thesis)

(2) the measurement of internal friction in solids (Pelmore 1974)

(3) the investigation of resonant modes in many structures

(4) the investigation of fluid properties; in particular, density, viscosity and pressure

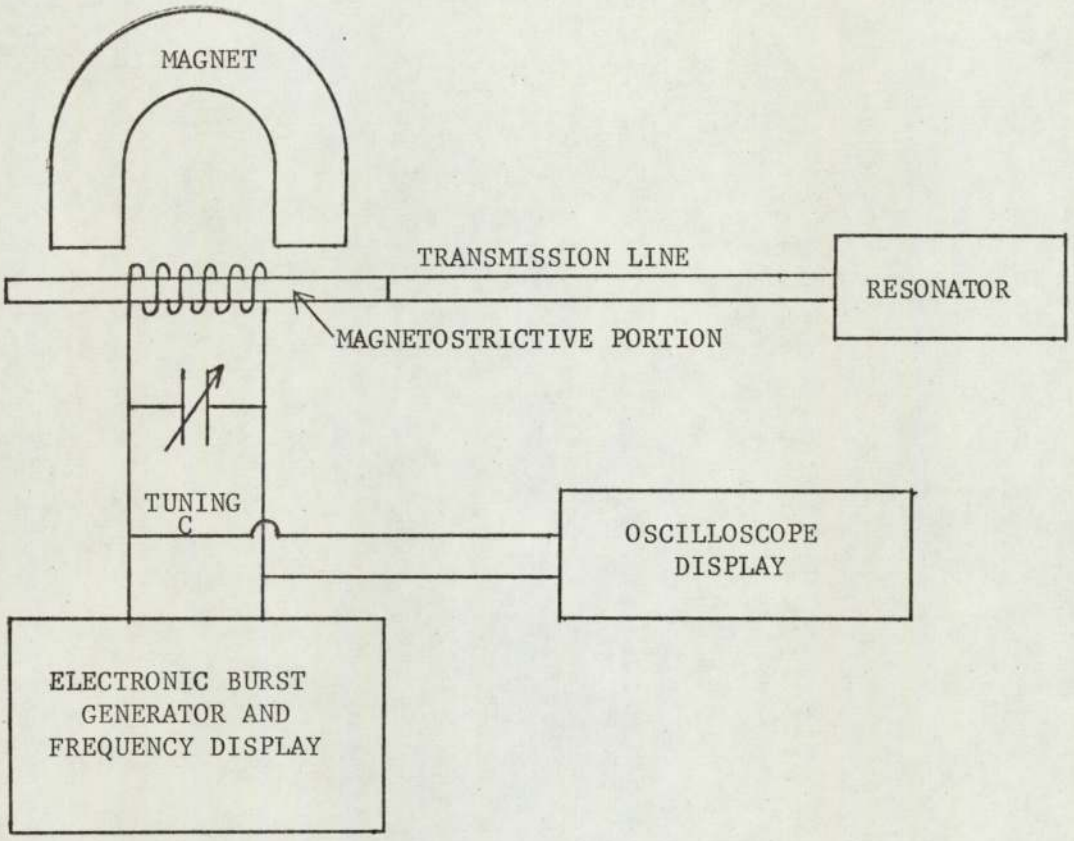

Fig.2.1.1 The bias produced by the magnet is necessary because of the quadratic nature of the magnetostrictive effect. The line must be long enough to accommodate the oscillation burst without producing standing waves. Particular forms of resonator are chosen for particular applications.

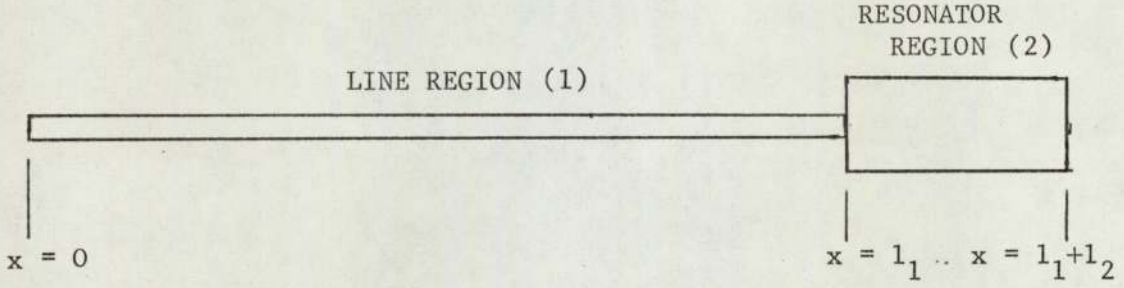

Fig.2.2.1 The analysis is accomplished by considering the line region ($0 < x < l_1$) and the resonator region ($l_1 < x < l_1 + l_2$) as boundary value problems.

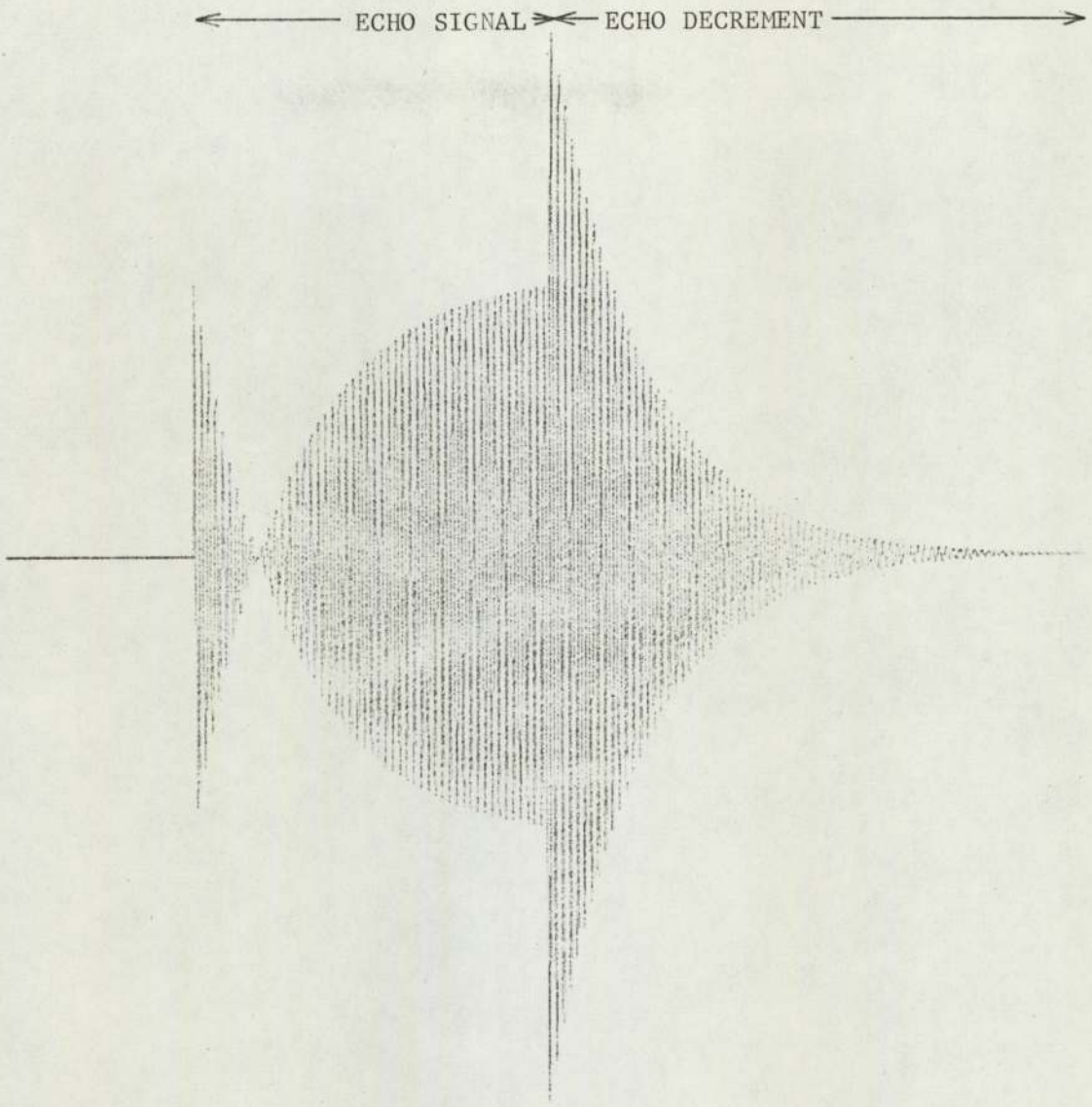

Fig. 2.1.2

The two components of the echo are shown; the echo signal which has the same duration as the transmitted burst, and the echo decrement which is the re-radiation of the energy stored.

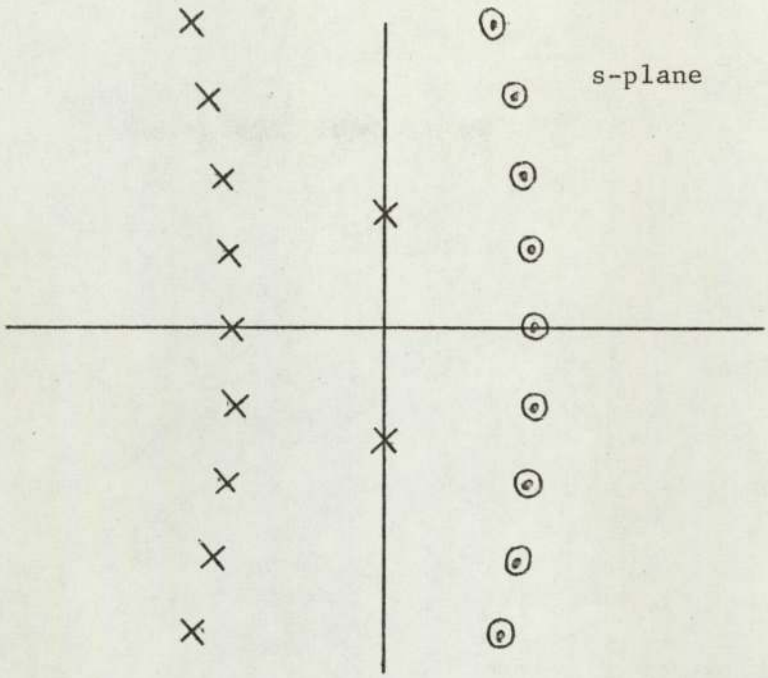

Fig.2.2.2 This diagram has unequal scale factors. In general the imaginary ordinate of a pole will be greater than fifty times the real ordinate. A ratio of fifty will be shown later to give about five oscillations to the crossover point. All s-plane diagrams in this thesis are shown with unequal scales for clarity.

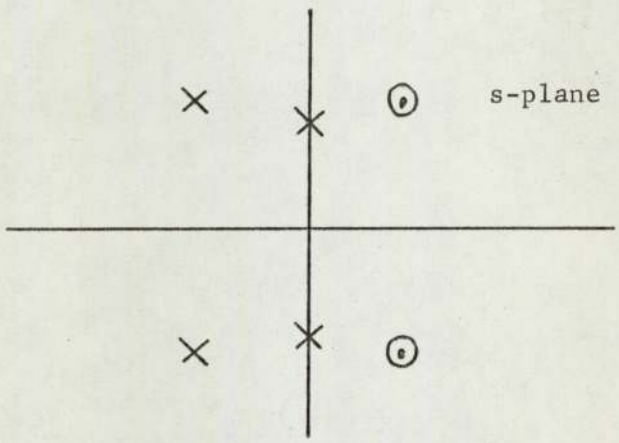

Fig.2.3.1 In this diagram for the dominant pole approximation, other poles of the system are neglected. The typical error produced is 1% because of the small distance separating the poles of the system and the poles of the forcing function.

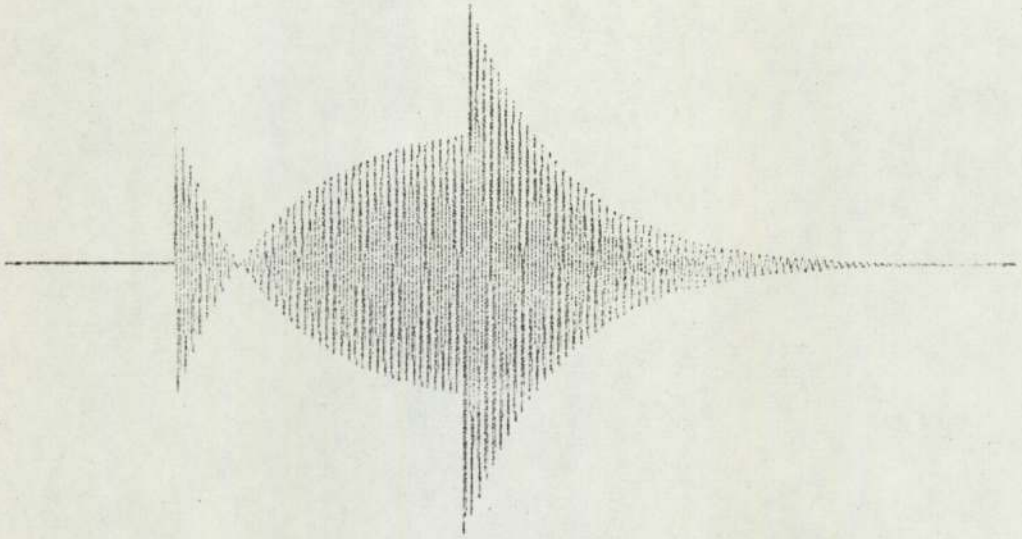

Fig. 2.4.1(a)

Resultant computer plot for the aluminium line resonator using the data calculated in Table 2.4.2.

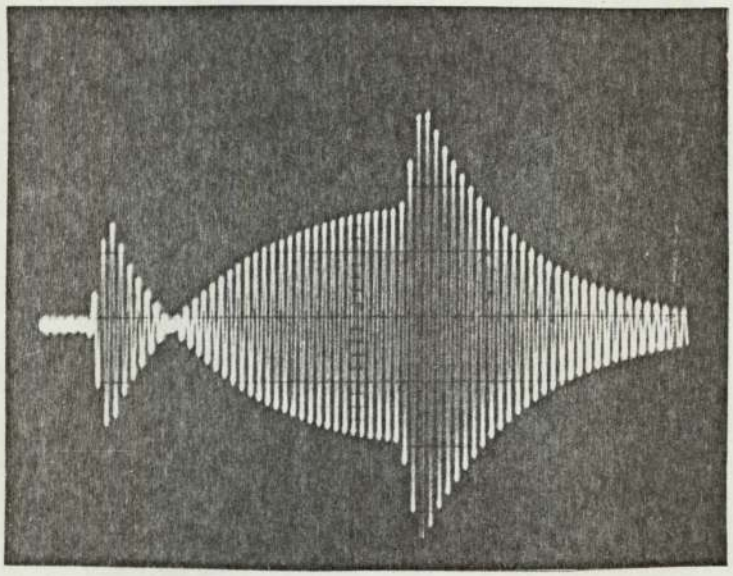

Fig.2.4.1(b)

Oscilloscope trace of the actual aluminium line resonator in its lowest mode.

The resonator is lossless, consequently the steady-state echo-signal is equal to the initial signal, and the decrement begins at twice this value. The equality of the exponential rise and fall is apparent. The stepped nature of the echo appears with the higher order resonances (see Fig.2.5.1).

Line/resonator cross-sectional area ratio	measured	$A_1/A_2 = 0.0128$
$\frac{\rho c \text{ line}}{\rho c \text{ resonator}}$	known data	$\rho_1 c_1 / \rho_2 c_2 = 2.88$
Longitudinal velocity in resonator	known data	$c_2 = 5240$ m/s
Resonator length	measured	$l_2 = 9.9$ cm
Fundamental natural resonant frequency	$\omega_1 = c_2\pi/l_2$	$\omega_1 = 2\pi\ 26500\ s^{-1}$
Reflection coefficient	$r = \frac{1 - \frac{\rho_1 c_1 A_1}{\rho_2 c_2 A_2}}{1 + \frac{\rho_1 c_1 A_1}{\rho_2 c_2 A_2}}$	$r = 0.93$
Factor k	$k = \log_e r$	$k = 0.076$
Ordinate β	$\beta = kc_2/2l_2$	$\beta = 2000 s^{-1}$
Loss coefficient	known data	$H_2 \simeq 0\ m^2 s^{-1}$
Ordinate α	$\alpha = H_2^2/2l_2^2$	$\alpha = 0\ s^{-1}$

Fig.2.4.2 This table shows the calculation process from first principles for the aluminium line resonator using the basic acoustical data. The resulting values for α, β, and ω_1 were used to obtain the computer plot of Fig.2.4.1(a)

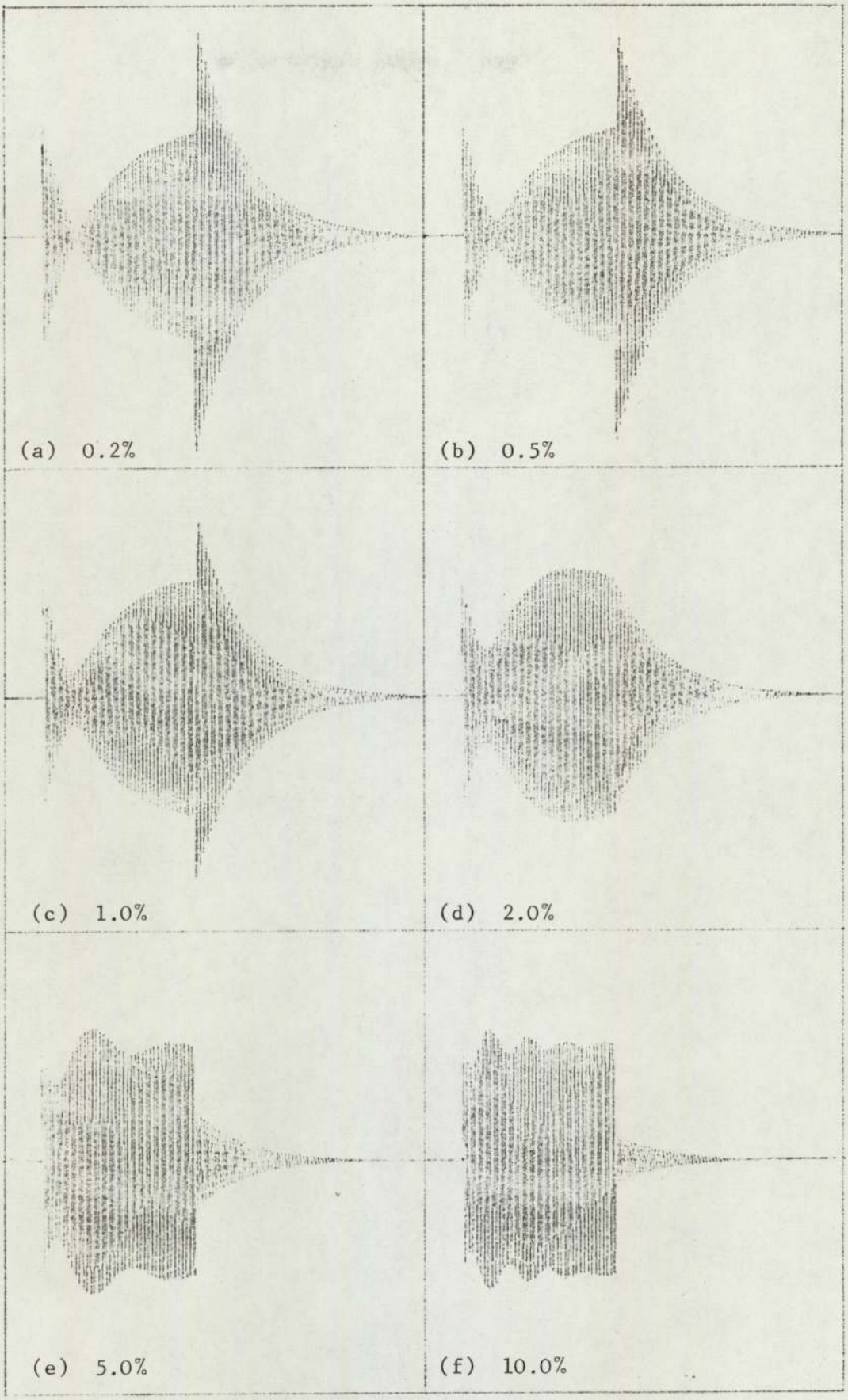

Fig.2.4.3

The echo is shown with successive amounts of detuning which cause a rapid fall in the energy stored, shown by the fall in the decrement amplitude. The modulation of the echo signal indicates the beat frequency difference between the transmitted signal frequency and the resonant frequency.

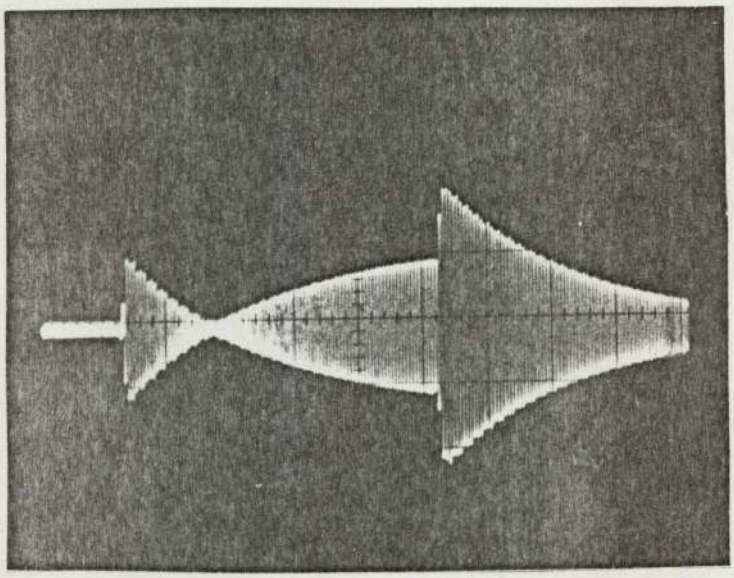

Fig. 2.5.1

Oscilloscope photograph showing the stepped nature of the echo for mode m = 3 of the aluminium line resonator. The steps correspond to the transit time for a return signal in the resonator.

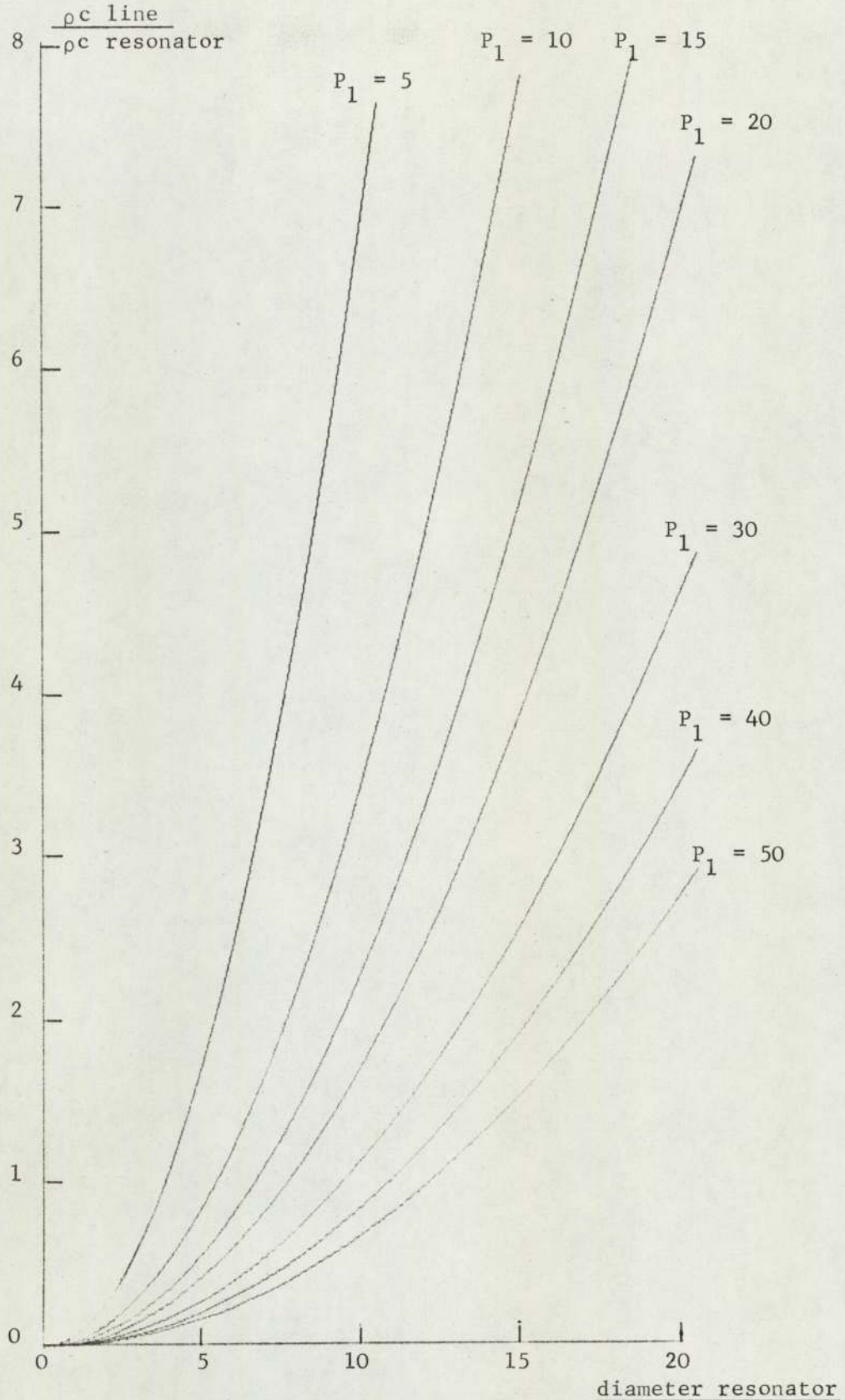

Fig.2.5.2

This graph is useful for choosing a line size in order to give a desirable coupling Q for a particular experiment. P_1 is the number of oscillations to crossover for the fundamental (m = 1). For overtones $P_m = mP_1$ so long as the material is lossless.

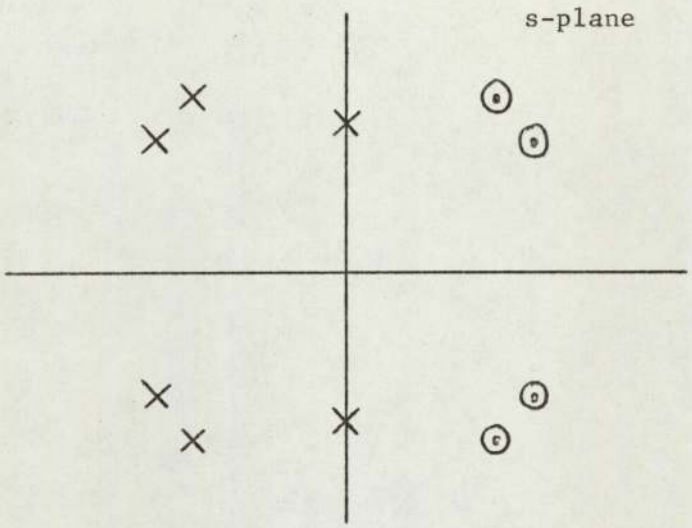

Fig. 2.6.1

This is the diagram for a coupled resonance involving two lossless resonant modes.

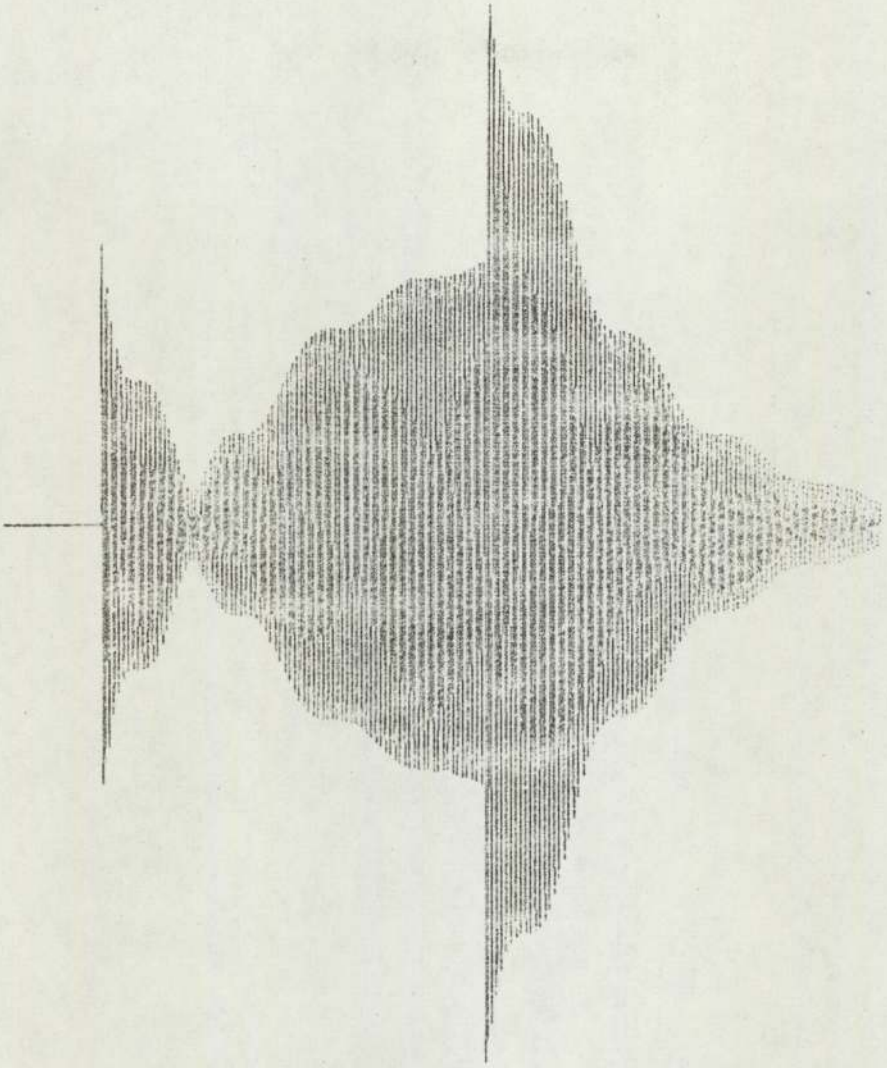

Fig.2.6.2

Echo return showing the effect of two coupled resonant modes as in Fig.2.6.1. The frequency separation of the modes is 5% and the coupling is the same for both. The transmitted frequency is tuned to one of the modes.

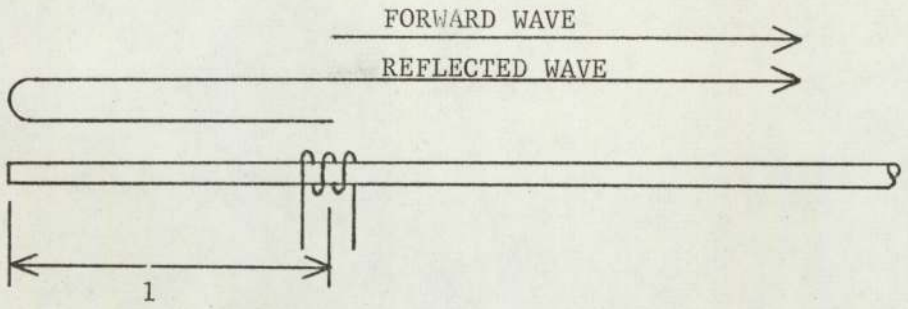

Fig.2.7.1(a)

The total forward travelling wave is the sum of the reflected and forward waves shown here.

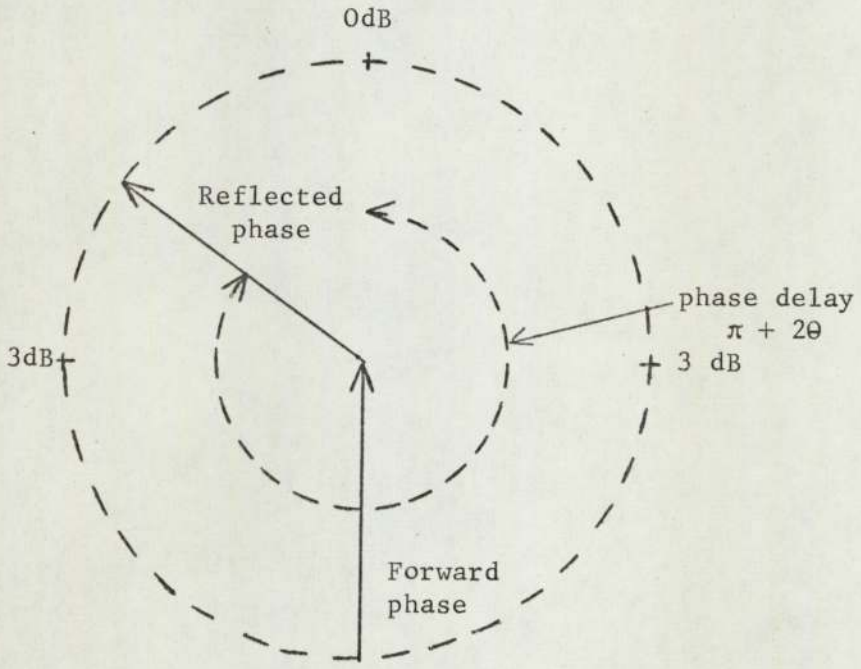

Fig.2.7.1(b)

This vector diagram shows the relation between θ and the 3 dB points and hence defines the bandwidth.

Fig.2.7.2

This photograph shows the burst generator, the tuning capacitor and the frequency meter used in the laboratory.

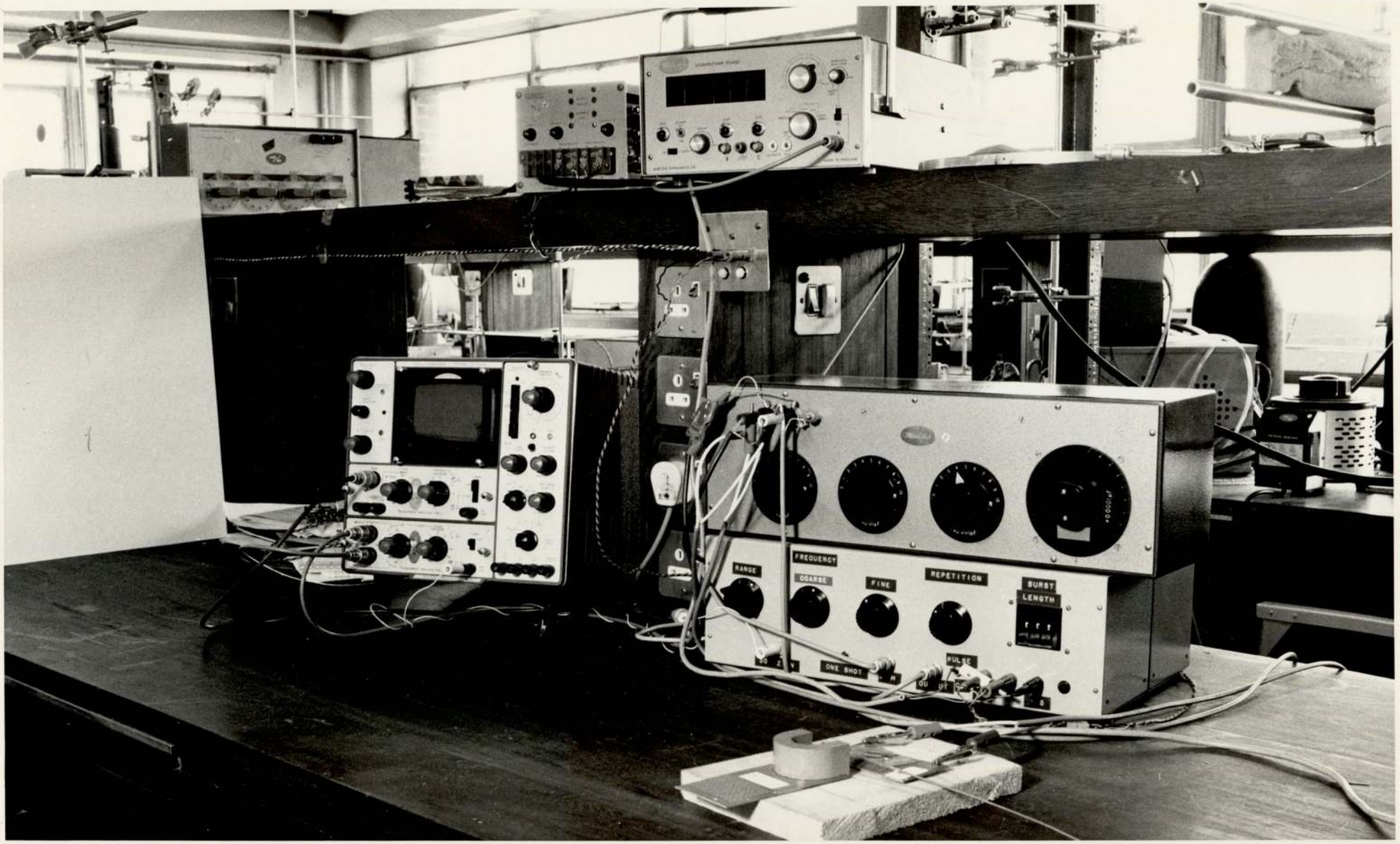
RANGE
FREQUENCY
COARSE
FINE
REPETITION
BURST
LENGTH
ONE SHOT
PULSE

Fig.2.7.3

A typical launching coil and bias magnet are shown here. A range of coils of various lengths allows optimum performance to be achieved at the frequencies being used. To achieve maximum electroacoustic coupling the coil must be close to the magnetostrictive material, so a range of various diameter coils was available.

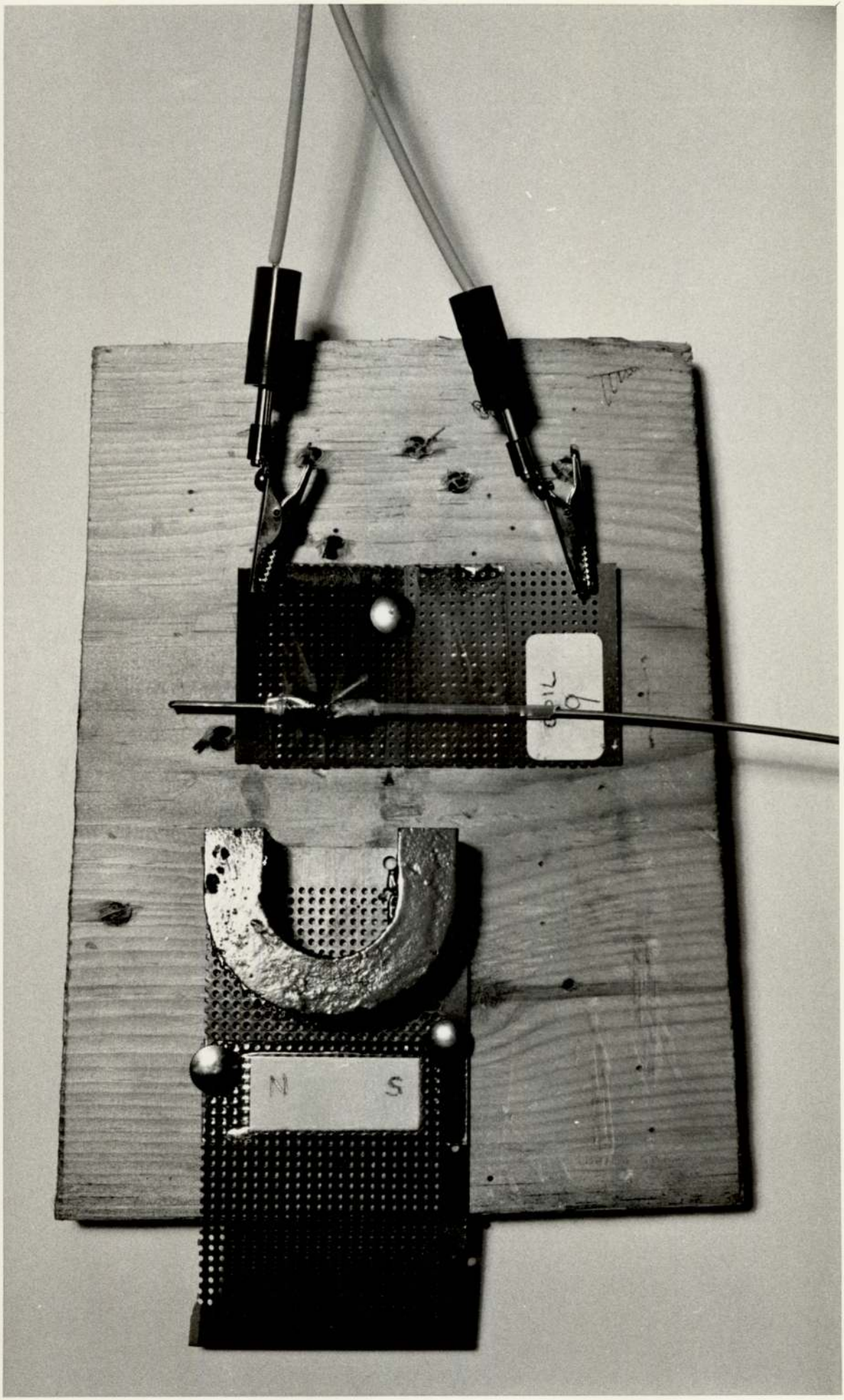
N
S

3. DISK RESONATORS

3.1 Introduction

The complex pattern of vibrations in disks and plates has been known and studied for about two centuries. Their analysis has been attempted by many mathematicians, and while the differential equations are readily derived, the boundary conditions can make certain solutions extremely difficult.

Here, thin disks with planar isotropy in particular are considered. There are two basic types of vibration, flexural (Chladni 1787, Ravenhall 1973), and contour extensional (in plane) modes. The latter, until comparatively recently have not been seriously considered for two principal reasons. First, the solution of the frequency equations without the help of a digital computer would have been a formidable task. Secondly there was no convenient method to excite these modes. In fact Love 1927 concluded, "these modes of vibration seem not to be of sufficient physical importance to make it worth while to attempt to calculate the roots numerically". With the general availability of highly active ferroelectric ceramics, the latter difficulty was removed and Onoe 1956 derived solutions for certain cases. Holland 1966, making extensive use of digital computers, completed the solutions for the difficult compound modes.

The contour extensional modes themselves subdivide into three groups:-

(1) Radial Modes characterised by the absence of rotation. In these modes ξ_θ vanishes and ξ_r is independent of θ.

(2) Tangential Modes characterised by the absence of areal dilatation. In these modes ξ_r vanishes and ξ_θ is independent of θ.

(3) Compound modes in which neither ξ_θ nor ξ_r vanish.

Frequency equations for these three groups of vibrational modes are given by Love 1927. The essence of Love's derivation of these equations is given in Appendix A.3.1. The equations can be rewritten in the following form.

(1) Radial modes frequency equation

$$M_1(K_{mR}) = 1 - \sigma \qquad 3.1.1$$

(2) Tangential modes frequency equation

$$M_1(K_{mT}\Theta) = 2 \qquad 3.1.2$$

(3) Compound modes. The frequency equation is formed by eliminating A/B.

$$\frac{A}{B} = \frac{J_n(\Theta K_{m,n})}{J_n(K_{m,n})} \cdot \frac{n(M_n(\Theta K_{m,n})-(n+1))}{\tfrac{1}{2}(K_{m,n})^2-n(n+1)+M_n(K_{m,n})} \qquad 3.1.3$$

$$\frac{A}{B} = \frac{J_n(\Theta K_{m,n})}{J_n(K_{m,n})} \cdot \frac{2M_n(\Theta K_{m,n})+(\Theta K_{m,n})^2-2n(n+1)}{2n(M_n(K_{m,n})-(n+1))} \qquad 3.1.4$$

K is a normalised dilatational wave number,

$$K = ha = \omega a(\rho(1-\sigma^2)/E)^{\frac{1}{2}} \qquad 3.1.5$$

Θ is the ratio of shear and dilatational wave numbers.

$$\Theta = k/h = (2/(1-\sigma))^{\frac{1}{2}} \qquad 3.1.6$$

$$\text{and } M_n(\Lambda) = \Lambda J_{n-1}(\Lambda)/J_n(\Lambda) \qquad 3.1.7$$

A brief explanation of the subscripts of K is in order here. For radial modes the integer m is the number of nodal circles associated with any particular mode. The centre point is always a node (i.e. a circle with zero radius). For tangential modes m is the number of nodal circles but now the centre is never a node.

The compound modes are described by two integers m and n. m is again the number of nodal circles. n is the number of nodal diameters. The centre is always a nodal point except when n=1.

From the tabulated values of K, resonant frequencies can be found from the equation, $K = \omega a \left[\rho\ (1-\sigma^2)/E\right]^{\frac{1}{2}}$.

Onoe 1956 solved the lower order modes publishing his results in the form of a small graph. Holland 1966 published tabulated values of $K_{m,n}$ for many modes extending to higher orders. He produced these for poissons ratio between 0.25 and 0.50 in intervals of 0.05. For much of the current work this documentation is not comprehensive enough, so Ambati 1973 produced K values for poissons ratio from 0.00 to 0.50 in intervals of 0.01. All modes that are easily excited by the delay-line method of section 2 were included. These tables have been extended to Poisson's Ratio values up to 1.00 and are available from the author.

3.2 Comparison with experiment

The apparatus for all disk experiments was as described in section 2.7; in this case the resonator was a disk. To excite the contour extensional modes the transmission line was coupled radially into the disk. Thermally setting epoxy resin proved an adequate adhesive for this purpose. The electrical drive was provided by the burst generator of section 6.3.

Tests were carried out on a variety of disks and the results are shown in Table 3.2.1. The agreement between measured and calculated frequencies is extremely good. Thickness to diameter ratios were kept to about 20, and the close agreement establishes that any thickness correction is unnecessary. The results would indicate that manual tuning gives a frequency, accurate to 0.05

per cent.

The ability to drive disks of any material is an important feature of this method and it enables very precise measurements of elastic constants, of a variety of materials, over a wide temperature range to be determined. Disks need only be isotropic in-plane so this allows measurements on orthotropic materials.

Making Q_c high improves the sensitivity of adjusting to resonance and still further reduces the effect of the selectivity of the transducer. These high values of Q_c and hence P_m, require the use of long lines, sometimes up to 20 metres in length.

Typical oscilloscope traces are shown in Fig. 3.2.2.

3.3 Multiple Resonances

The case of two interacting resonances was considered in section 2.6. This sometimes occurs with disks, in particular with modes (1,R) and (1,3) in Aluminium or Steel. Figs. 3.3.1 and 3.3.2 show photographs and corresponding computer plots for Aluminium and Steel disks. Computer plotting would allow the true resonant frequencies to be inferred. However for the measurements made in this report other more convenient modes were available so a detailed investigation of these coupled modes was not pursued.

3.4 Measurement of Elastic Constants

Traditionally elastic constants are measured by observing longitudinal and shear wave velocities in a specimen (Love 1927, Tzannes 1966), normally using a pulse technique. A consideration of disk resonators has led to alternative methods for piezoelectric materials (McMahon 1963, Meitzler 1973).

The method described here has greater accuracy than a pulse technique, and uses the phase technique described in section 3.2. Employing the system of excitation described, the method becomes applicable to all materials rather than piezoelectrics hitherto.

For the tests carried out, Poissons Ratio was measured at room temperature and above. A photograph of the furnace assembly is shown in Fig. 3.4.1. The gas supplied to the furnace tube was argon, flowing into the bottom at a slow rate. A Chromel-Alumel thermocouple was situated close to the disk for temperature measurement. The furnace itself could be raised and lowered over the tube. The disk was attached to the line with a high-temperature adhesive, "Autostick".

The compound modes having nodal diameters all have similar dependence on Poissons Ratio (see Fig. 3.4.2). The pure radial modes (1,R) and (2,R) and the mode (2,1) which has only one nodal diameter have a completely different dependence and comparison of these modes with the adjacent compound modes gives Poisson's Ratio with good sensitivity. In practice mode (1,R) is compared with (1,3), (2,1) with (1,5) and (2,R) with (1,8) or (1,9). For this reason Ambati 1973 tabulated

$$\frac{K_{1R}-K_{13}}{K_{13}} \text{ , } \frac{K_{21}-K_{15}}{K_{15}} \text{ , } \frac{K_{2R}-K_{18}}{K_{2R}} \text{ , and } \frac{K_{2R}-K_{19}}{K_{2R}}$$

all against Poisson's Ratio. Table 3.4.3 gives these results which are also shown graphically in Fig. 3.4.4.

Comprehensive tests were carried out on two specimen disks. One was high-conductivity copper, cut from sheet, with a 99.98% purity. The other was E1C aluminium sliced from bar with the following composition:-

Al	Cu	Mg	Si	Fe	Mn
99.0	0.1	-	0.5	0.7	0.1

Both disks were made 35 mm in diameter. This meant that modes (2,1) and (1,5) were the most convenient because (1,8), (1,9) and (2,R) would have been rather high in frequency.

Two temperature runs were performed on each specimen, so that any annealing effects would take place on the first run. The furnace was set to a constant power and values of $f_{1,5}$, $f_{2,1}$ and thermocouple millivolts were taken at equal intervals of time. Each experiment was terminated when Q_M became equal to Q_C, for after this point manual tuning becomes less accurate. The raw data from these four experiments is plotted out in Figs. 3.4.5/6/7/8. After these heating runs a further calibration run was performed for both specimens. For this calibration, a furnace controller was used so that isothermal conditions could be established.

Readings of $f_{2,1}$, $f_{1,5}$ and thermocouple mV were taken so that the disk could be regarded as its own thermometer for the previous experiments (Bell 1968, Seth 1973).

In processing this raw data, computer least-squares curve fitting is extensively used. (see Appendix A.3.4.)

Polynomials are fitted directly to the observed values of $f_{2,1}$, $f_{1,5}$ and mV, time being the independent variable. Where apparent singularities appear the curve is split into sections for the curve fitting process. The resultant polynomials are then used to calculate $(f_{21}-f_{15})/f_{15}$ and mV at selected intervals of time. The temperature readings are cross checked by using the disk as its own thermometer via the calibration curves. To find Poisson's Ratio a polynomial is fitted locally to the data from Table 3.4.3; in this

case for σ from 0.32 to 0.39 (a cubic curve gave a perfect fit). Hence pairs of values for Poisson's Ratio and temperature are obtained.

The derived curves of $(f_{21} - f_{15})/f_{15}$ are shown in Figs. 3.4.9/10/11/12, together with the resultant curves for Poisson's Ratio against temperature.

3.5 Discussion of results

Assuming an overall accuracy of frequency measurement of 0.05% (that is $\pm$50Hz for the 35 mm disks) gives Poisson's Ratio to an accuracy of 0.0015. However for a particular specimen the frequency tuning sensitivity is about $\pm$10Hz so changes in Poisson's Ratio of 0.0003 can be detected (with larger disks giving $f_{1,5}$ around 50KHz a frequency sensitivity of $\pm$1Hz can be obtained).

After the initial annealing runs on each specimen, the second runs can be used to give the temperature coefficient of Poisson's Ratio. The change in Poisson's Ratio for the aluminium disk was large and the curve permits the curvature to be detected.

3.6 Possible extension to anisotropic disks

The effect of anisotropy is to split one of the disk modes of section 3.1 into two or more. A simulated anisotropic disk was made by machining the faces of a steel disk to be non-parallel. On this specimen the mode splitting was clearly observed by coupling at a series of different positions on the circumference. A mathematical investigation of anisotropic disks would require the derivation of new equations of motion from first principals. It would facilitate an important extension of the work in that anisotropic elastic constants and elastic anisotropy could be investigated. The method would then be applicable to disks cut at various angles from single crystals and

also to disks constructed from laminated carbon fibres.

At the present time this work has not been pursued.

RESONANT MODE	Frequencies in KHz			
	Mild Steel Disk 7.5 cm dia. σ = 0.29		Aluminium Disk 7.5 cm dia. σ = 0.34	
	measured	calculated	measured	calculated
1,T	71.30	71.3	67.18	67.1
1,R	46.27	46.3	47.35	47.1
2,1	80.14	79.7	79.66	79.7
1,1	36.71	36.6	36.24	36.0
1,2	31.83	31.3	30.54	30.6
1,3	48.65	48.1	47.35	47.0
1,4	63.41	62.6	61.39	61.3
1,5	77.35	76.2	74.33	74.8
1,6	90.98	89.5	87.72	87.6
1,7	103.27	102.5	100.62	100.3
1,8	116.25	115.2	112.94	112.8
1,9	129.46	127.2	124.55	125.2
	Quartz Disk 5 cm dia. σ = 0.16		Glass Disk 9 cm dia σ = 0.25	
	measured	calculated	measured	calculated
1,T	124.8	124.7	-----	60.8
1,R	73.53	73.4	39.82	39.0
2,1	131.96	128.3	69.79	69.5
1,1	63.15	63.3	32.61	32.5
1,2	56.48	55.9	28.40	28.5
1,3	86.78	86.6	43.45	43.6
1,4	112.09	112.0	56.51	56.7
1,5	135.40	135.9	68.75	68.8
1,6	159.80	160.2	80.59	80.7
1,7	183.0	182.5	92.20	92.3
1,8	200.9	204.8	103.68	103.6
1,9	-----	227.1	115.06	115.1

Table 3.2.1

This table shows the close agreement between calculated and experimentally measured frequencies. The values of σ used in the calculations are recognised values for these materials (Kaye/Laby 1958).

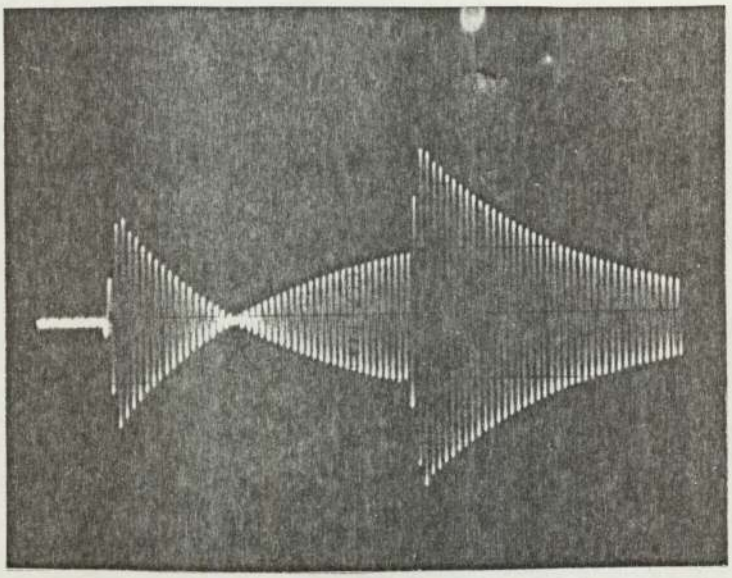

Fig.3.2.2(a) The echo for mode (1,1) of a 1.5 inch diameter aluminium disk shown here is a typical echo as described in Section 2.4.

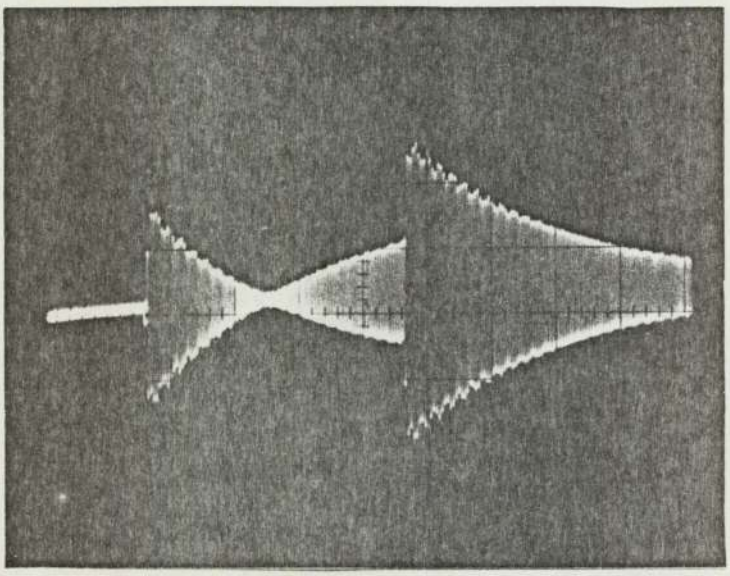

Fig.3.2.2(b) The echo for mode (1,4) of the same disk shows a stepped envelope suggesting that the wave travels circumferentially in the disk (see Section 2.5).

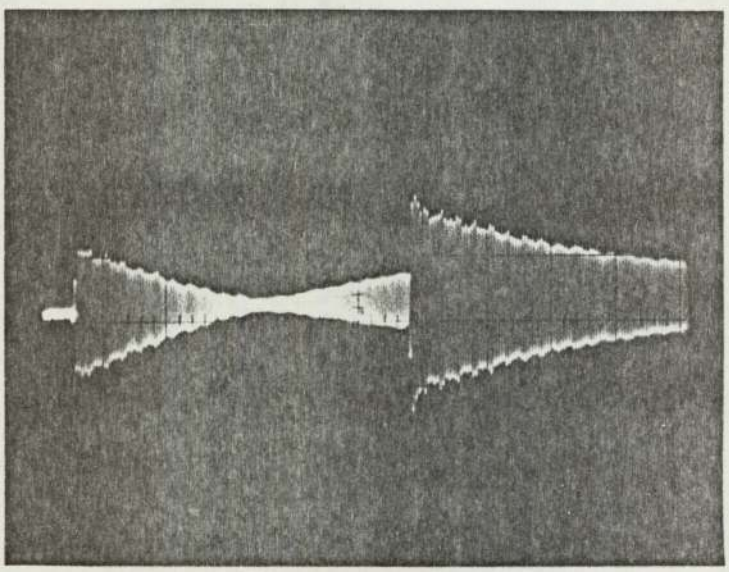

Fig.3.2.2(c) The echo for mode (1,5) of the same disk.

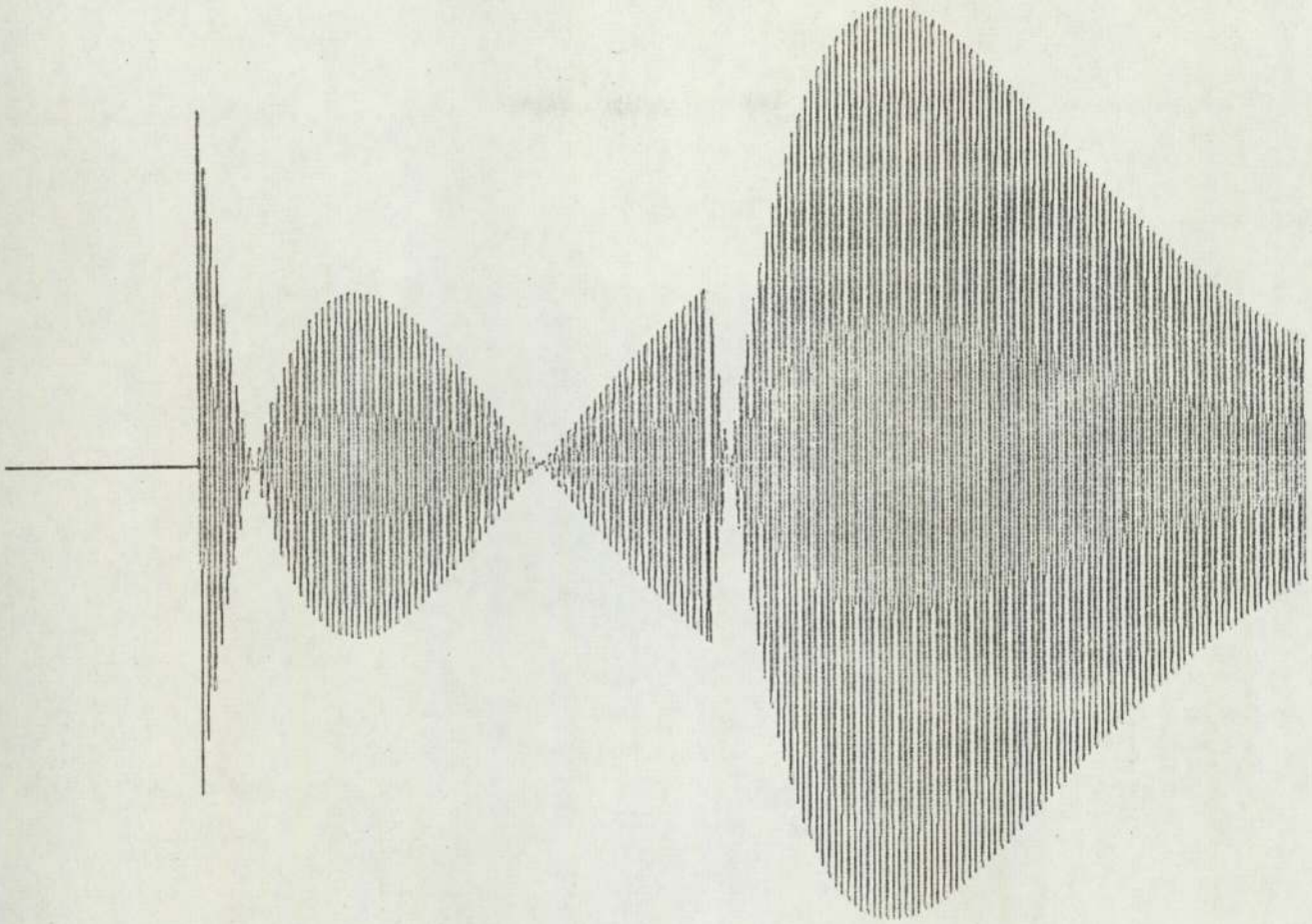

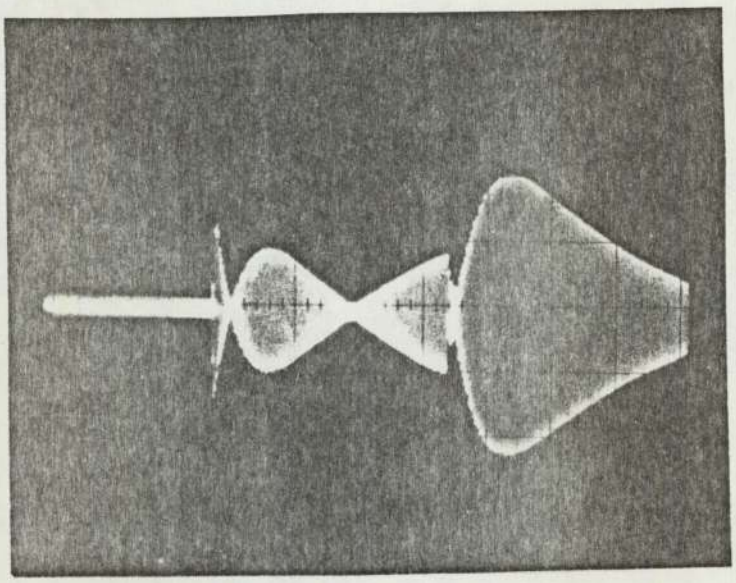

Fig.3.3.1

The oscilloscope trace shown here was observed from an aluminium disk for the coupled modes (1,3) and (1,R). The Poissons Ratio for aluminium is such that these two modes occur at the same frequency (see Fig.3.4.2) With frequencies equal and with coupling Q values of 80 for both modes the corresponding computer plot was obtained.

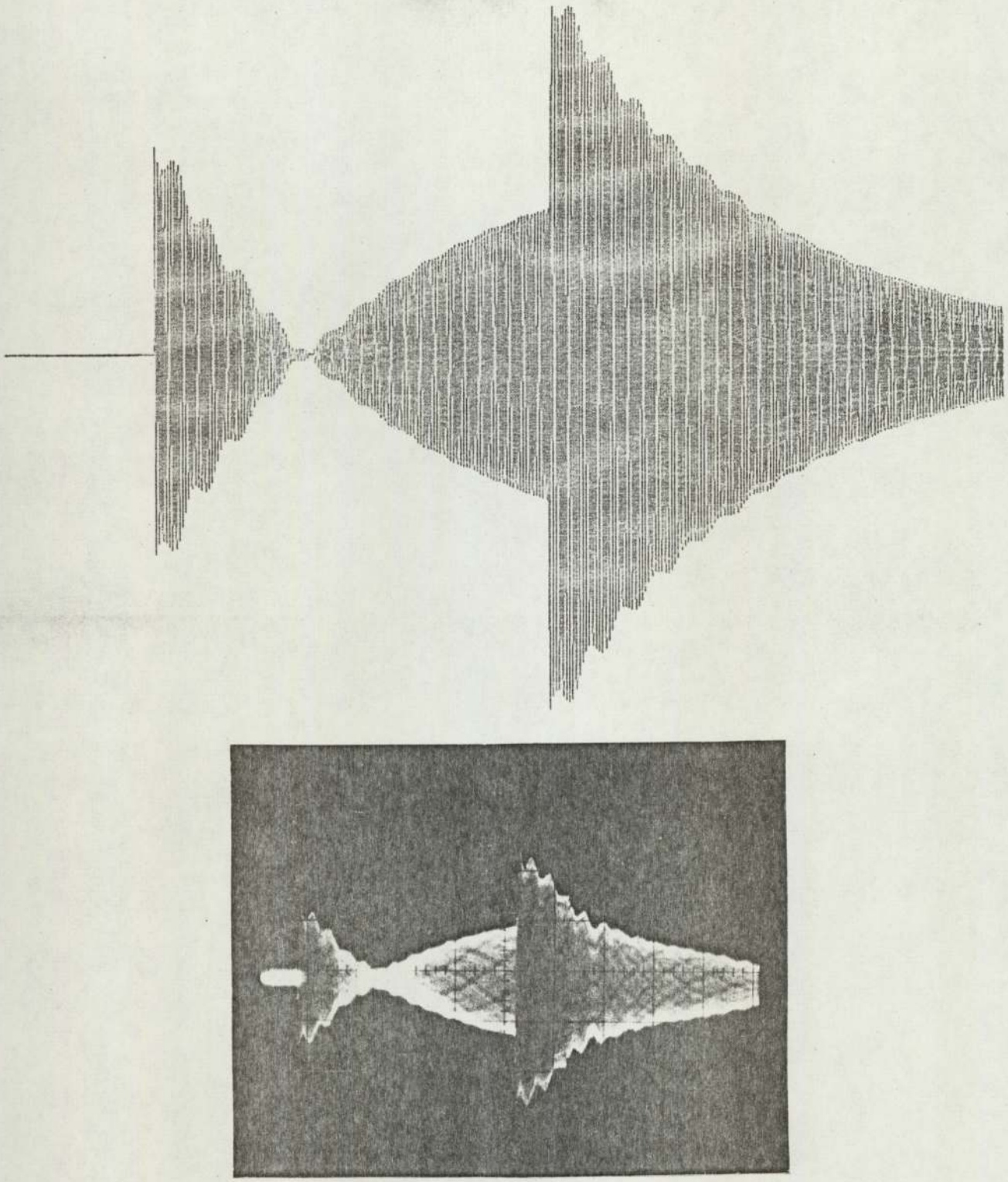

Fig.3.3.2

The oscilloscope trace was from a mild steel disk for the modes (1,3) and (1,R). The computer plot was obtained with a 10% frequency separation between the two resonant modes. The signal frequency was equal to that of one mode with Q_c = 210. The other mode had Q_c = 115.

Fig.3.4.1

This furnace rig was constructed by J.M. Pelmore. The element moves up over the silica tube and is capable of 1000° C maximum temperature. The transmission line fits through a rubber bung at the top, and small brackets keep the line and resonator in place inside the tube. A thermocouple outside the tube but inside the heater was used to supply a signal for the furnace controller. A second thermocouple inside the tube was used to measure the specimen temperature. The pipes supplying the argon can be clearly seen in the photograph.

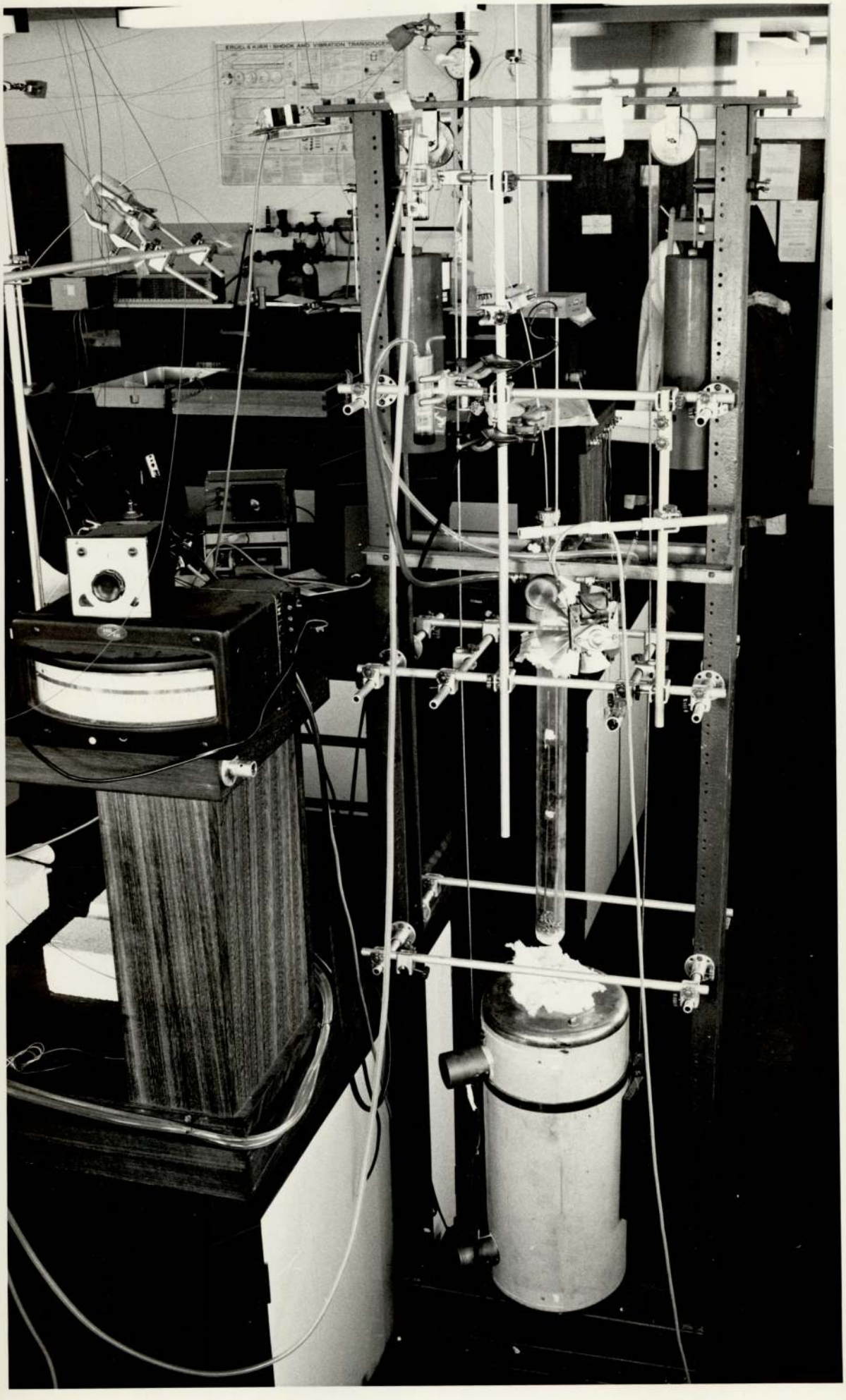

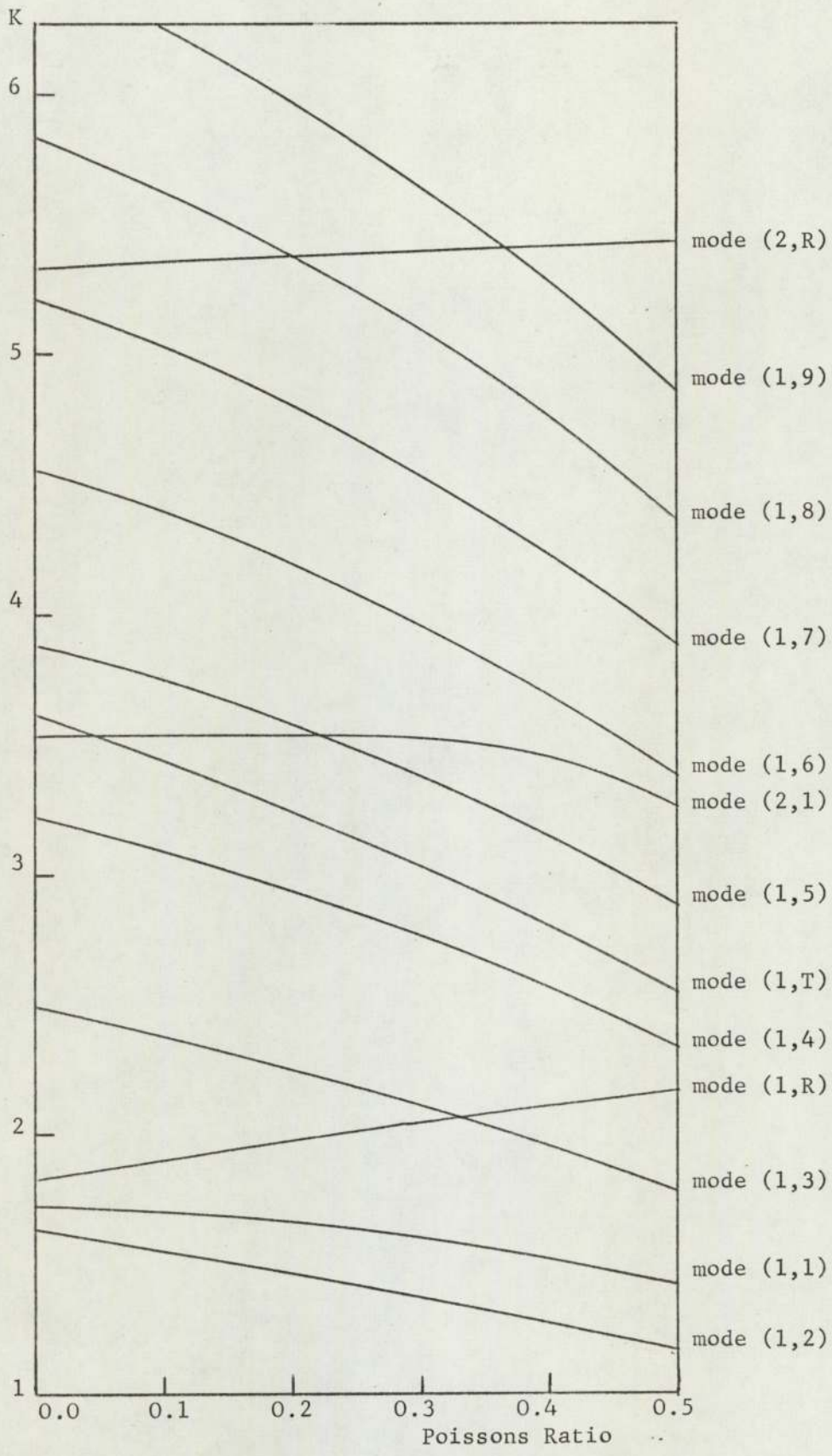

Fig.3.4.2

These are graphs of the data from Ambati 1973. The differing trends of the K parameters for radial and distortional modes are the basis for a measurment of Poissons Ratio.

Poissons Ratio	$\frac{100(K_{1R} - K_{13})}{K_{13}}$	$\frac{100(K_{21} - K_{15})}{K_{15}}$	$\frac{100(K_{2R} - K_{18})}{K_{2R}}$	$\frac{100(K_{2R} - K_{19})}{K_{2R}}$
0.00	-26.552	-9.568	-9.705	-21.601
0.01	-25.933	-9.197	-9.328	-21.213
0.02	-25.309	-8.876	-8.950	-20.798
0.03	-24.674	-8.545	-8.556	-20.361
0.04	-24.032	-8.203	-8.147	-19.906
0.05	-23.382	-7.851	-7.728	-19.450
0.06	-22.724	-7.486	-7.311	-18.995
0.07	-22.057	-7.110	-6.879	-18.522
0.08	-21.383	-6.724	-6.433	-18.015
0.09	-20.699	-6.325	-5.975	-17.505
0.10	-20.003	-5.916	-5.516	-16.995
0.11	-19.305	-5.496	-5.051	-16.484
0.12	-18.596	-5.065	-4.575	-15.968
0.13	-17.877	-4.622	-4.083	-15.459
0.14	-17.146	-4.169	-3.589	-14.922
0.15	-16.400	-3.706	-3.086	-14.365
0.16	-15.650	-3.230	-2.583	-13.784
0.17	-14.888	-2.744	-2.064	-13.202
0.18	-14.115	-2.246	-1.531	-12.621
0.19	-13.331	-1.737	-0.998	-12.033
0.20	-12.531	-1.218	-0.452	-11.440
0.21	-11.722	-0.687	+0.096	-10.834
0.22	-10.901	-0.148	+0.652	-10.247
0.23	-10.067	0.401	1.218	- 9.633
0.24	- 9.219	0.962	1.788	- 9.003
0.25	- 8.357	1.531	2.364	- 8.356
0.26	- 7.481	2.109	2.952	- 7.689
0.27	- 6.592	2.695	3.550	- 7.033
0.28	- 5.688	3.288	4.154	- 6.368
0.29	- 4.765	3.888	4.762	- 5.700
0.30	- 3.824	4.492	5.378	- 5.032
0.31	- 2.868	5.100	6.004	- 4.353
0.32	- 1.895	5.710	6.636	- 3.645
0.33	- 0.903	6.319	7.281	- 2.938
0.34	0.108	6.924	7.925	- 2.229
0.35	1.137	7.523	8.578	- 1.508
0.36	2.188	8.111	9.242	- 0.774
0.37	3.261	8.686	9.918	- 0.023
0.38	4.357	9.243	10.598	0.726
0.39	5.470	9.778	11.278	1.477
0.40	6.615	10.285	11.973	2.240
0.41	7.784	10.762	12.680	3.036
0.42	8.979	11.141	13.391	3.830
0.43	10.201	11.612	14.110	4.622
0.44	11.451	11.981	14.833	5.417
0.45	12.733	12.314	15.566	6.221
0.46	14.048	12.610	16.313	7.064
0.47	15.393	12.872	17.069	7.897
0.48	16.773	13.103	17.832	8.740
0.49	18.190	13.304	18.599	9.583
0.50	19.644	13.480	19.375	10.434

TABLE 3.4.3

By considering these ratios the constant of proportionality between K and frequency cancels and Poissons Ratio can be determined by experimentally measuring two frequencies. (See Fig. 3.4.4).

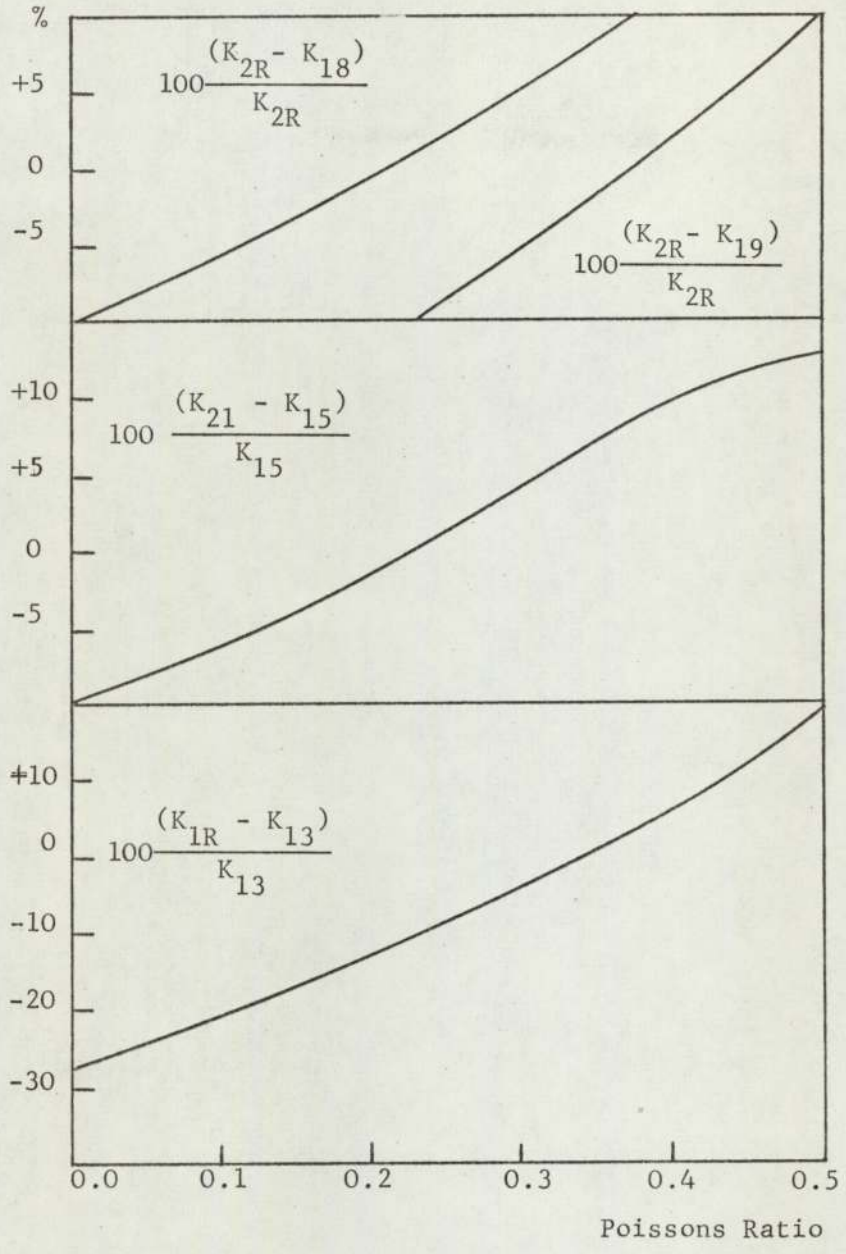

Fig.3.4.4

These graphs indicate the sensitivity of the three methods. If R is the ratio of two frequencies then a measure of the sensitivity is $\left|\frac{1}{R}\ \frac{dR}{d\sigma}\right|$. Using this criterion the sensitivities for K_{1R}/K_{13}, K_{21}/K_{15}, K_{18}/K_{2R}, and K_{19}/K_{2R} respectively are 1.0, 0.6, 0.65, and 0.65 for $\sigma = 0.3$.

Fig.3.4.5

Measured data from first test on copper. For metals modes (1,R) and (1,3) usually give a coupled resonance, so modes (2,1) and (1,5) are the most convenient. In practice these graphs are plotted on large sheets of graph paper so that the fitted polynomial curves can be checked.

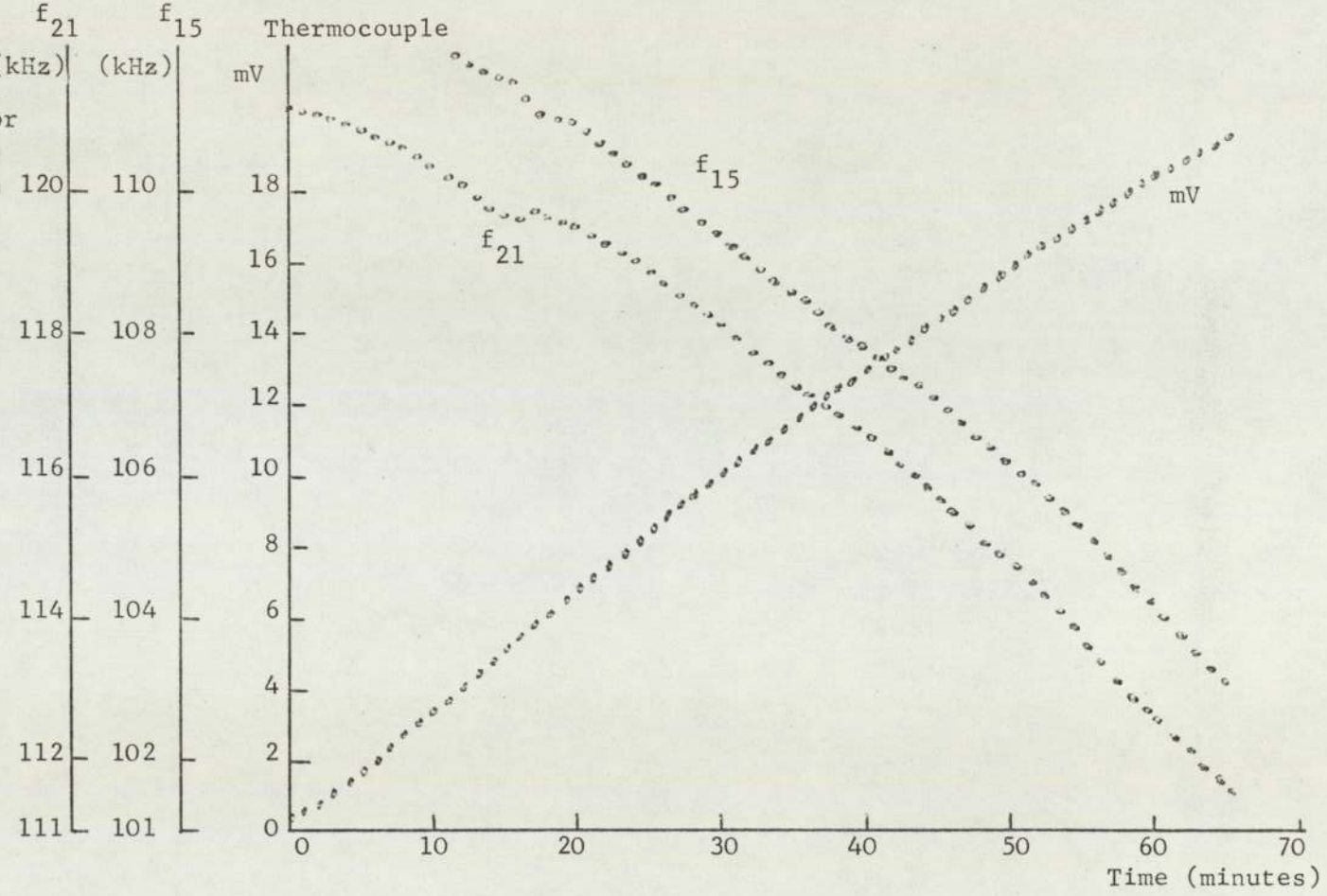

Fig. 3.4.6

Measured data from second test on copper

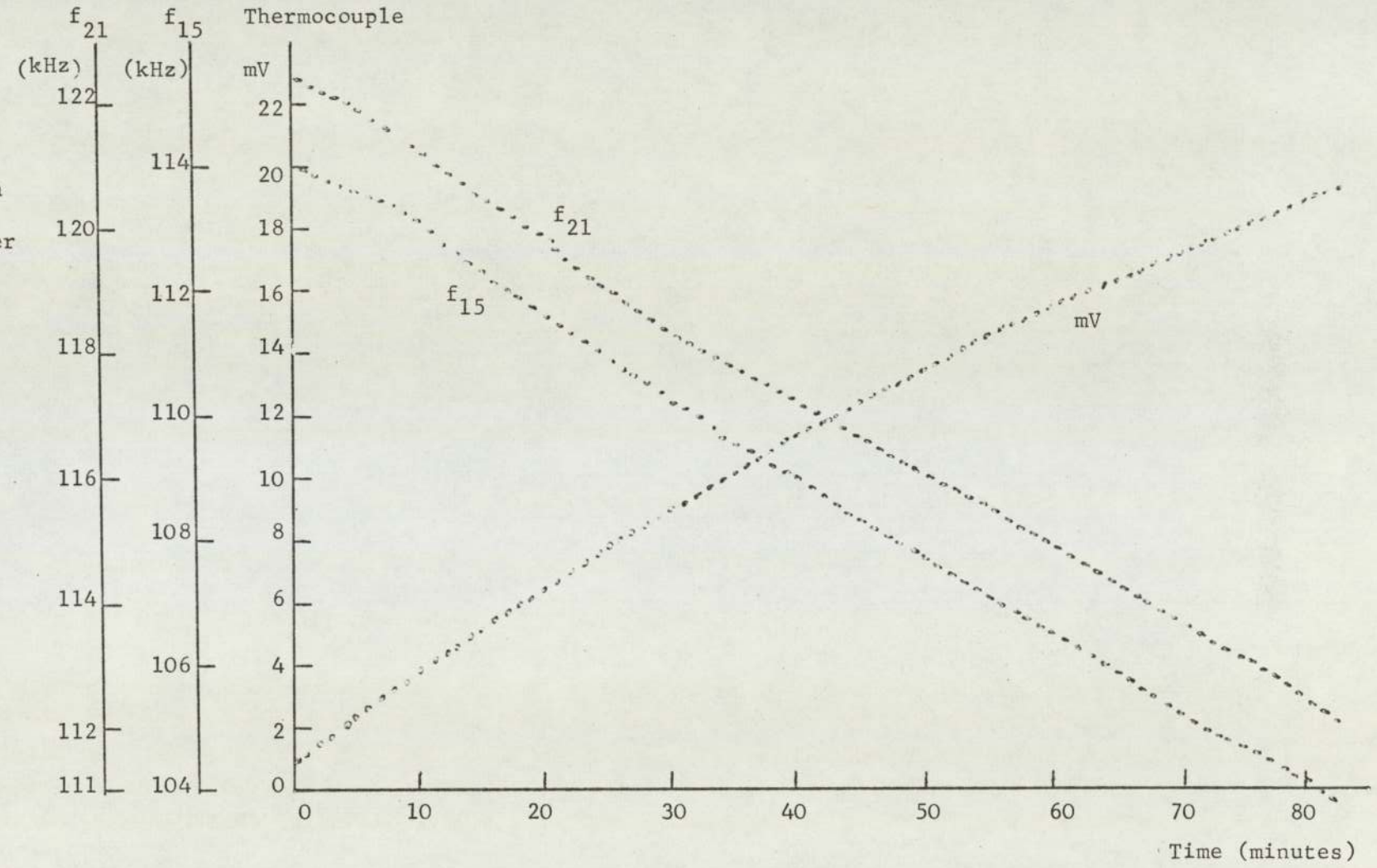

Fig. 3.4.7

Measured data from first test on aluminium.

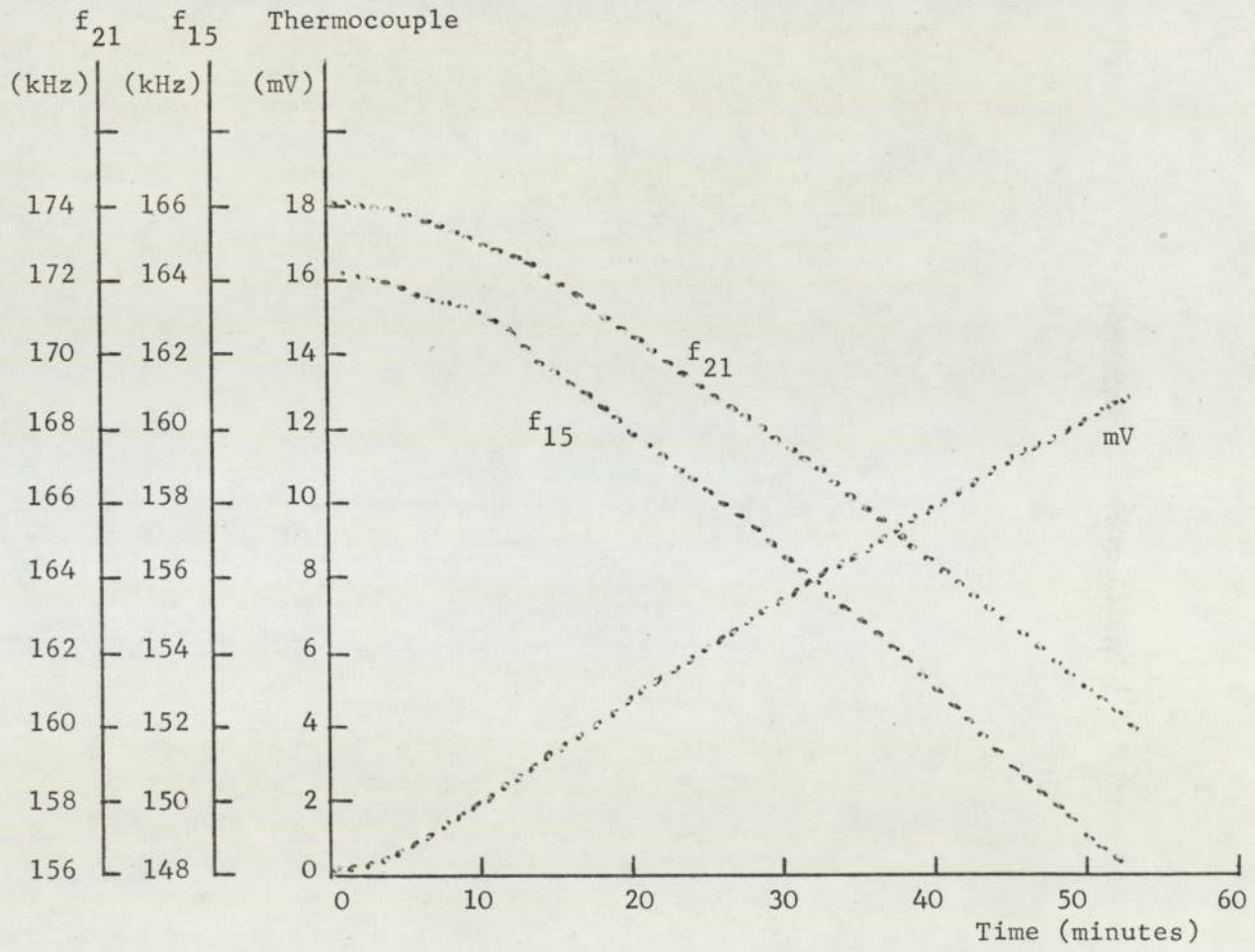

Fig. 3.4.8

Measured data from second test on aluminium.

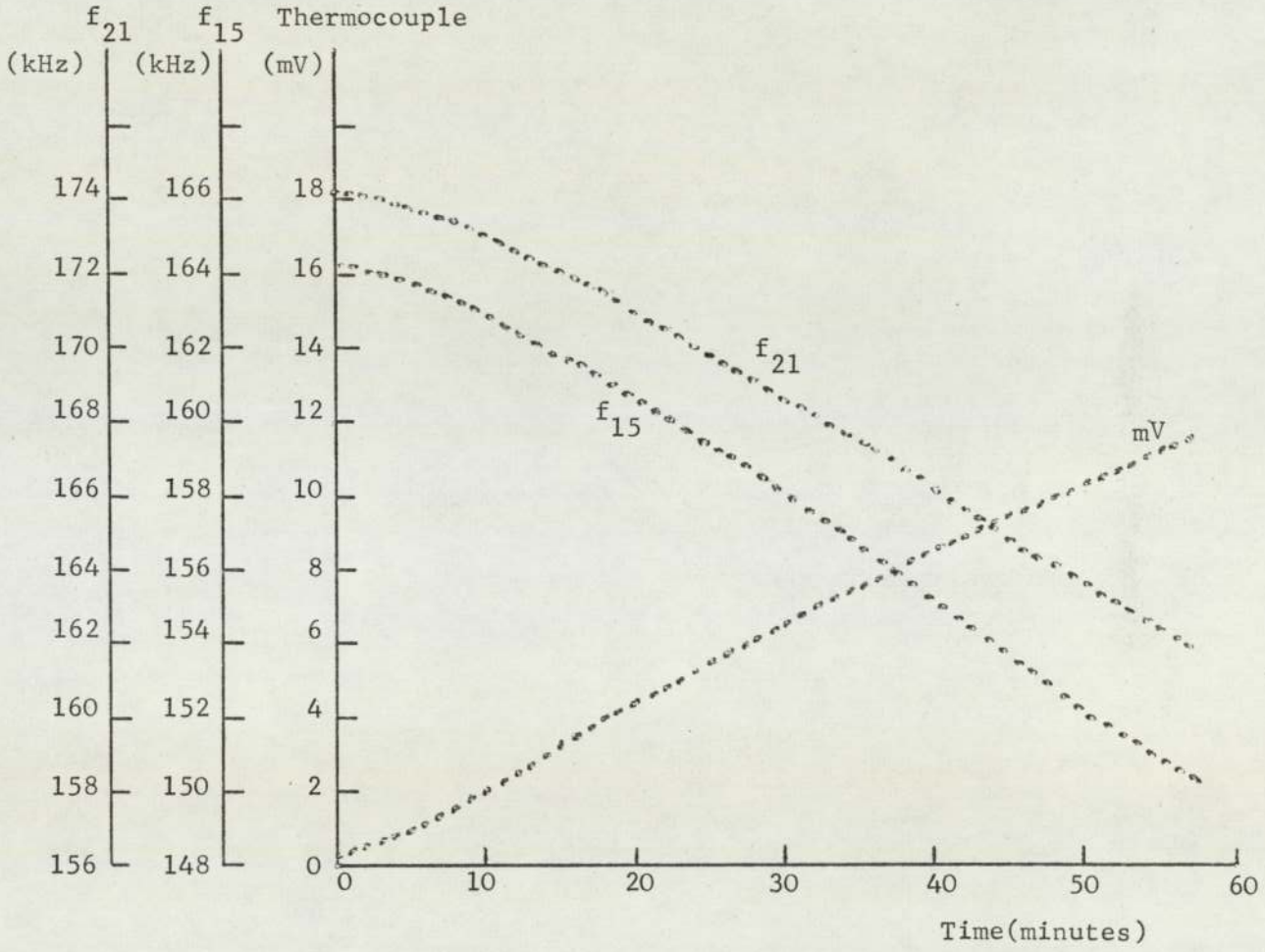

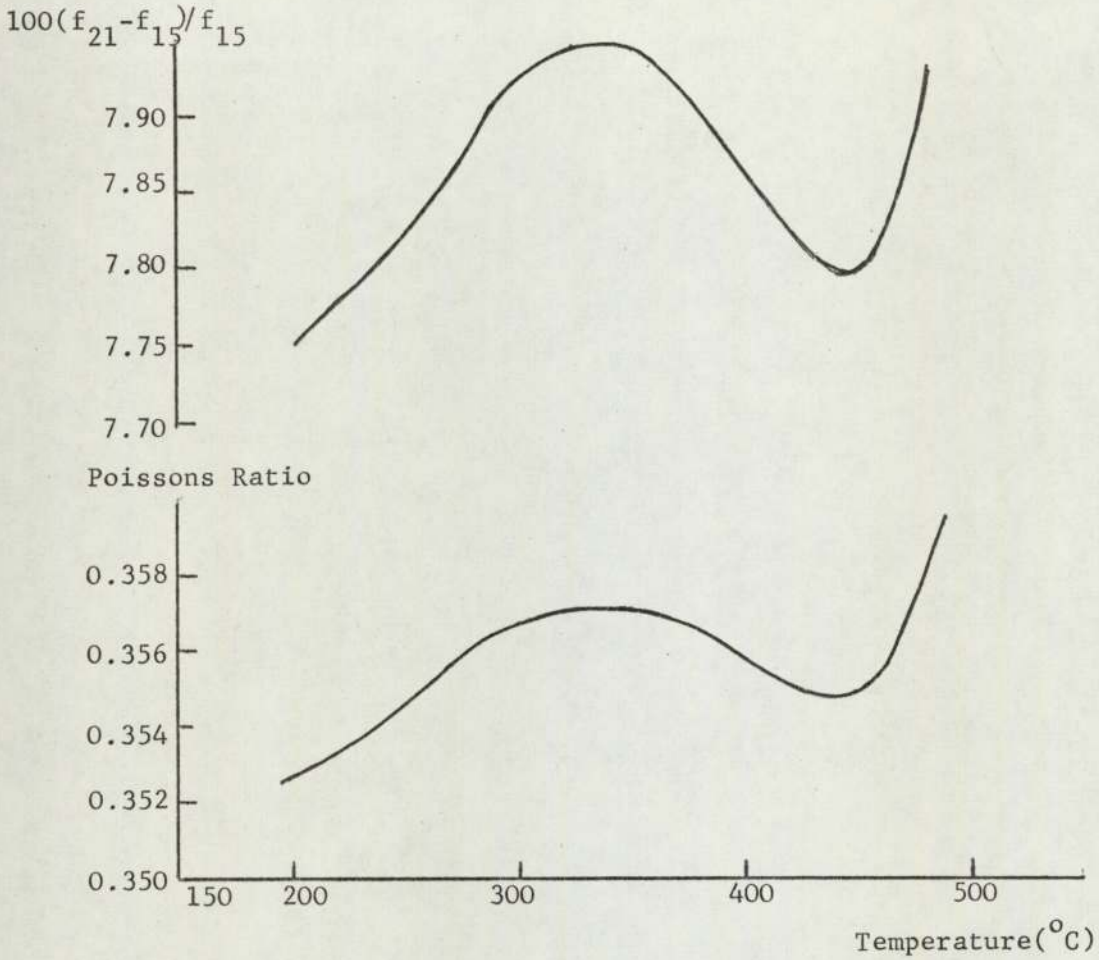

Fig. 3.4.9

Resultant curves from first test on copper. A curve of Youngs Modulus can be derived by measuring the diameter and density of the disk and using equation 3.1.5.

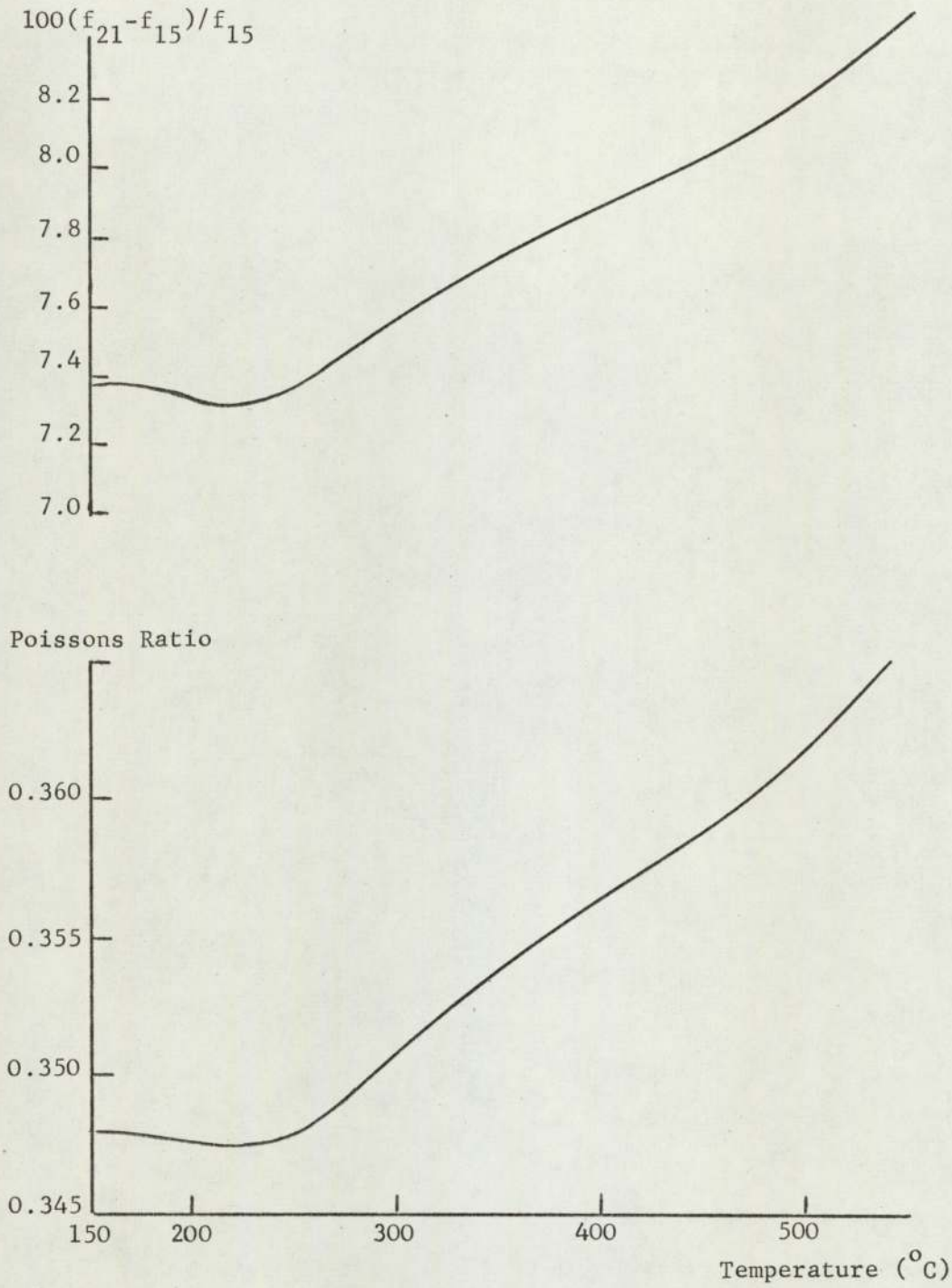

Fig.3.4.10

Resultant curves from second test on copper.
Defining the temperature coefficient as $d\sigma/dT$ (where T is temperature) gives $d\sigma/dT = 5.6 \times 10^{-5}/^{o}C$ over the range 250° C to 500° C.

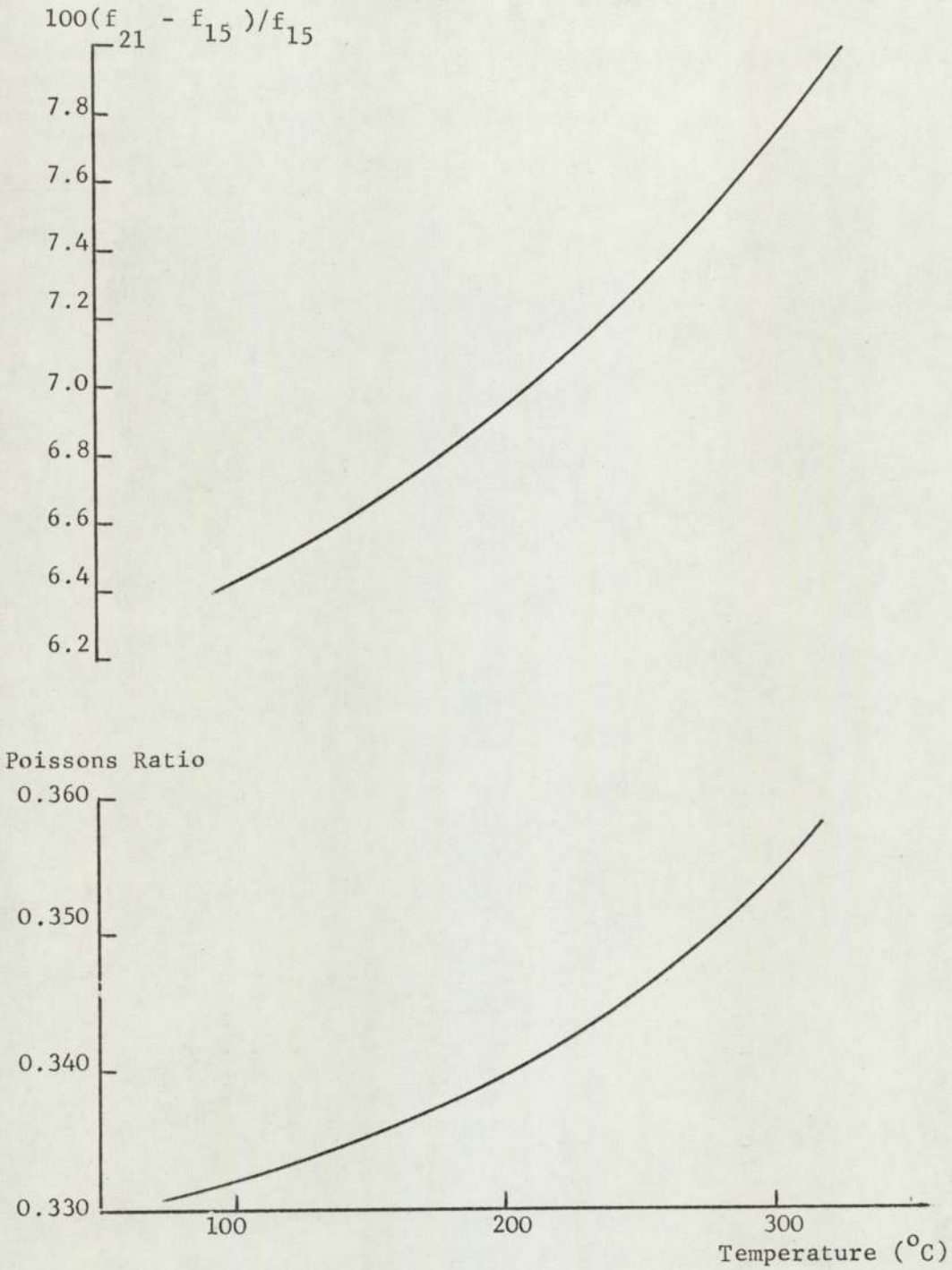

Fig.3.4.11

Resultant curves from first test on aluminium.
Temperature coefficient d σ/dT = 11.0 x 10^{-5}/°C.

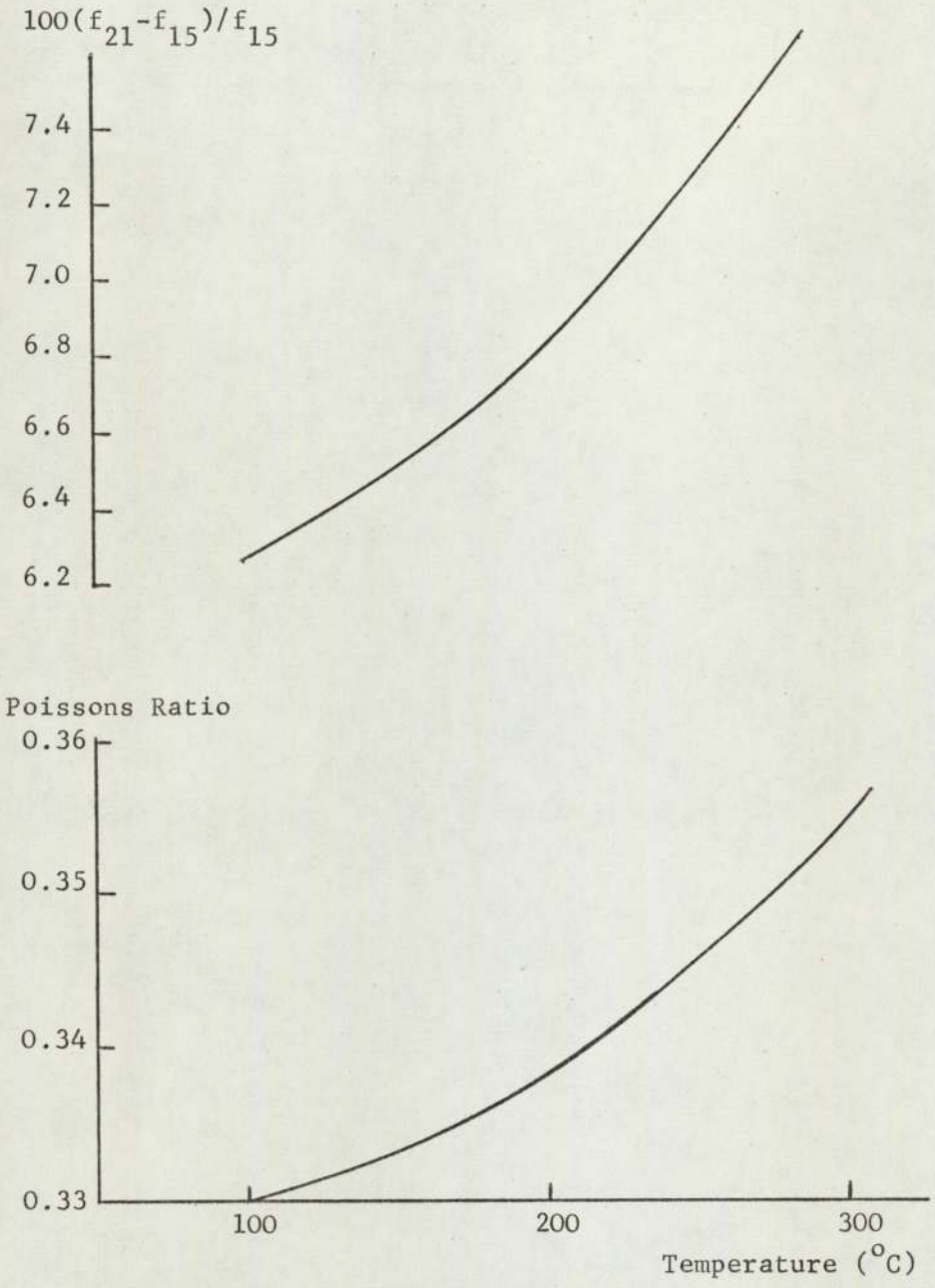

Fig.3.4.12

Resultant curves from second test on aluminium. Temperature coefficient, $d\sigma/dT = 11.5 \times 10^{-5}/^{o}C$. The temperature coefficient given is an average over the range of the graph. However the data was good enough here to allow the curvature to be taken from this graph. $d\sigma/dT$ varies from $7.5 \times 10^{-5}/^{o}C$ to $15.5 \times 10^{-5}/^{o}C$ over the range 150 ^{o}C to 250^{o}C.

4. DISK/RING RESONATORS

4.1 Introduction

The vibrations of thin rings, both in the plane of the ring and perpendicular to it are readily analysible and have been studied by many authors (Love 1927, Timoshenko 1959). This work deals with the inplane vibrations. Buckens (1950) takes into account shear stresses but the resulting theory is difficult to apply, and approximations in the theory become invalid when the relative radial thickness is large.

A study of Hollands analysis (Appendix A.3.1) of disks indicated that the general case of the ring, though of greatly increased complexity as it involves a second boundary, was soluable within the limits of algebraic effort, and computational cost. The resulting theoretical values are applicable to rings with rectangular cross-section where the ratio of out-of-plane thickness to wavelength is small.

4.2 Existing Theory

The frequency equations for the thin ring are easily derived by considering an elemental portion. Here it is sufficient to quote the results obtained by Love 1927. The frequency equation for the simple radial mode is,

$$\omega^2 = \frac{E}{\rho} \frac{1}{a_1^2} \qquad 4.2.1$$

where a_1 is the mean radius of the ring.

The frequency equation for other modes of vibration in the plane of the ring is,

$$\omega^2 = \frac{E}{\rho} \frac{K^2}{a_1^4} \frac{n^2(n^2-1)^2}{n^2+1} \qquad 4.2.2$$

where K is the radius of gyration of the cross-sectional area, and n = 2,3,4 etc.

The modes will be referred to by the notation used for disks so that the simple radial mode (equation 4.2.1) is (1,R) and the modes of equation 4.2.2 are (1,2), (1,3), (1,4) etc. Clearly all disk modes of type (2,n), (3,n) etc. and of type (1,T), (2,T) etc. which have nodal circules, approach infinite frequency for the thin ring. Fig. 4.2.1 shows calculated frequencies for a steel ring.

4.2 Analysis of Disk with Central Hole

The derivation from first principles is given in Appendix A.3.1 obtaining the general solutions, A.3.1.28 and A.3.1.29 repeated here.

$$\triangle = \left[A_7 J_n(hr) + A_8 Y_n(hr)\right] \cos n\theta \cos \omega t \qquad 4.3.1$$

$$\bar{\omega} = \left[A_9 J_n(kr) + A_{10} Y_n(kr)\right] \sin n\theta \cos \omega t \qquad 4.3.2$$

However the boundary conditions for a disk of radius a, with a central hole radius b, are now as follows

$$T_{rr} = 0 \quad \text{at } r = a \qquad 4.3.3$$

$$T_{rr} = 0 \quad \text{at } r = b \qquad 4.3.4$$

$$T_{r\theta} = 0 \quad \text{at } r = a \qquad 4.3.5$$

$$T_{r\theta} = 0 \quad \text{at } r = b \qquad 4.3.6$$

The equations for the stress resultants (A.3.1.18, A.3.1.19) repeated here are,

$$T_{rr} = \frac{E}{(1-\sigma^2)}\left[\frac{\partial \xi_r}{\partial r} + \sigma\left(\frac{\xi_r}{r} + \frac{1}{r}\frac{\partial \xi_\theta}{\partial \theta}\right)\right] \qquad 4.3.7$$

$$T_{r\theta} = \frac{E}{(1+\sigma)2}\left[\frac{\partial \xi_\theta}{\partial r} - \frac{\xi_\theta}{r} + \frac{1}{r}\frac{\partial \xi_r}{\partial \theta}\right] \qquad 4.3.8$$

and the equations of motion (A.3.1.30, A.3.1.31) are,

$$\frac{\partial \Delta}{\partial r} - (1-\sigma)\frac{1}{r}\frac{\partial \bar{\omega}}{\partial \theta} = -\rho\omega^2\frac{(1-\sigma^2)}{E}\xi_r \qquad 4.3.9$$

$$(1-\sigma)\frac{\partial \bar{\omega}}{\partial r} + \frac{1}{r}\frac{\partial \Delta}{\partial \theta} = -\rho\omega^2\frac{(1-\sigma^2)}{E}\xi_\theta \qquad 4.3.10$$

Substituting into 4.3.9 and 4.3.10 with the general solutions 4.3.1 and 4.3.2 gives the form for the solutions of ξ_r and ξ_θ.

$$\xi_r = \left[A_{13}\frac{\partial J_n(hr)}{\partial r} + nA_{14}\frac{J_n(kr)}{r} + A_{15}\frac{\partial Y_n(hr)}{\partial r} + nA_{16}\frac{Y_n(kr)}{r}\right]\cos n\theta \cos\omega t \qquad 4.3.11$$

$$\xi_\theta = -\left[nA_{13}\frac{J_n(hr)}{r} + A_{14}\frac{\partial J_n(kr)}{\partial r} + nA_{15}\frac{Y_n(hr)}{r} + A_{16}\frac{\partial Y_n(kr)}{\partial r}\right]\sin n\theta \cos\omega t \qquad 4.3.12$$

For radial modes ξ_θ vanishes and ξ_r is independent of θ. This occurs when n=0. Equation 4.3.7 and boundary conditions 4.3.3 and 4.3.4 give,

$$\left[\frac{\partial \xi_r}{\partial r} + \sigma\left(\frac{\xi_r}{r} + \frac{1}{r}\frac{\partial \xi_\theta}{\partial \theta}\right)\right]_{r=a} = 0 \qquad 4.3.13$$

and

$$\left[\frac{\partial \xi_r}{\partial r} + \sigma\left(\frac{\xi_r}{r} + \frac{1}{r}\frac{\partial \xi_\theta}{\partial \theta}\right)\right]_{r=b} = 0 \qquad 4.3.14$$

Substituting into 4.3.13 and 4.3.14 with 4.3.11 yields,

$$\frac{A_{13}}{A_{15}} = -\left[\frac{d^2Y_0(ha)}{da^2} + \frac{\sigma}{a}\frac{dY_0(ha)}{da}\right] \Big/ \left[\frac{d^2J_0(ha)}{da^2} + \frac{\sigma}{a}\frac{dJ_0(ha)}{da}\right] \qquad 4.3.15$$

and

$$\frac{A_{13}}{A_{15}} = -\left[\frac{d^2Y_0(hb)}{db^2} + \frac{\sigma}{a}\frac{dY_0(hb)}{db}\right] \Big/ \left[\frac{d^2J_0(hb)}{db^2} + \frac{\sigma}{b}\frac{dJ_0(hb)}{db}\right] \qquad 4.3.16$$

Equation 4.3.15 becomes,

$$\frac{A_{13}}{A_{15}} = -\left[\frac{dY_1(ha)}{da} + \frac{\sigma}{a}Y_1(ha)\right] \Big/ \left[\frac{dJ_1(ha)}{da} + \frac{\sigma}{a}J_1(ha)\right] \qquad 4.3.17$$

and equation 4.3.16 becomes

$$\frac{A_{13}}{A_{15}} = -\left[\frac{dY_1(hb)}{db} + \frac{\sigma}{b}Y_1(hb)\right] \Big/ \left[\frac{dJ_1(hb)}{db} + \frac{\sigma}{b}J_1(hb)\right] \qquad 4.3.18$$

The radial modes frequency equation is formed by eliminating A_{13}/A_{15}.

Now letting K=ha, L=hb, Θ = k/h and also defining, $M_n(\Lambda) = \Lambda J_{n-1}(\Lambda)/J_n(\Lambda)$ and, $N_n(\Lambda) = \Lambda Y_{n-1}(\Lambda)/Y_n(\Lambda)$, equations, 4.3.17 and 4.3.18 become,

$$\frac{A_{13}}{A_{15}} = -\frac{KY_0(K)-(1-\sigma)Y_1(K)}{KJ_0(K)-(1-\sigma)J_1(K)} \qquad 4.3.19$$

$$\frac{A_{13}}{A_{15}} = -\frac{LY_0(L)-(1-\sigma)Y_1(L)}{LJ_0(L)-(1-\sigma)J_1(L)} \qquad 4.3.20$$

Now if Φ =b/a then L=ΦK, and equations 4.3.19 and 4.3.20 form a single frequency equation, giving solutions in K for particular values of σ, and Φ.

The frequency equation for compound modes becomes cumbersome, so matrix equations will be used to simplify the presentation.

Boundary conditions 4.3.5 and 4.3.6 with equation 4.3.8 give,

$$\left[\frac{\partial \xi_\theta}{\partial r} - \frac{\xi_\theta}{r} + \frac{1}{r}\frac{\partial \xi_r}{\partial \theta}\right]_{r=a} = 0 \qquad 4.3.21$$

and

$$\left[\frac{\partial \xi_\theta}{\partial r} - \frac{\xi_\theta}{r} + \frac{1}{r}\frac{\partial \xi_r}{\partial \theta}\right]_{r=b} = 0 \qquad 4.3.22$$

Now substituting into equations 4.3.13, 4.3.14, 4.3.21 and 4.3.22 with the results 4.3.11 and 4.3.12 gives four equations which can be written.

$$\begin{bmatrix} a_{11} & a_{12} & a_{13} & a_{14} \\ a_{21} & a_{22} & a_{23} & a_{24} \\ a_{31} & a_{32} & a_{33} & a_{34} \\ a_{41} & a_{42} & a_{43} & a_{44} \end{bmatrix} \begin{bmatrix} A_{13} \\ A_{14} \\ A_{15} \\ A_{16} \end{bmatrix} = \begin{bmatrix} 0 \\ 0 \\ 0 \\ 0 \end{bmatrix} \qquad 4.3.23$$

where,

$$a_{11} = -J_n(K)\left[(K\Theta)^2/2 - n(n+1) + M_n(K)\right]\left[2/a^2\,\Theta^2\right]$$

$$a_{12} = J_n(K\Theta)n\left[M_n(K\Theta) - (n+1)\right]\left[2/a^2\,\Theta^2\right]$$

$$a_{13} = -Y_n(K)\left[(K\Theta)^2/2 - n(n+1) + N_n(K)\right]\left[2/a^2\,\Theta^2\right]$$

$$a_{14} = Y_n(K\Theta)n\left[N_n(K\Theta) - (n+1)\right]\left[2/a^2\,\Theta^2\right]$$

$$a_{21} = -J_n(L)\left[(L\Theta)^2/2 - n(n+1) + M_n(L)\right]\left[2/b^2\,\Theta^2\right]$$

$$a_{22} = J_n(L\Theta)n\left[M_n(L\Theta) - (n+1)\right]\left[2/b^2\,\Theta^2\right]$$

$$a_{23} = -Y_n(L)\left[(L\Theta)^2/2 - n(n+1) + N_n(L)\right]\left[2/b^2\,\Theta^2\right]$$

$$a_{24} = Y_n(L\Theta)n\left[N_n(L\Theta) - (n+1)\right]\left[2/b^2\,\Theta^2\right]$$

$$a_{31} = -J_n(K)2n\left[M_n(K)-(n+1)\right]\left[1/a^2\right]$$

$$a_{32} = J_n(K\,\Theta)\left[2M_n(K\Theta)+(K\Theta)^2-2n(n+1)\right]\left[1/a^2\right]$$

$$a_{33} = -Y_n(K)2n\left[N_n(K)-(n+1)\right]\left[1/a^2\right]$$

$$a_{34} = Y_n(K\,\Theta)\left[2N_n(K\Theta)+(K\Theta)^2-2n(n+1)\right]\left[1/a^2\right]$$

$$a_{41} = -J_n(L)2n\left[M_n(L)-(n+1)\right]\left[1/b^2\right]$$

$$a_{42} = J_n(L\,\Theta)\left[2M_n(L\Theta)+(L\Theta)^2-2n(n+1)\right]\left[1/b^2\right]$$

$$a_{43} = -Y_n(L)2n\left[N_n(L)-(n+1)\right]\left[1/b^2\right]$$

$$a_{44} = Y_n(L\,\Theta)\left[2N_n(L\Theta)+(L\Theta)^2-2n(n+1)\right]\left[1/b^2\right]$$

Eliminating the arbitary constants A_{13}, A_{14}, A_{15} and A_{16} the frequency equation is formed thus,

$$\begin{vmatrix} a_{11} & a_{12} & a_{13} & a_{14} \\ a_{21} & a_{22} & a_{23} & a_{24} \\ a_{32} & a_{32} & a_{33} & a_{34} \\ a_{41} & a_{42} & a_{43} & a_{44} \end{vmatrix} = 0 \qquad 4.3.24$$

It will be noticed that as the last factor in each of the a_{1q} $(q=1,2,3,4)$ is $2/a^2\Theta^2$ this can be taken from row one as a common factor. Similarly the other three rows also have a common factor.

The frequency equations for radial and compound modes have been solved. Tabulations of K values for Φ from 0.00 to 1.00 and Poissons Ratio from 0.00 to 1.00 are available. Values are tabulated to four decimal places so that local curve fitting can be used to obtain intermediate points. A condensed form of these tables is given in Appendix A.4.3 of this thesis.

As stated in section 3, Poissons Ratio is given for values above 0.5 to facilitate the investigation of orthotropic materials.

4.4 Comparison with Experiment

The specimen was a mild steel disk with a diameter of three inches. The central hole was machined in steps until a radially-thin ring was formed. At each step the family of resonances was investigated by the Echo Method of section 2. The raw data from the experiment is given in table 4.4.1. Theoretical values of frequency have been calculated using the tabulated values of K and the formula,

$$\omega = K/\left[a\sqrt{\rho\,(1-\sigma^2)/E} \right] \qquad 4.4.1$$

The physical properties of the specimen were taken to be,

$a = 1.5$ inch $= 0.0381$ m

$\rho = 7.9$ g/ml $= 7.9 \times 10^3$ kg/m^3

$\sigma = 0.30$

$E = 21 \times 10^{11}$ dyne/cm^2 $= 2.1 \times 10^{11}$ N/m^2

The calculated curves are shown in Fig. 4.4.2. The experimental curves obtained from Table 4.4.1 coincide precisely with these.

4.5 Discussion

The radial mode (1,R) is an important one for the thin ring because the stress is uniform over the whole of the ring, and is used to investigate amplitude sensitive effects. Fig.4.4.2 shows that the thin ring approximate frequency equation 4.2.1 is still quite accurate as Φ decreases. The radial mode equation 4.2.1 can be rewritten,

$$\omega_{ring} = \frac{V_L}{a}\,\frac{2}{(1+\Phi)} \qquad 4.5.1$$

where $V_L = \sqrt{(E/\rho)}$ and a is the outside radius. The actual frequency, ω can be found using equation 4.4.1; rewritten here,

$$\omega = \frac{V_L}{a}\,\frac{K}{(1-\sigma^2)^{1/2}} \qquad 4.5.2$$

K is obtained from the tables of Appendix A.4.3, and is a function of σ and Φ . Now dividing equation 4.5.2 by equation 4.5.1,

$$\omega/\omega_{ring} = \frac{1}{2} K(1 + \Phi)/(1 - \sigma^2)^{1/2} \qquad 4.5.3$$

Equation 4.5.3 was used to investigate the departure from the thin ring radial mode frequency equation as a function of σ and Φ , and the resultant curves are shown in Fig.4.5.1. An interesting point is that for a Poisson's Ratio of 0.18 a disk fits the thin ring frequency equation perfectly. Fig.4.5.2 shows a direct plot of the radial mode K values, K_{1R}. As Φ increases the curves approach a curve due to the function $(1 - \sigma^2)^{1/2}$. This verifies that ω is independent of σ for very thin rings, as assumed by the simple equation 4.5.1.

The in-plane flexural modes are examined in an exactly similar way. Equation 4.2.2 becomes,

$$\omega_{ring} = \frac{V_L}{a} \frac{2}{\sqrt{3}} \frac{(1 - \Phi)}{(1 + \Phi)^2} (f(n))^{1/2} \qquad 4.5.4$$

where

$$f(n) = n^2 (n^2 - 1)^2/(n^2 + 1)$$

Dividing equation 4.5.2 by equation 4.5.4

$$\omega/\omega_{ring} = \frac{2}{\sqrt{3}} \frac{K}{(1 - \sigma^2)^{1/2}} \frac{(1+\Phi)^2}{(1 - \Phi)} (f(n))^{-1/2} \qquad 4.5.5$$

Curves resulting from equation 4.5.5 are shown in Figs. 4.5.3 and 4.5.4. The error produced by using the simple equation 4.2.2 is generally much larger than for the case of the radial mode.

Approximate methods are available for the determination of resonant frequencies, such as that due to Rayleigh and Ritz (see Bishop/Gladwell/Michaelson 1965). However, and advantage of the high accuracy frequency equation solved in Section 4.3 is that the effect on frequency of small changes in any parameter can be determined.

The digital computer gives the possibility of solving many associated boundary value problems. However obtaining a set of solutions is as much a matter of economics as of mathematical skill. On the I.C.L. 1900E computer, a disk program was using 5p worth of time per K value found. Solutions for ten modes with Poisson's Ratio from 0.00 to 1.00 in 0.05 steps therefore cost £10. The program to find K values for the disk with a central hole, used 10p worth of time per K value. For Φ from 0.00 to 1.00 in 0.1 steps and Poisson's Ratio as for disks, the resultant cost for ten modes was £200. Introducing damped or pinned edges to the disk with the hole would produce problems with the same order of complexity which could also be solved for 10p per K value.

Problems of greater complexity could also be solved. Consider, for example, accounting for ring thickness. The cost per value with the increased complexity would be about 20p per value. However the cost of a comprehensive set of results would be greatly elevated by the requirement for a number of steps in the new thickness parameter. In this case it would probably be necessary to limit the results to a small set applicable to a particular specimen being studied. Further results would then be obtained as the need arose.

To summarise, from the experience gained in dealing with the ring, it is feasible to obtain a rough estimate of the effort and cost of solving a number of associated problems.

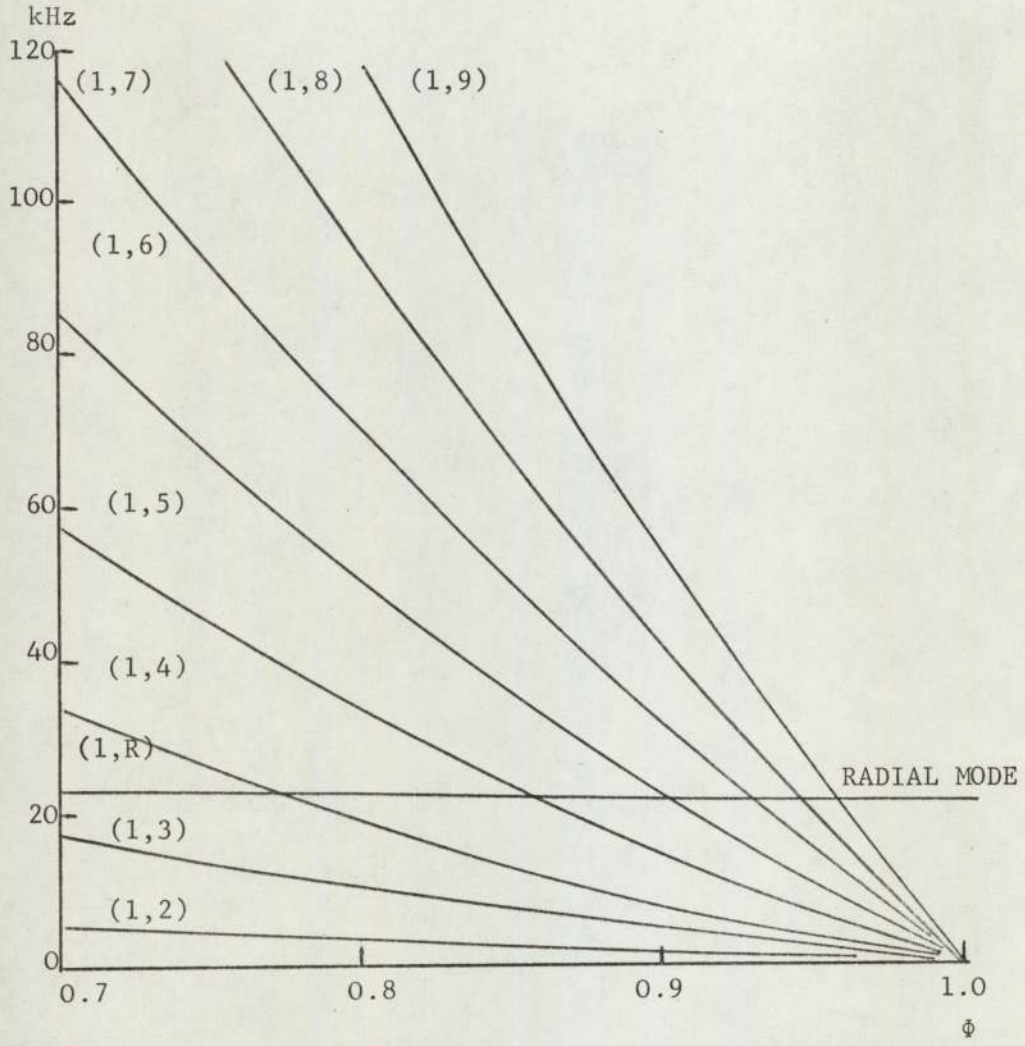

Fig.4.2.1

A typical family of mode frequencies calculated from the classical thin ring theory. Φ is the ratio of internal to external diameters. Notice that for the infinitely thin ring (Φ = 1.0) the in-plane flexural modes have zero frequency but the radial mode shown has finite frequency.

MODE	NO HOLE	¼ INCH HOLE Φ =0.0833	½ INCH HOLE Φ = 0.1667	¾ INCH HOLE Φ =0.2500	1 INCH HOLE Φ =0.3333
1,R	45.81	44.83	41.84	38.19	34.84
1,1	36.67	36.90	37.25	38.19	38.10
2,1	79.98	81.79	85.33	-----	-----
1,2	31.55	30.22	26.64	22.39	18.76
1,3	48.09	48.14	47.71	44.93	40.74
1,4	63.21	63.24	63.13	62.43	59.86
1,5	77.24	77.25	77.26	77.27	77.31
1,6	89.07	89.06	89.82	89.97	89.77
1,7	103.02	102.96	102.83	102.95	102.99
1,8	115.95	115.63	115.43	115.71	115.84
1,9	128.19	128.12	127.91	128.27	128.25

MODE	1¼ INCH HOLE Φ=0.4167	1½ INCH HOLE Φ=0.5000	1¾ INCH HOLE Φ =0.5833	2 INCH HOLE Φ = 0.6667	2¼ INCH HOLE Φ =0.7500
1,R	32.23	29.86	27.88	26.21	24.78
1,1	38.11	37.70	36.80	35.64	34.37
2,1	-----	-----	-----	-----	-----
1,2	15.68	12.68	9.97	7.46	5.25
1,3	35.64	30.09	24.53	19.30	14.10
1,4	55.15	48.53	41.24	33.40	25.32
1,5	72.94	66.78	58.24	48.64	38.15
1,6	88.48	84.47	75.85	64.64	51.90
1,7	102.51	99.59	91.90	81.12	66.48
1,8	115.61	113.98	108.08	96.75	81.57
1,9	128.15	127.41	123.28	112.53	96.38

MODE	2 3/8 INCH HOLE Φ =0.7917	2½ INCH HOLE Φ =0.8333	2 9/16 INCH HOLE Φ =0.8540	2 5/8 INCH HOLE Φ =0.8750	2¾ INCH HOLE Φ =0.9167
1,R	24.15	23.55	23.33	23.05	22.53
1,1	33.67	32.99	32.68	32.35	31.70
2,1	-----	-----	-----	-----	-----
1,2	4.20	2.98	2.56	2.17	2.0
1,3	11.48	8.93	7.80	6.46	5.1
1,4	20.98	16.59	14.51	12.23	7.81
1,5	32.10	25.86	22.76	19.40	12.71
1,6	44.60	36.46	32.38	27.73	18.41
1,7	57.67	47.99	43.01	37.14	25.03
1,8	71.63	60.36	54.32	47.32	32.46
1,9	86.22	73.41	66.52	58.40	40.76

TABLE 4.4.1

The observed data from the mild steel ring is shown. These values can be compared with the curves of Fig.4.4.2. The agreement is to the limit of experimental accuracy.

Fig.4.4.2

The theoretical curves for the mild steel ring calculated from the data given in Appendix A.4.3 are shown in solid lines. The points from Table 4.4.1 are not plotted as this graph is too small for any error to be detected. The dotted lines indicate the frequency predicted by the thin ring theory of equations 4.2.1 and 4.2.2.

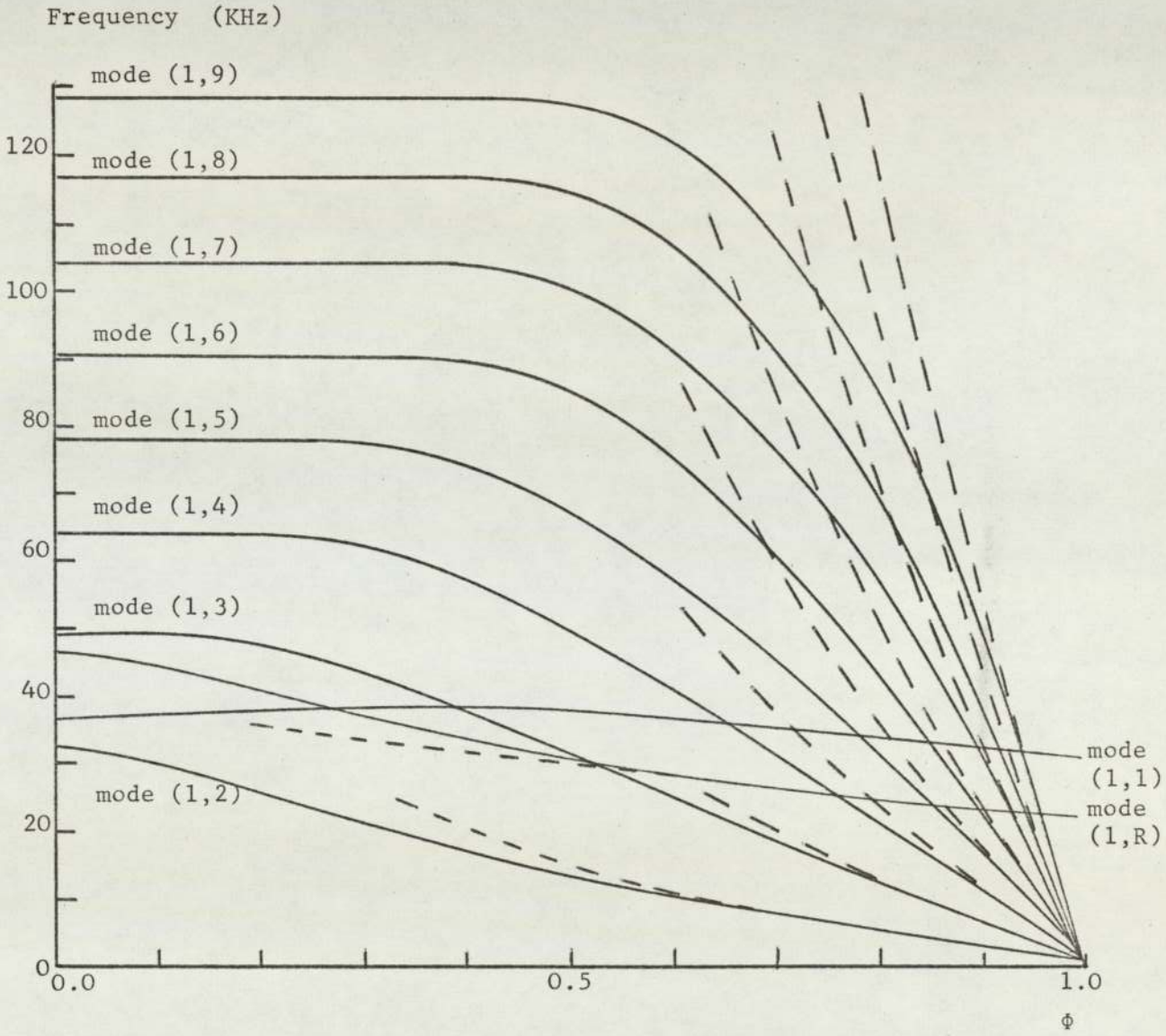

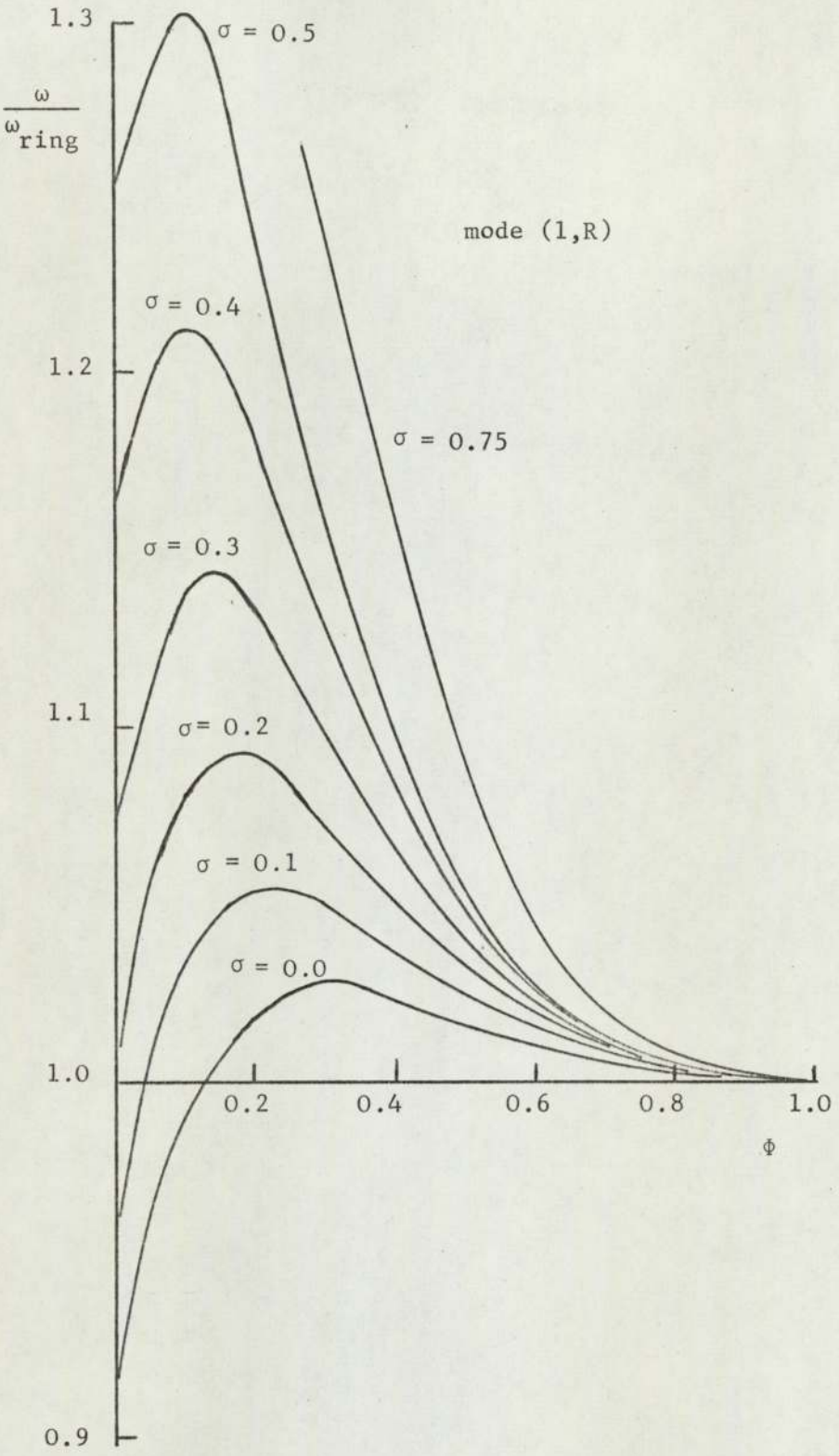

Fig. 4.5.1

This shows the deviation of the frequency predicted by the simple thin ring theory for the radial mode (1,R) over a range of σ and Φ.

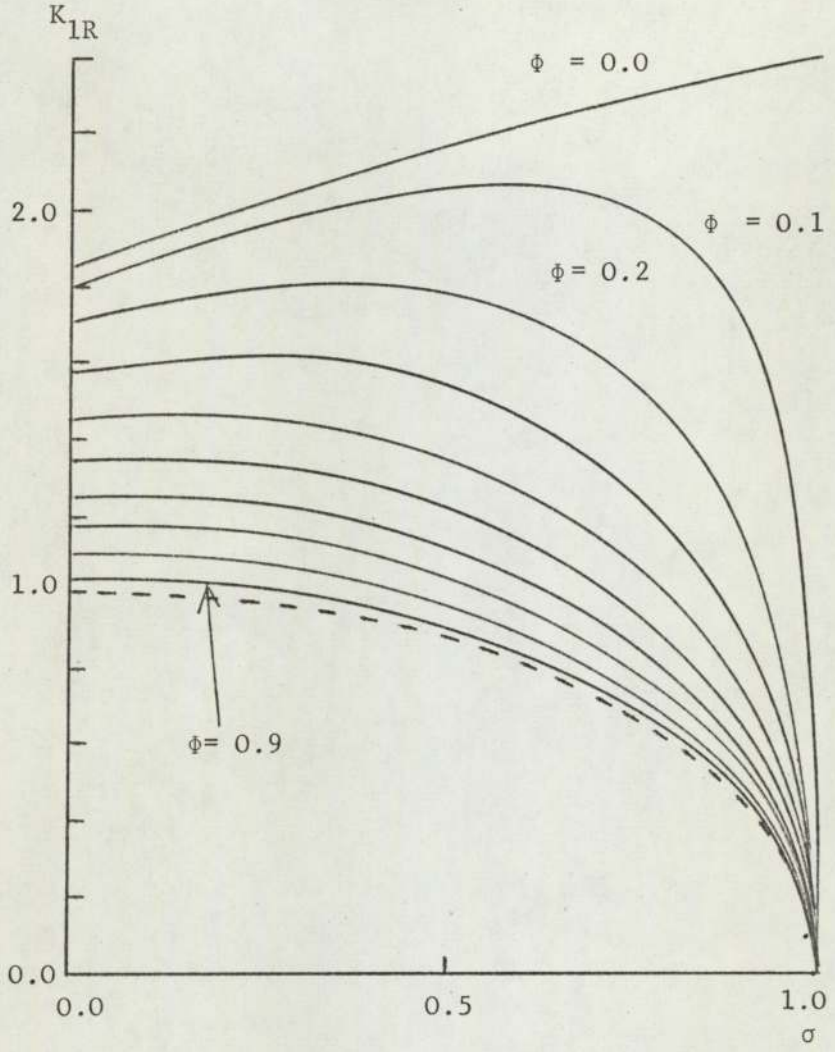

Fig.4.5.2

These graphs of K_{1R} values, show how the frequency becomes independent of Poissons Ratio for an infinitely thin ring. A graph of $(1 - \sigma^2)^{1/2}$ against σ is shown dotted. Notice that K = 0 when σ = 1.0 and the plate modulus is infinite.

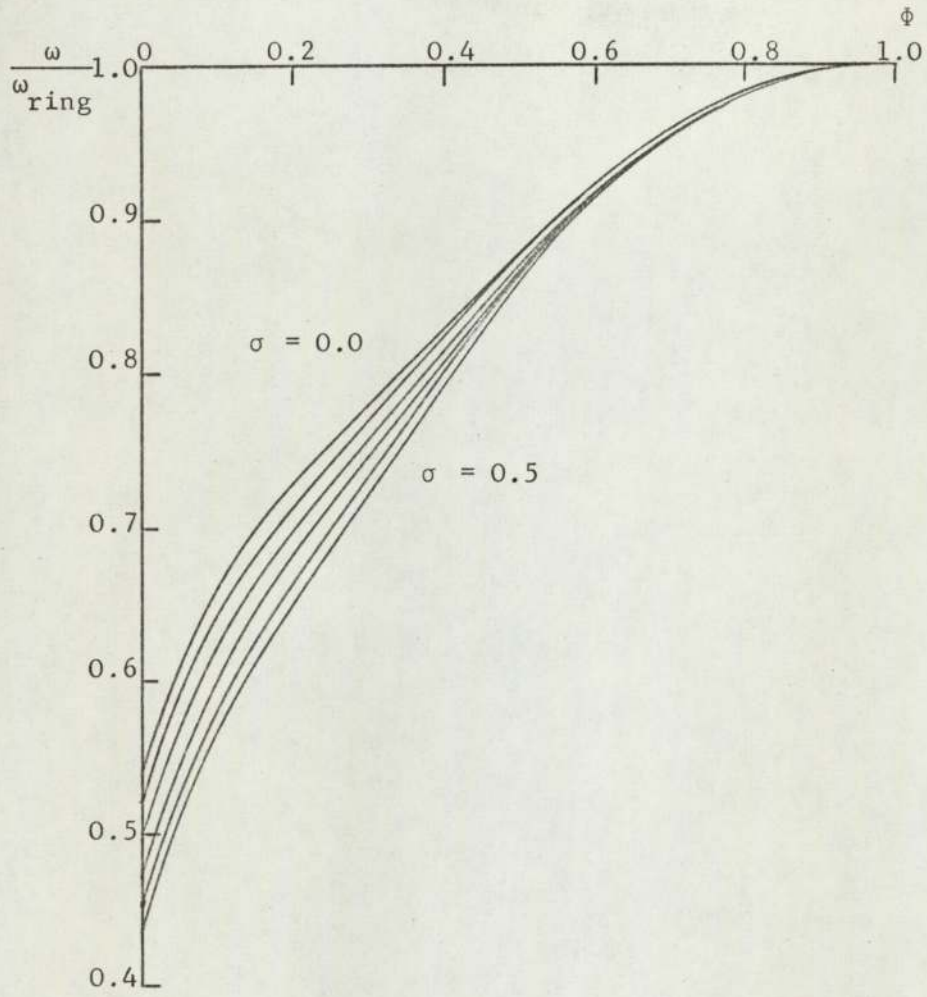

Fig.4.5.3

The variation of the thin ring frequency equation for mode (1,2) is shown. All modes of type (1,n) with $n \geq 2$ will have similar dependence on σ and Φ .

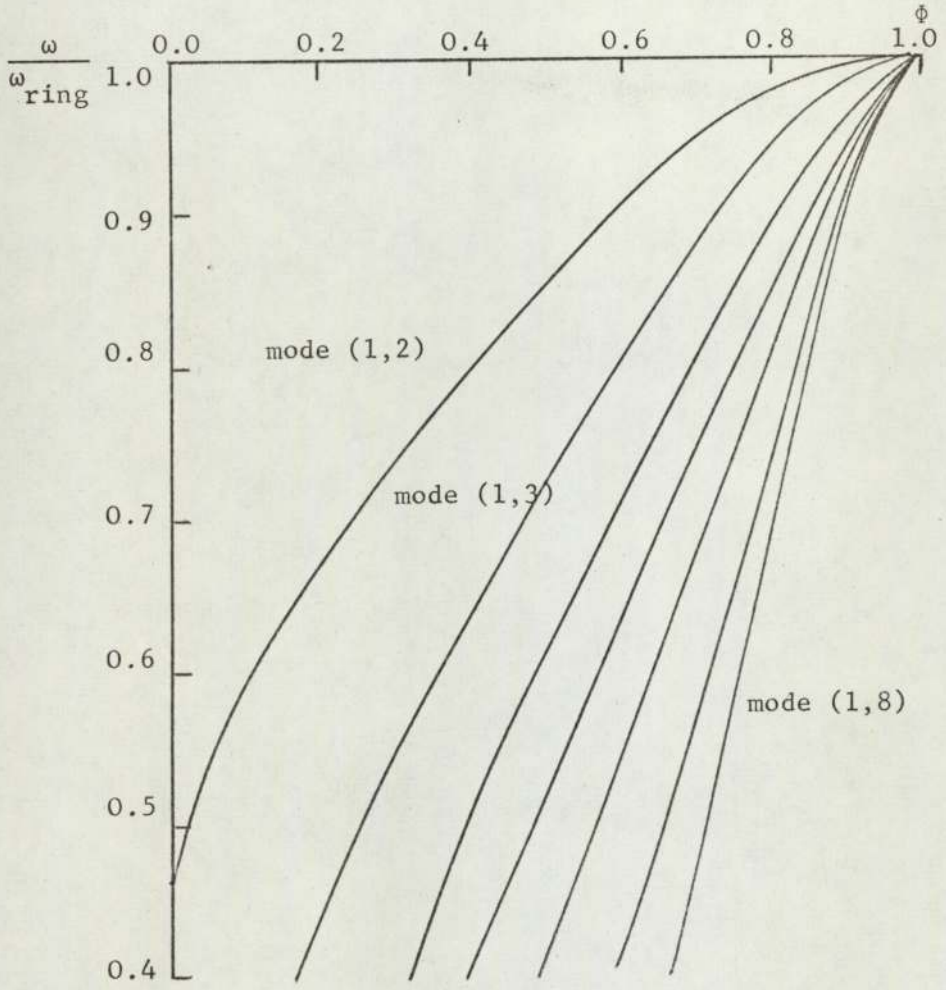

Fig.4.5.4

The variation of the thin ring frequency equation is shown. For the higher order modes the radial thickness to wavelength ratio becomes larger, and hence the error produced is larger.

5. INTERNAL FRICTION

5.1 Introduction

The attenuation of acoustic waves was first treated by Stokes 1845 who considered the effect of viscosity on the transmission of sound through gases. Navier added the second transport phenomenon term, thermal conductivity, which resulted in the classical Navier-Stokes equation (section 2.2, equation 2.2.1). An enormous number of other loss mechanisms occur, particularly in solids, and these are studied for the information they give of molecular effects in liquids and gases and lattice and grain boundary effects in solids, where they are classified under the general heading of Internal Friction (see Fig. 5.1.1). The H term in equation 2.2.1 expresses the total internal friction. This is a volume effect and is therefore independent of the shape of the material being studied. In general the internal friction varies strongly with temperature and to a much smaller extent with frequency. Considerable success has been achieved in identifying the sources, particularly by Bordoni 1947, Snoek 1941, Granato 1956 and Powers 1959.

The measurement of internal friction over a wide range of temperature and frequency is of current importance and a number of methods are available, typically the torsional pendulum (Kê 1947) and the single pulse echo system used by Bell 1957 and Lynworth 1967. This single pulse traverses a fixed length of specimen, held at a fixed uniform temperature. From the attenuation of this pulse, the internal friction shown by the specimen material can be evaluated, for that temperature.

The method described here is a resonance method based on an acoustic transmission line. An advantage of this system is that the resonator which terminates the line can, for example, be a tuning fork, where only a physically small specimen is necessary. The excitation and return signals are as described in section 2.4. The echo decrement exponential is evaluated by measuring amplitude at two points on its envelope. From this information Q_T can be determined and then if Q_C is known Q_M (a measure of internal frction) can be derived ($Q_T^{-1}=Q_M^{-1}+Q_C^{-1}$). In this way Q_M can be determined as a function of temperature and for several frequencies (if the resonator has several resonant modes of vibration). See Fig.5.1.2.

A problem common to all transmission line methods considered so far is the evaluation of Q_C. This is often done by assuming the low temperature material loss to be negligible, and Q_C then becomes Q_T. While this is a reasonable assumption for most cases it is to some extent unsatisfactory and the multimode method described allows Q_C to be evaluated with certainty. This is an important feature of the method of measurement and is described in detail.

5.2 Multimode Method of Measuring Q_C and Q_M

A set of resonant modes for any resonator can be utilised to greater advantage if the coupling Q factor, Q_C can be calculated for each mode. This is the case for the line resonator the equations of which were derived in section 2.3. They are used here to determine Q_M for a range of frequencies and temperatures. For many materials Q_M alters little for, say, a factor of five change in frequency. In this case the multimode method is advantageous in that it increases redundancy in the readings taken.

The equations for the line resonator from section 2.3, repeated here are as follows:-

Relative steady-state echo signal amplitude,

$$E_\infty/E_0 = -(\beta - m^2\alpha)/(\beta + m^2\alpha) \qquad 5.2.1$$

Oscillations to crossover point,

$$P_m = \left[\omega_m/2\pi(\beta + m^2\alpha)\right]\ln(2\beta/(\beta - m^2\alpha)) \qquad 5.2.2$$

Q relationships,

$$Q_{Cm} = \omega_m/2\beta \qquad 5.2.3$$

$$Q_{Mm} = \omega_m/2m^2\alpha \qquad 5.2.4$$

$$Q_{Tm} = \omega_m/2(\beta + m^2\alpha) \qquad 5.2.5$$

Using the Q relationships E_∞/E_0 and P_m can be expressed in terms of Q_{Cm} and Q_{Mm}.

$$E_\infty/E_0 = -(1-Q_{Cm}/Q_{Mm})/(1+Q_{Cm}/Q_{Mm}) \qquad 5.2.6$$

$$P_m = \frac{Q_{Cm}}{\pi(1+Q_{Cm}/Q_{Mm})}\ln(2/(1-Q_{Cm}/Q_{Mm})) \qquad 5.2.7$$

Let $P'_m = P_m/m$; then,

$$P'_m = \frac{Q_{C1}}{\pi(1+Q_{Cm}/Q_{Mm})}\ln(2/(1-Q_{Cm}/Q_{Mm})) \qquad 5.2.8$$

because $Q_{Cm} = \omega_m/2\beta = m\omega_1/2\beta = mQ_{C1}$

From the echo observations E_∞/E_0, P_m, and Q_{Tm} can be determined directly for any particular mode.

E_∞/E_0 is in general not used numerically because E_0 cannot be observed very accurately. This occurs because the echo signal has maximum rate of change of envelope amplitude at the beginning of the echo, and because of the finite bandwidth of the magnetostrictive launcher, the true envelope amplitude takes one or two oscillations to be established.

However E_∞/E_0 does serve as a direct qualitative indication of Q_M (see Fig. 5.2.1). One accurate value can be obtained when $E_\infty/E_0 = 0$ (i.e. $Q_{Cm}=Q_{Mm}$) because $E_\infty=0$ at this point and E_0 need not be measured.

Another measure of Q_M observed from the echo is P_m, the number of oscillations to the crossover point for mode m. The form of equation 5.2.8 immediately suggests a useful approach. If m=0 then from equation 5.2.4, $Q_{Mm} = \infty$. Equation 5.2.8 then becomes,

$$P_0' = (Q_{C1}/\pi)\ \ln 2 \qquad 5.2.9$$

m=0 (where ω_0 would be zero) is not a physically realisable condition but it can be deduced by extrapolation. If a graph is plotted from experimental P_m' values for m=1,2,3 etc., this graph can then be extrapolated to m=0 to give a value P_0' from which Q_{C1} can be directly calculated.

Let $mQ_{C1}Q_{Mm}^{-1} = h_m$; then equation 5.2.8 becomes,

$$P_m' = \frac{Q_{C1}}{(1+h_m)}\ \ln(2/(1-h_m)) \qquad 5.2.10$$

therefore

$$P_m'/P_0' = \frac{1}{(1+h_m)}\ \frac{\ln(2/(1-h_m))}{\ln 2} \qquad 5.2.11$$

Table 5.2.2 gives pairs of values of P_m'/P_0' and h_m; Fig. 5.2.3 shows a graph of P_m'/P_0' against h_m. In practice a graph of P_m' against m can be extrapolated to give a value P_0' and then a subsequent graph of P_m'/P_0' against m can be plotted. (Fig. 5.2.4 shows a typical graph obtained from an experiment of section 5.3.) Values of P_m'/P_0' are taken from the graph and then with table 5.2.2

(or Fig. 5.2.3), h_m can be found. From P'_0, Q_{C1} is found from equation 5.2.9 then,

$$Q_{Mm} = mQ_{C1}/h_m \qquad 5.2.12$$

gives the value of Q_{Mm}.

If the dependance of Q_M on frequency is known (or determined empirically), a suitable function can be chosen and plotted against m to give a straight line graph.

The last measure of Q_M, which can be observed from the echo, is a direct evaluation of Q_{Tm}. This can be accomplished by observing two amplitudes in the echo-decrement and noting their separation interval, from which Q_{Tm} can be directly calculated.

Summarising, for the line resonator three methods to determine Q_{C1} ($Q_{Cm}=mQ_{C1}$) have been established:-

1. By direct calculation from acoustical data.

   $$Q_{Cm} = \pi\, m/\ln((\rho_2 C_2 A_2+\rho_1 C_1 A_1)/(\rho_2 C_2 A_2-\rho_1 C_1 A_1)) \qquad 5.2.13$$

   The graph of Fig. 2.5.2 (section 2.5) is based on the same equation and gives P_1 against the diameter ratio of resonator and line for values of $\rho_2 C_2/\rho_1 C_1$.

2. By extrapolation of the P'_m against m graph as previously described.

3. By elimination between the two equations containing P_m and Q_{Tm}. Using $Q_{Mm}=Q_{Tm}Q_{Cm}/(Q_{Cm}-Q_{Tm})$ to substitute in equation 5.2.7 gives

   $$Q_{Cm} = 2Q_{Tm}-2\exp(-\pi P_m/Q_{Tm}) \qquad 5.2.14$$

When the coupling has been determined by one or more of these three methods, Q_{Mm} can be found from observed values of P_m and Q_{Tm} (and E_∞/E_0 at certain points).

5.3 Experimental Work

An experiment was required that would test the multimode method in practice. An ideal material would be one which showed no variation of Q_M with frequency, and an absence of any internal friction peaks over the temperature range used. The Q_M of copper is reported (Wegel 1935) to be independent of frequency and while having the normal fall of Q_M with temperature does not have any relaxation peaks. A 99.999% pure copper rod (supplied by Johnson Matthey Metals Ltd.) was first annealed at a high temperature. Observations were then carried out over a moderate temperature range.

The choice of transmission line diameter is important. A thin wire gives a high value of P_m and determines Q_M more accurately than a low value for two reasons. First, P_m can be observed more accurately. Secondly, Q_{Mm} has a greater effect on Q_{Tm}, and hence a greater effect on P_m. However the disadvantage of a high initial value of P_m is that the temperature point where $Q_{Mm}=Q_{Cm}$ and $P_m=\infty$ is soon reached. Hence a given line size gives the optimum experiment at particular values of Q_M. The graph of Fig. 2.5.2 (section 2.5) aids choosing a line diameter. For the experiment here an initial P_1 (P_m for mode m=1) of 15 was convenient. The specimen of copper was 7 mm in diameter, so a line 1 mm in diameter was used. The specimen was cut to 63 mm long to give a fundamental frequency of about 30KHz.

The furnace constructed by J.M. Pelmore and referred to in section 3.4 of this thesis was again used for this experiment. The specimen was gradually heated and observations were taken using the first five modes of the resonator. The raw data from the experiment is given in table 5.3.1.

5.4. Discussion of Results

At room temperature P'_m against m gives the straight line graph of Fig. 5.4.1. A value of P'_0=16.5 has been taken to perform all subsequent calculations. The values of Q_{Mm}^{-1} have then been calculated for each mode in turn. The calculation process for mode m=2 is given here as an example.

Equation 5.2.9 can be written,

$$Q_{C1} = \pi P'_0/\ln 2 \qquad 5.4.1$$

Then $$Q_{C2} = 2\pi P'_0/\ln 2 \qquad 5.4.2$$

Equation 5.2.12 becomes,

$$Q_{M2}^{-1} = h_m \ln 2/(2\pi P'_0) \qquad 5.4.3$$

So using P'_0=16.5,

$$Q_{M2}^{-1} = h_m \times 0.00668 \qquad 5.4.4$$

The values of Q_{M2}^{-1} are then found as shown in table 5.4.2.

The complete results from all five modes are shown in Fig. 5.4.3

The higher order modes tend to give greater accuracy, because of the division by m in evaluating P'_m. The lower order modes however, are useful up to higher temperatures. To extend the temperature range (lower values of Q_M) the line diameter would have to be increased so that Q_{C1} (and hence P'_0) is reduced.

The results are completely consistent with the theory and give values for copper similar to those obtained by other workers. Further work by Pelmore 1974 in the comparison of various methods of measurement, has confirmed the convenience and accuracy of the multimode technique.

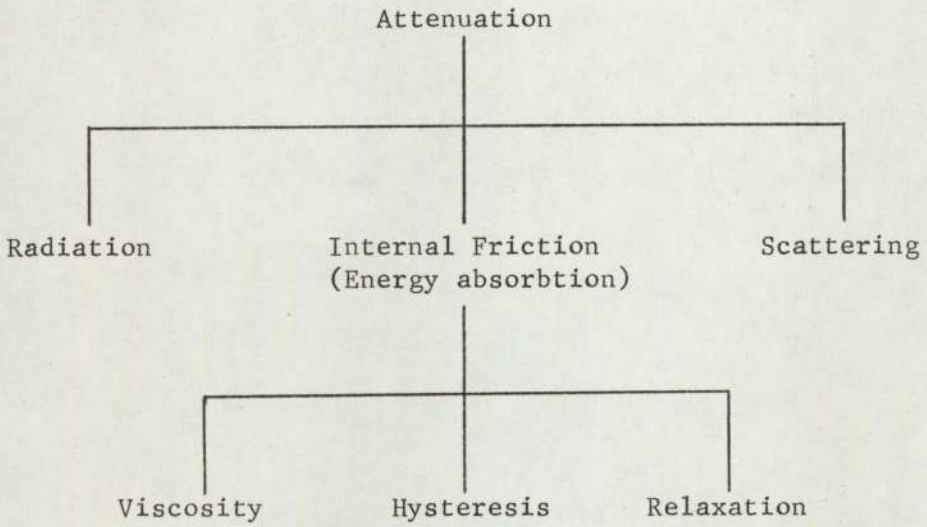

Fig.5.1.1

This shows a family tree of the terminology of energy loss effects.

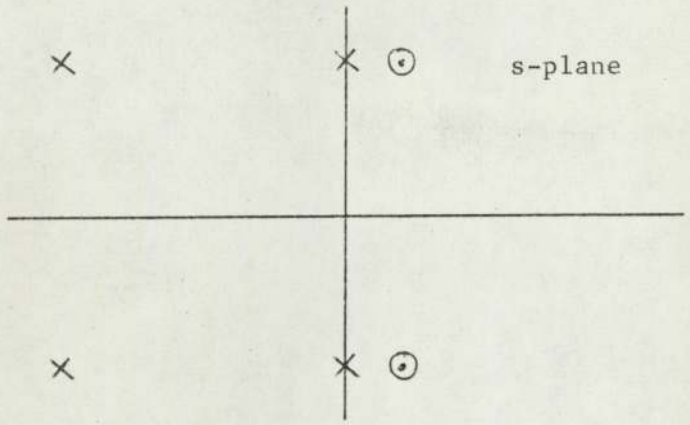

Fig.5.1.2(a)

This displacement of the poles and zeros is due to material losses. The echo corresponding to this diagram is shown below.

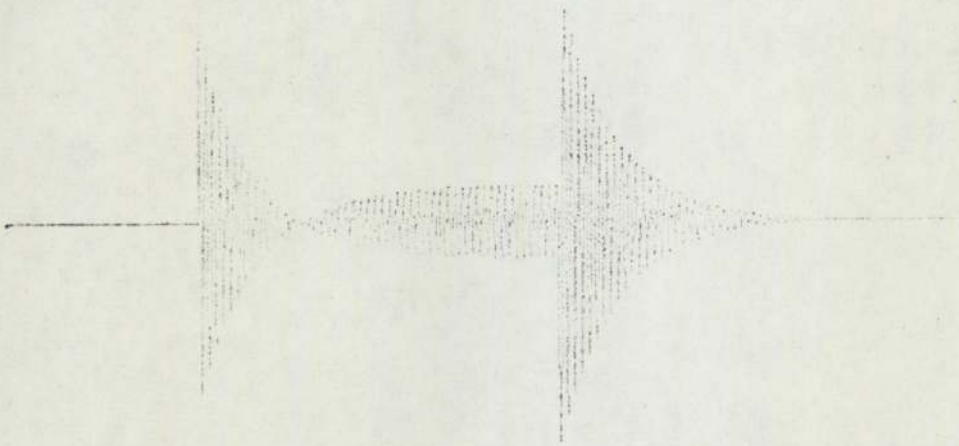

Fig.5.1.2(b)

This shows the effect of material losses in a resonator with $Q_M = 60$, $Q_C = 40$, $Q_T = 24$. The steady-state power dissipation by the internal friction losses leads to a reduction of the steady-state signal and echo-decrement amplitudes. The echo with no material loss but with the same coupling (i.e. $Q_M = \infty$, $Q_C = 40$) is shown in Fig.2.1.2.

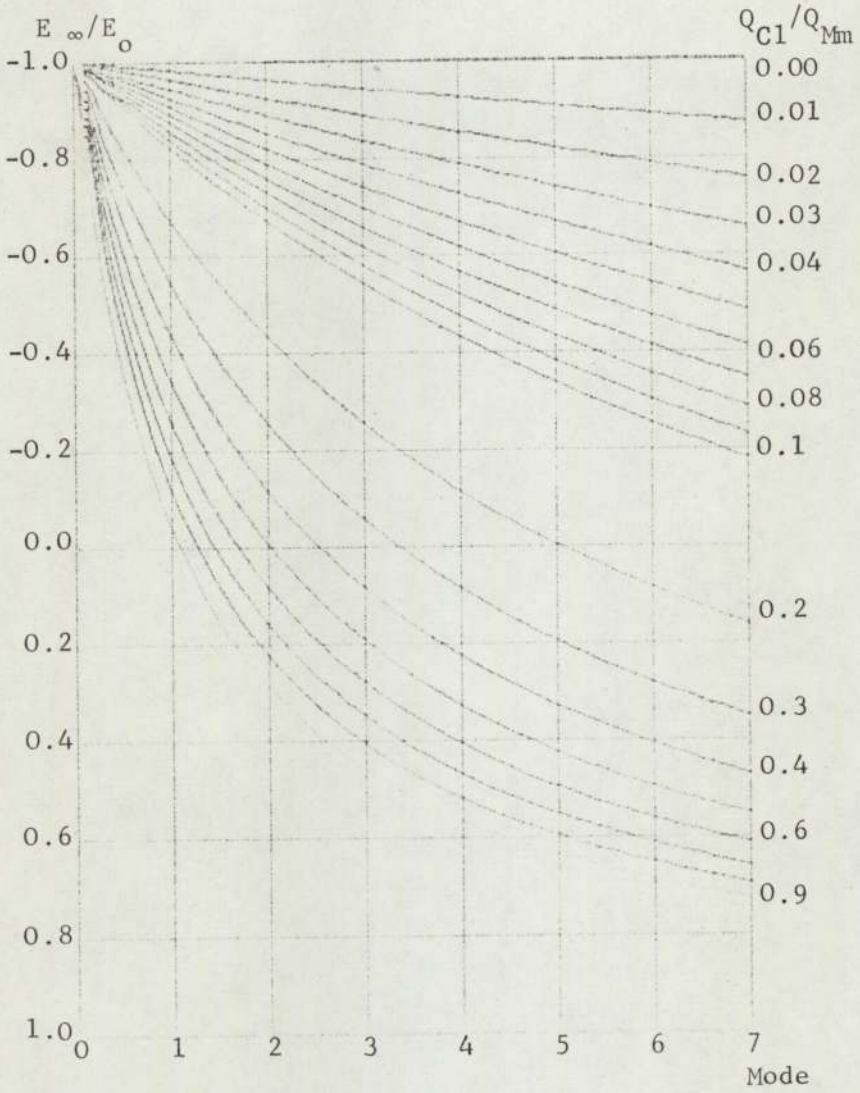

Fig.5.2.1

This gives E_∞/E_o for seven modes of the line resonator. Positive values of E_∞/E_o indicate that there is no crossover point (i.e. no phase reversal). Each curve is for a constant value of Q_M indicated at the right.

h_m	P'_m/P'_o	h_m	P'_m/P'_o
0.000	1.000	0.500	1.333
0.010	1.005	0.510	1.344
0.020	1.009	0.520	1.355
0.030	1.014	0.530	1.366
0.040	1.018	0.540	1.377
0.050	1.023	0.550	1.388
0.060	1.028	0.560	1.400
0.070	1.033	0.570	1.413
0.080	1.037	0.580	1.425
0.090	1.042	0.590	1.438
0.100	1.047	0.600	1.451
0.110	1.052	0.610	1.465
0.120	1.058	0.620	1.479
0.130	1.063	0.630	1.494
0.140	1.068	0.640	1.509
0.150	1.074	0.650	1.524
0.160	1.079	0.660	1.540
0.170	1.085	0.670	1.557
0.180	1.090	0.680	1.574
0.190	1.096	0.690	1.592
0.200	1.102	0.700	1.610
0.210	1.108	0.710	1.629
0.220	1.114	0.720	1.649
0.230	1.120	0.730	1.670
0.240	1.126	0.740	1.692
0.250	1.132	0.750	1.714
0.260	1.139	0.760	1.738
0.270	1.145	0.770	1.763
0.280	1.152	0.780	1.789
0.290	1.158	0.790	1.817
0.300	1.165	0.800	1.846
0.310	1.172	0.810	1.876
0.320	1.179	0.820	1.909
0.330	1.186	0.830	1.943
0.340	1.194	0.840	1.980
0.350	1.201	0.850	2.020
0.360	1.209	0.860	2.063
0.370	1.217	0.870	2.109
0.380	1.224	0.880	2.159
0.390	1.233	0.890	2.214
0.400	1.241	0.900	2.275
0.410	1.249	0.910	2.342
0.420	1.258	0.920	2.419
0.430	1.267	0.930	2.506
0.440	1.275	0.940	2.608
0.450	1.285	0.950	2.729
0.460	1.294	0.960	2.880
0.470	1.303	0.970	3.076
0.480	1.313	0.980	3.356
0.490	1.323	0.990	3.841

TABLE 5.2.2

This gives values for equation 5.2.11. P'_m/P'_o is observed experimentally and then h_m can be found. The material Q is then calculated from the relationship $Q_{Mm} = Q_{Cm}/h_m$. These tabulated values are shown graphically in Fig.5.2.3

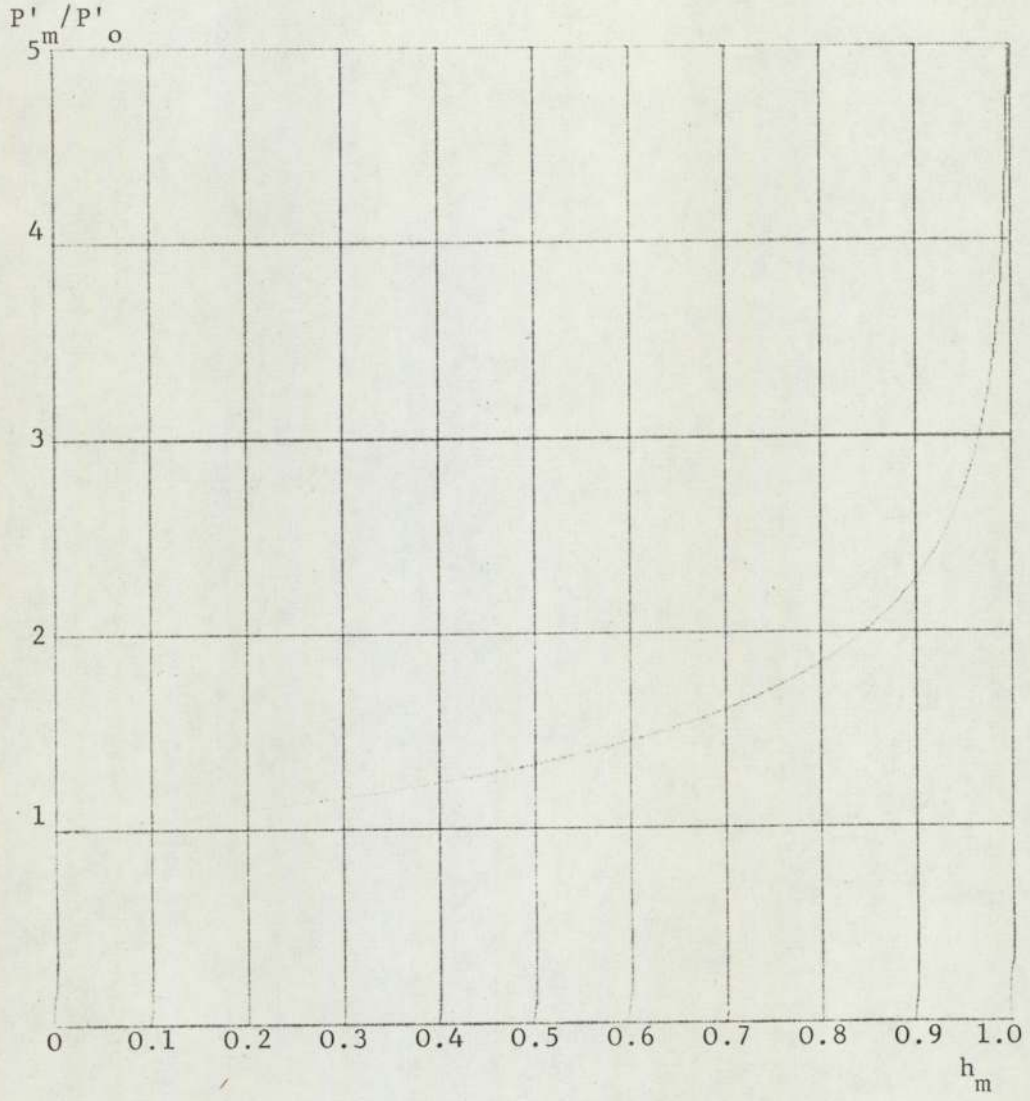

Fig.5.2.3

This graph is useful for quick reference while performing an experiment (see Fig.5.2.2).

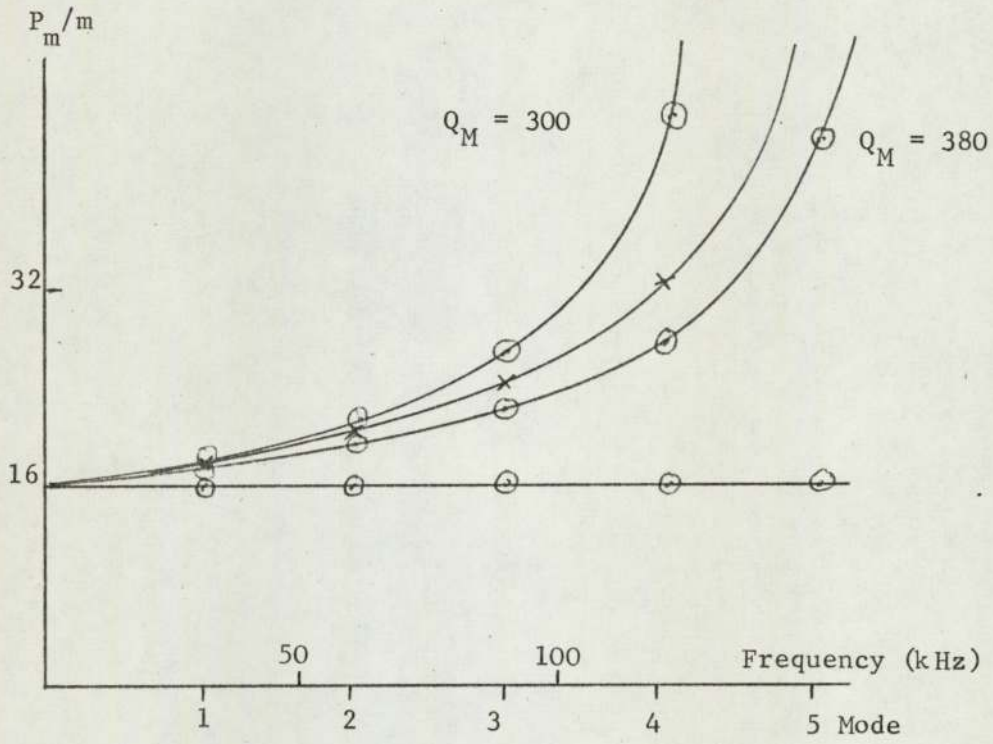

x Experimental curve for copper at 270° C.

θ Theoretical curves.

Fig.5.2.4

A spot set of values enable Q_C to be found by extrapolation to zero frequency. Then the absolute values of Q_M can be determined.

TABLE 5.3.1

Mode	Temperature (mV)	Frequency (kHz)	P_m	P_m/m
1	0.00	29.30	16.5	16.5
2	0.00	58.49	34.0	17.0
3	0.00	87.26	49.5	16.5
4	0.00	115.50	64.0	16.0
5	0.00	142.88	80.0	16.0
5	2.16	142.32	82.0	16.2
4	2.24	114.97	63.0	15.7
3	2.29	86.83	40.5	16.5
2	2.34	58.16	34.5	17.3
1	2.37	29.14	17.0	17.0
1	4.73	28.82	17.0	17.0
2	4.73	57.52	34.5	17.3
3	4.73	85.82	49.5	16.5
4	4.73	113.54	68.0	17.0
5	4.73	140.45	81.0	16.2
5	6.74	139.98	81.0	16.2
4	6.74	113.12	68.5	17.1
3	6.74	85.48	51.0	17.0
2	6.73	57.29	35.0	17.5
1	6.73	28.71	17.0	17.0
1	7.58	28.61	17.5	17.5
2	7.58	57.10	36.0	18.0
3	7.52	85.17	52.5	17.5
4	7.51	112.78	70.5	17.8
5	7.53	139.42	87.0	17.4
5	8.76	138.87	101.0	20.2
4	8.79	112.21	76.0	19.0
3	8.82	84.74	55.0	18.3
2	8.84	56.79	37.0	18.5
1	8.86	28.43	17.5	17.5
1	9.22	27.74	17.5	17.5
2	9.22	55.35	39.0	19.5
3	9.23	82.53	59.5	19.8
4	9.23	109.14	85.0	21.2
5	9.25	134.87	115.0	23.0
5	10.12	134.88	∞	∞
4	10.10	109.21	118.5	29.6
3	10.09	82.70	76.0	25.3
2	10.10	55.46	47.5	23.8
1	10.10	27.80	18.5	18.5
1	10.64	28.30	22.5	22.5
2	10.64	56.52	70.0	35.0
1	11.13	28.31	24.5	24.5

This shows the observed data from the experiment on pure copper. Any problems with low thickness to wavelength ratios can be detected by observing f_m/m.

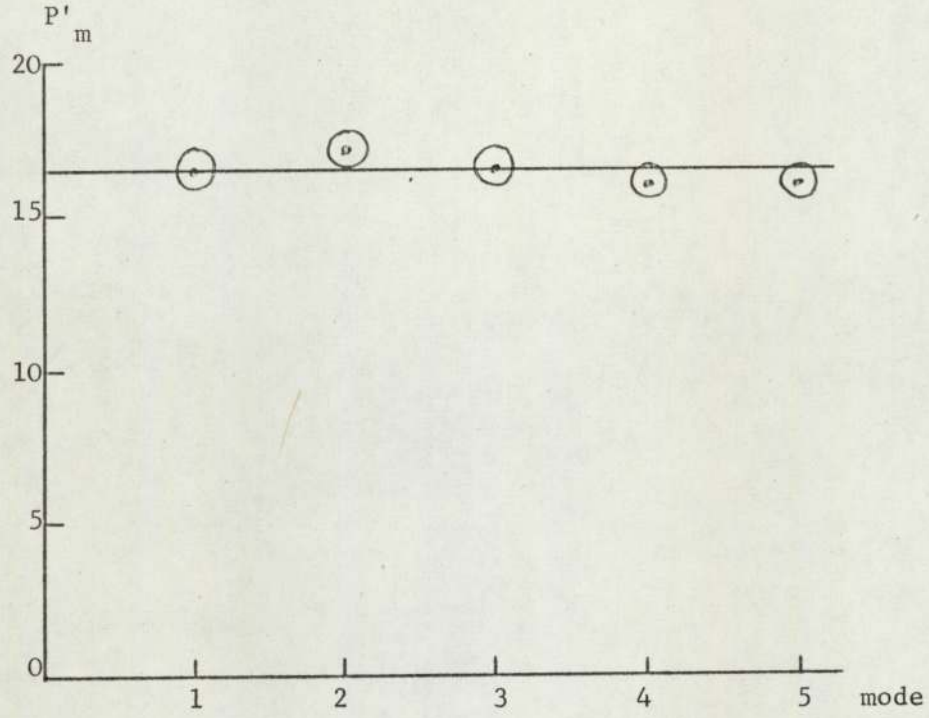

Fig.5.4.1

The P'_m values at room temperature indicate that $Q_M \simeq \infty$ and the extrapolation process can be performed with a straight line.

P'_2	Temperature (mV)	P'_2/P'_o	h_m	$Q_{M2}^{-1} \times 10^3$
measured	measured	$=P'_2/16.5$	Table 5.2.2	Equation 5.4.4
17.0	0.00	1.03	0.06	0.4
17.3	2.34	1.05	0.11	0.7
17.3	4.73	1.05	0.11	0.7
17.5	6.73	1.06	0.12	0.8
18.0	7.58	1.09	0.18	1.2
18.5	8.84	1.12	0.23	1.5
19.5	9.22	1.18	0.32	2.1
23.8	10.10	1.44	0.59	3.9
35.0	10.64	2.12	0.87	5.8

TABLE 5.4.2

Values of h_m are found from Table 5.2.2, and hence Q_{Mm}^{-1} can be calculated from equation 5.4.4.

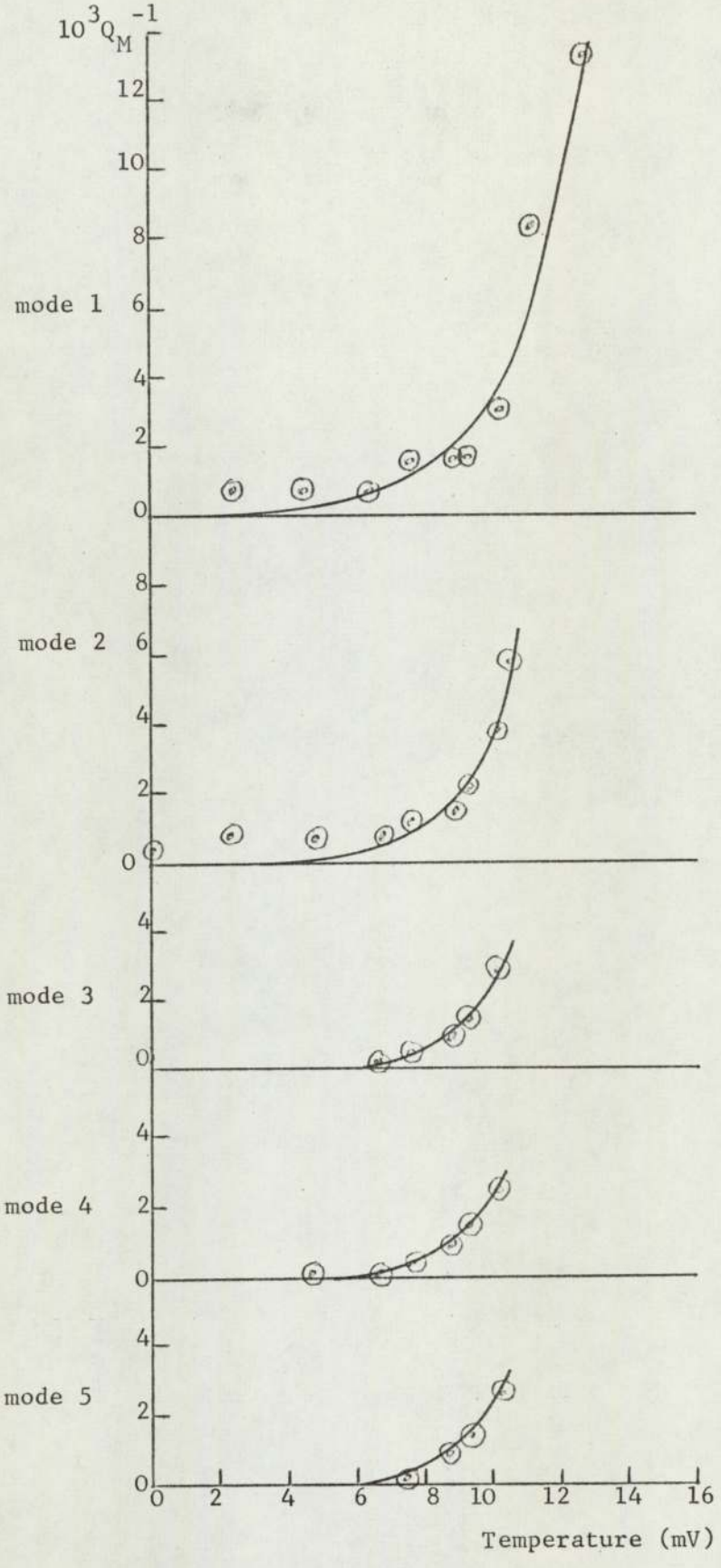

Fig.5.4.3

The complete results from the copper experiment give good agreement between the five modes.

6. THE ELECTRONIC SYSTEMS

6.1 Introduction

The electronic systems will not be described in detail. However the circuit diagrams of two simple transmitters, constructed by the author, are given. (Figs.6.3.1 and 6.3.3).

6.2 Oscillators

Comprehensive studies were carried out on oscillators suitable for the present electronic burst generators. The two main requirements for these oscillators were that they should have a T.T.L. compatible output and an adequate frequency stability for their application. Two such free-running oscillators are shown in Figs.6.2.1 and 6.2.2. The result of these oscillator investigations has been published - Bell/Sharp/Wong, 1974.

The Telequipment oscilloscope type D53A gives a mains locked output which is a convenient drive for a mains locked oscillator. Such an oscillator is shown in Fig.6.2.3.

6.3 Burst generators

Two burst generators were constructed by the author. The first, a simple portable model, was used mainly for demonstrations and is shown in Figs.6.3.1 and 6.3.2. The second burst generator (Figs.6.3.3 and 2.7.2) featured thumbwheel switches for selecting the number of burst oscillations. This is very helpful for measuring P_m (see chapter 5). Also a more stable burst frequency oscillator was used in order to reduce long term frequency drift. The output stage used in both generators is shown in Fig.6.3.4.

6.4 Automatic systems

For some applications, particularly temperature measurement it is desirable to use an electronic system which tracks the

frequency being studied. Two types of automatic system have been built to date.

(1) The first produces its error signal by examining phase in the echo-signal (Pelmore 1971).

(2) The second derives its error by measuring the frequency of the echo-decrement, and comparing with the burst frequency oscillator.

The analysis in chapter 2 of this thesis provides formulae which completely describe the echo. Computer programs were written to plot the phase of the echo. Figs.6.4.1 to 6.4.5 show plots for various cases. Fig.6.4.6 relates steady-state phase of the echo signal to the acoustic parameters.

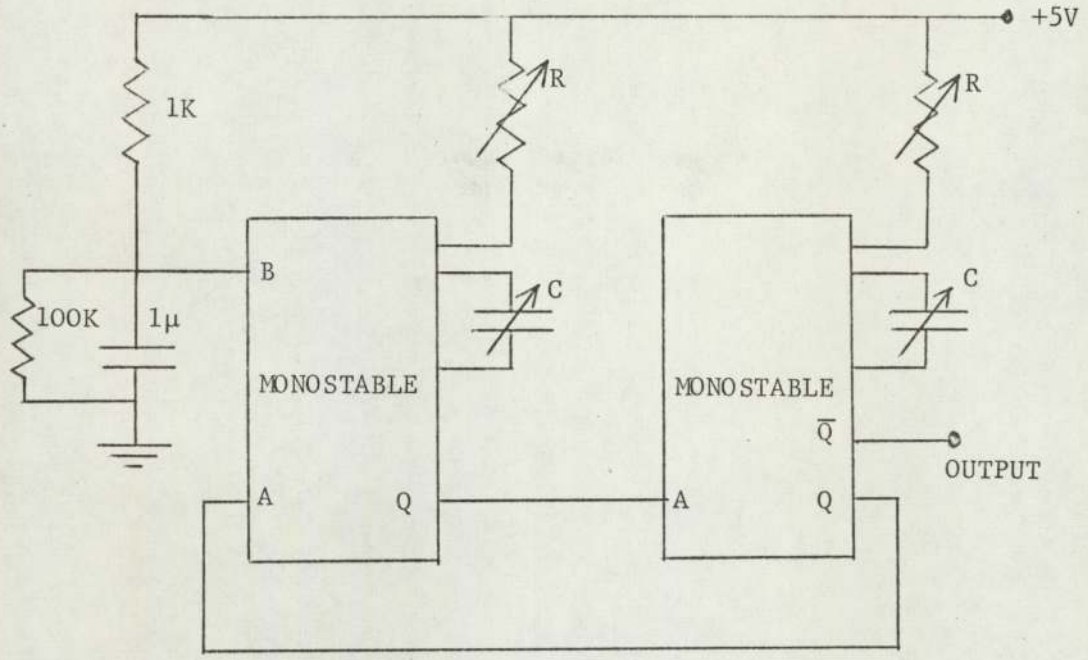

Fig.6.2.1

The two monostable multivibrators are cross-coupled to form a free-running oscillator. Point B can be used to stop and start the oscillator; it is shown here connected to a simple circuit to ensure the oscillator starting when the supply is switched on. The components C and R are changed to vary the frequency of the oscillator. (Integrated circuit numbers were Texas Instruments SN74121).

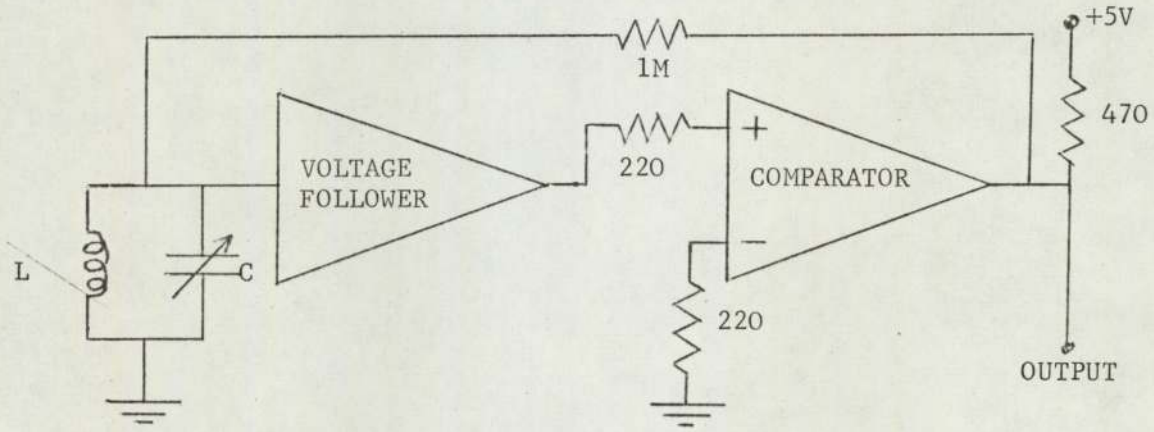

Fig.6.2.2

The oscillator shown here has a better frequency stability than that of the oscillator of Fig.6.2.1. However its frequency range is smaller, and so it is followed by a variable dividing circuit using standard digital techniques in order to obtain the required frequency range. (The voltage follower and comparator were National Semiconductor LM310 and LM306).

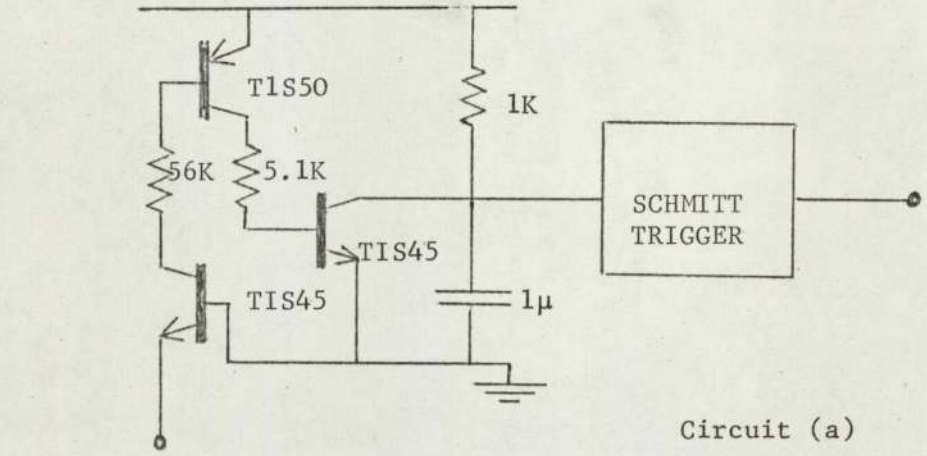

Circuit (a)

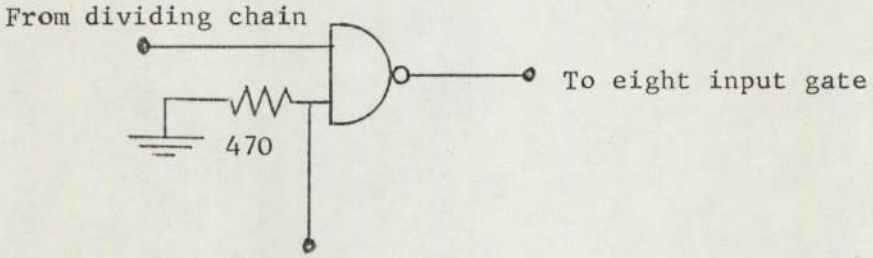

Circuit (b)

Fig.6.2.3

For some applications it is desirable to have an oscillator with its period locked to a fixed multiple of the mains supply period. The Telequipment D53A oscilloscope used by the author gives a 0V to -2V square wave output derived from the 50 Hz mains supply. This was used as the driving voltage for the circuit (a) above. The output of the Schmitt Trigger was fed into dividing chains constructed using J-K flip flops. These gave frequency division factors of 1,2,3,4,6,8,12 and 16. Each of these divided outputs was supplied to one input of a two input Nand gate as shown in circuit (b) above. The desired frequency was selected by switching +5 volts on to the appropriate Nand gate using an 8 way wafer switch. The outputs from the eight dual input Nand gates were supplied to an eight input Nand gate, which provided a single output from the mains locked oscillator. (Components were supplied by Texas Instruments).

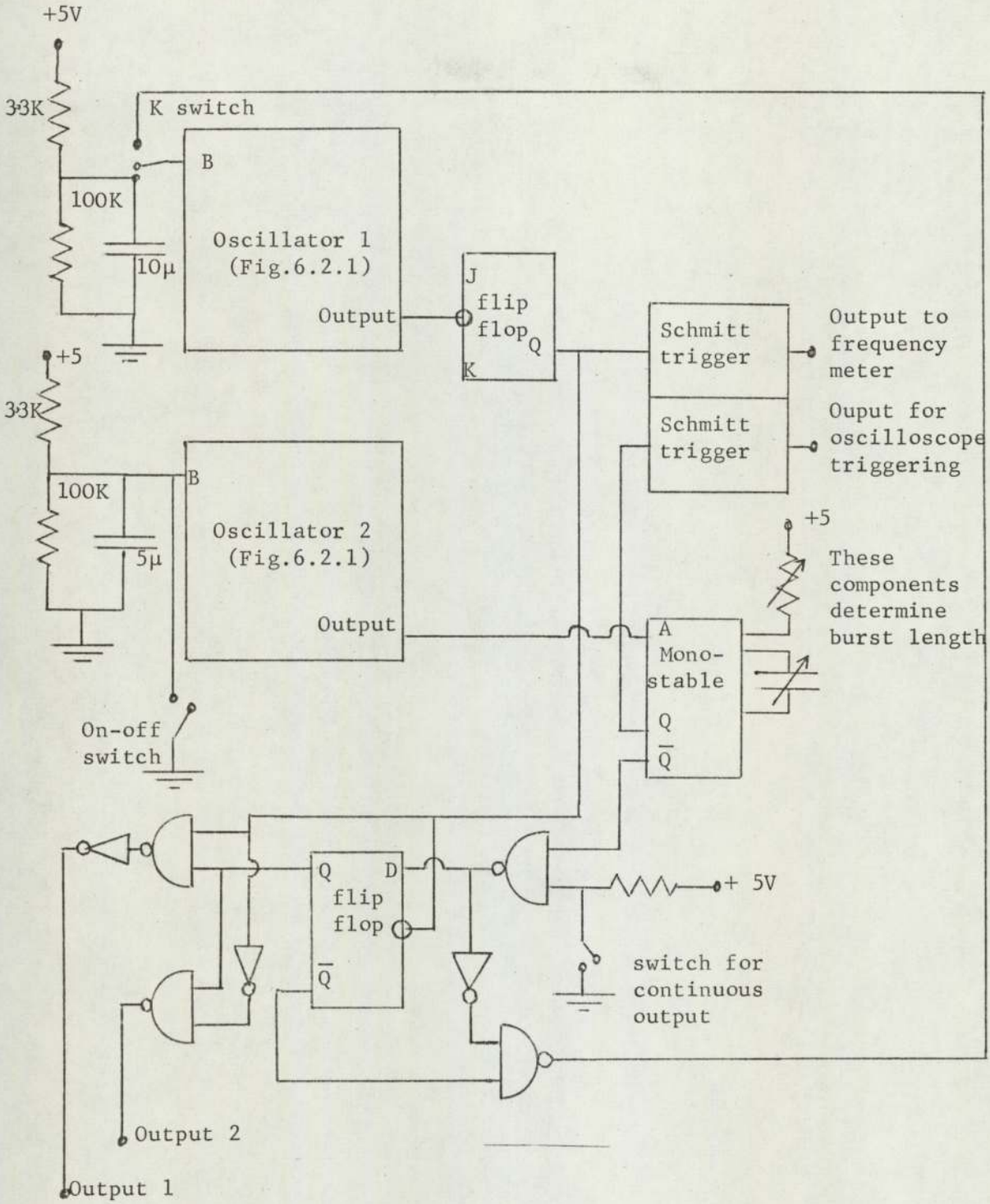

Fig.6.3.1

Oscillator 1 determines the transmitted frequency; the J-K flip flop ensures a unity mark-space ratio for the output. Oscillator 2 is of lower frequency and determines the repetition rate of the transmitted burst of oscillations. The D type flip flop ensures that a whole number of oscillations are transmitted. By using the K switch oscillator 1 can be changed from continuous running to running only during the burst length. Outputs 1 and 2 supply the output circuit of Fig.6.3.4. (All integrated circuits were supplied by Texas Instruments).

Fig.6.3.2

This portable burst generator was built for demonstration purposes. The transducer tuning capacitor was included inside the box.


J C K SHARP
JULY 1973
BURST
CONT.
TUNING CAPACITOR
BURST LENGTH
REP. RATE
FREQUENCY
OFF
ON
TRANSDUCER
D.F.M.
SCOPE TRIGGER

Fig.6.3.3

The main feature of this burst generator was the decade thumb-wheel switches which were used to select the number of oscillations in the burst.

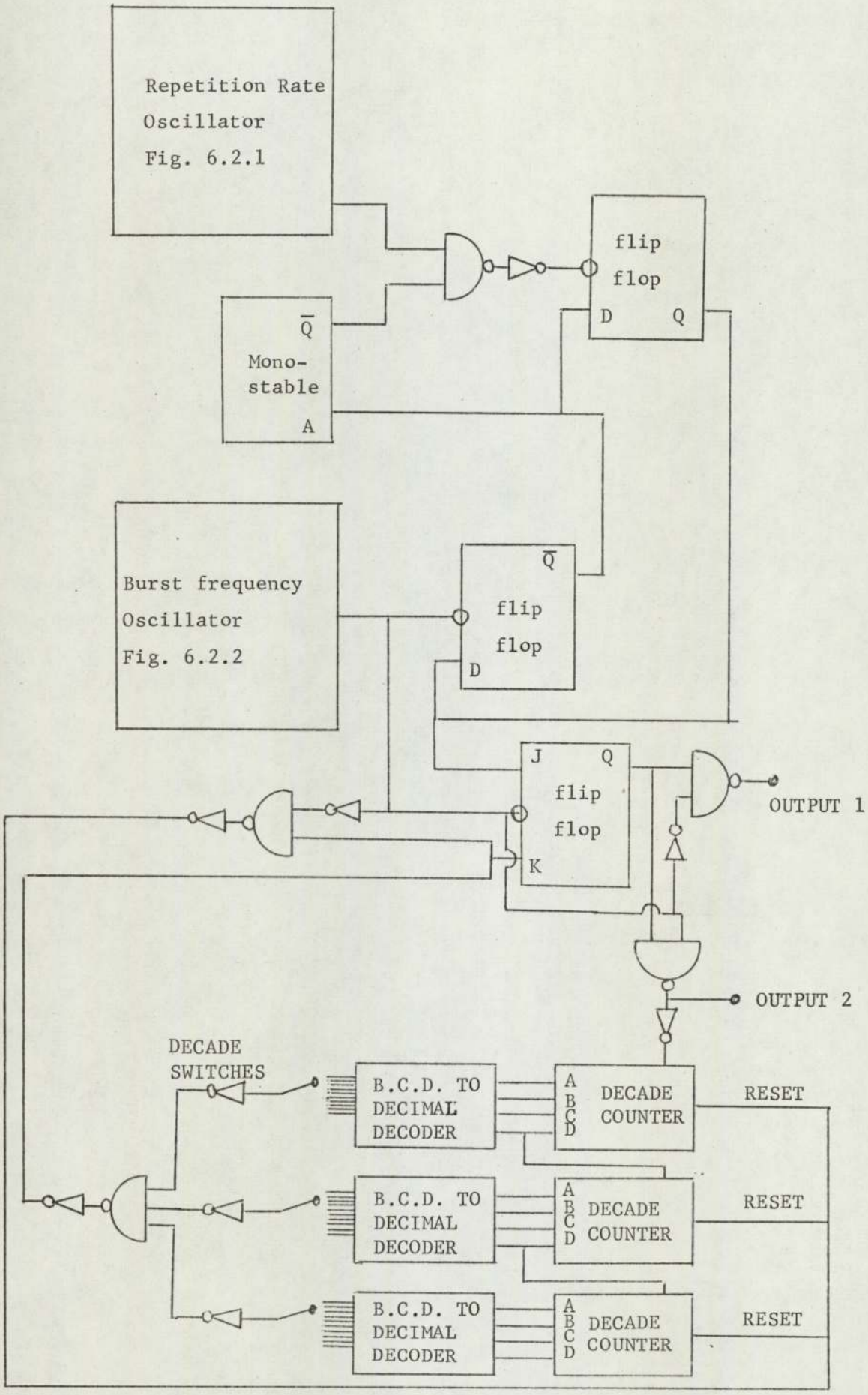

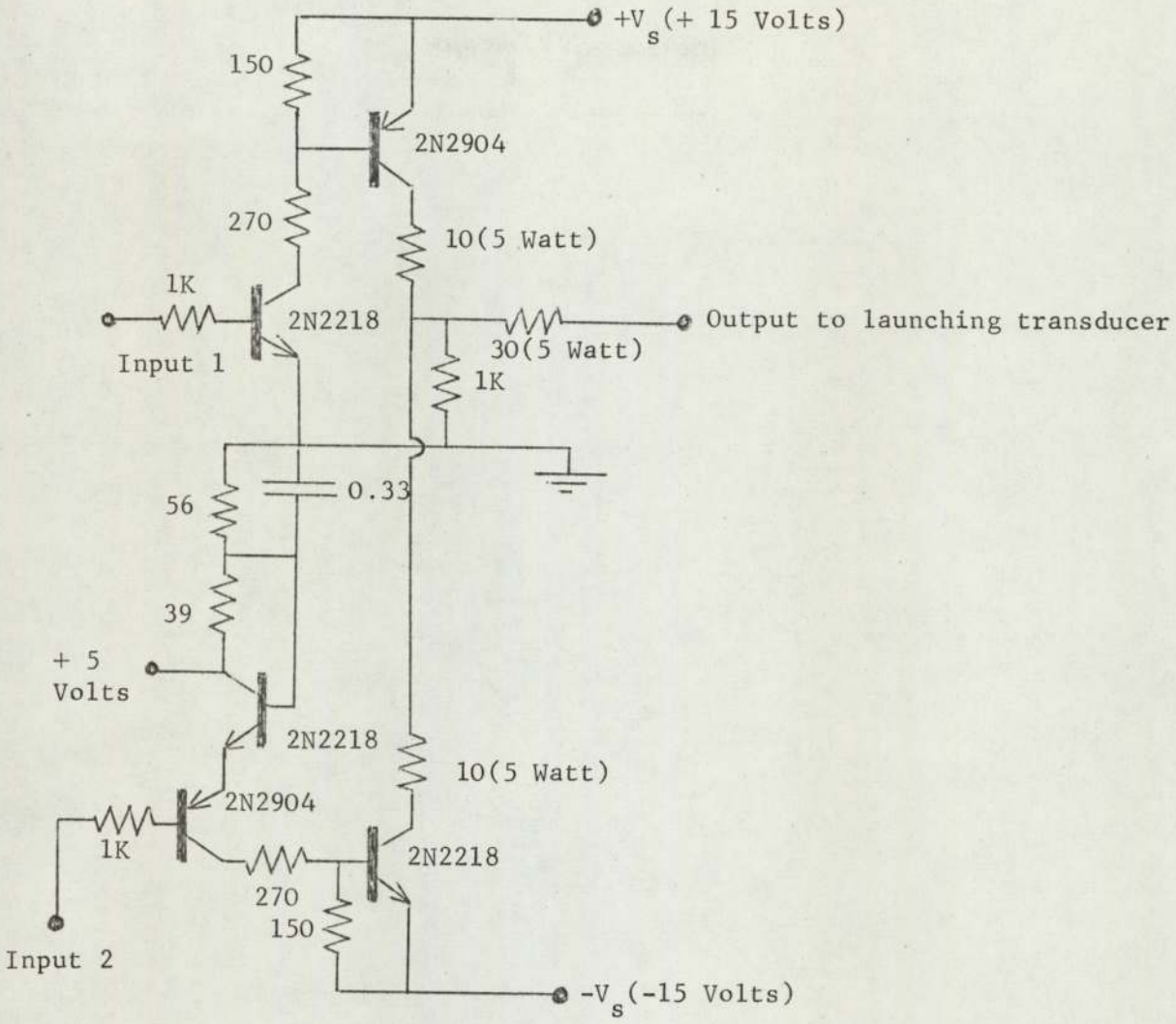

Fig.6.3.4

The output circuit for both burst generators is shown. The inputs 1 and 2 are taken from outputs 1 and 2 of Figs.6.3.1 and 6.3.2. The supply voltage $\pm V_s$ can be varied, but in this case it was fixed at $\pm$ 15V. (Transistors were supplied by Texas Instruments).

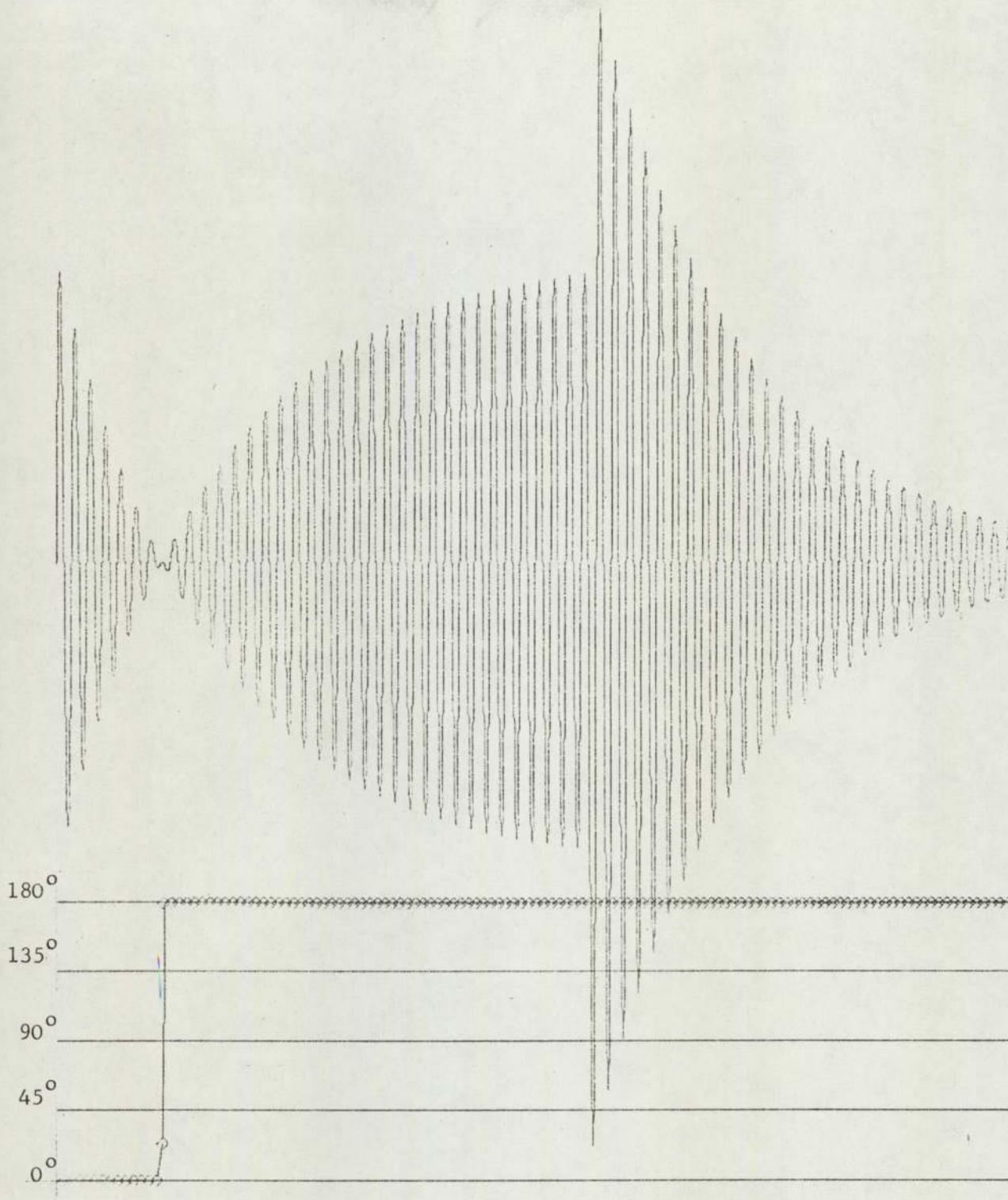

Fig. 6.4.1

The echo is shown with the transmitted frequency tuned to resonance and with Q_C = 30. The phase graph shows the 180° phase reversal at the cross-over point.

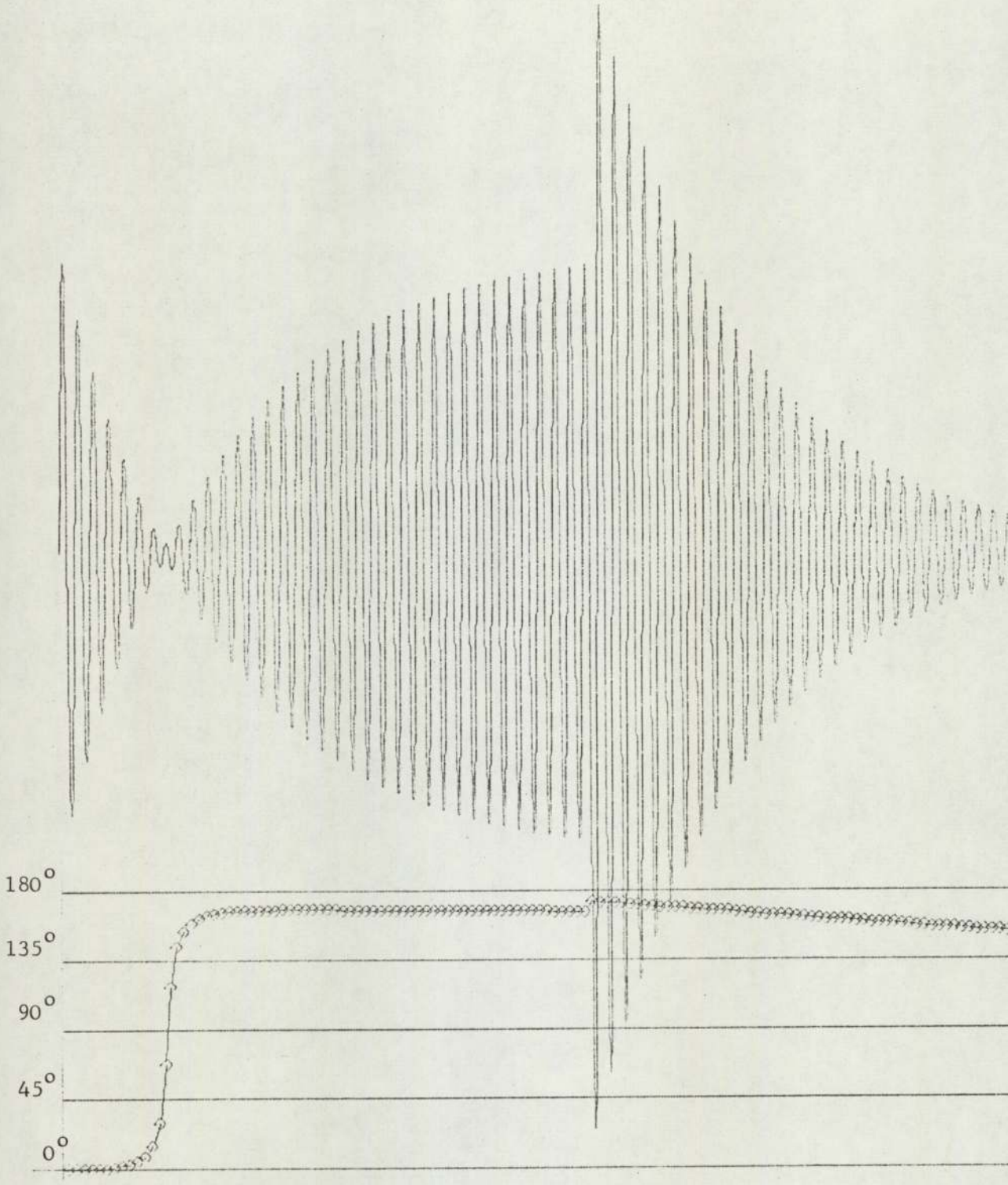

Fig.6.4.2

The echo is shown with 0.2% frequency detuning, again with $Q_C = 30$. The steady-state phase shift produced in the echo-signal is 12^{o}. During the echo-decrement the steady ramp of the phase graph indicates the difference between transmitted and resonant frequencies.

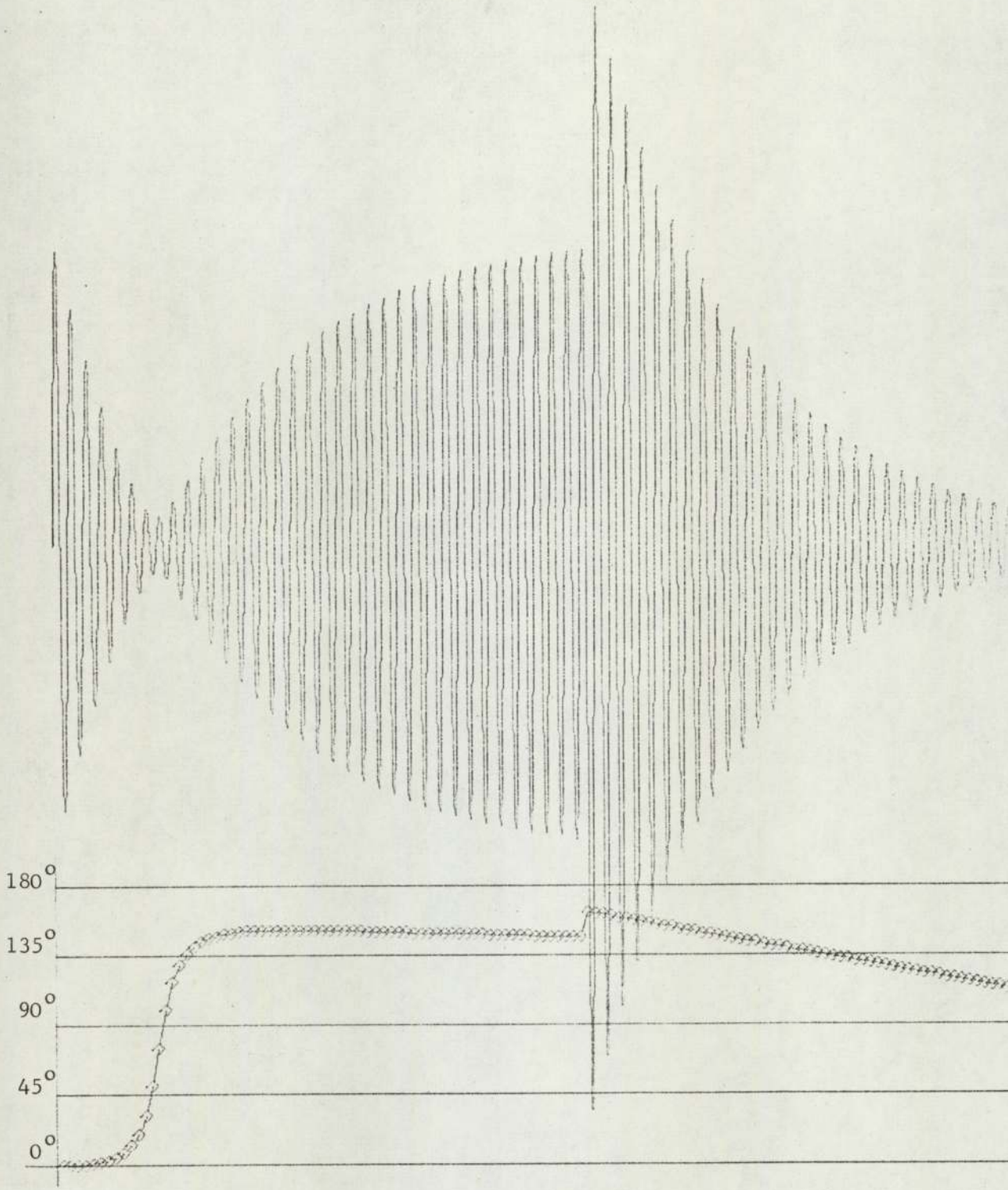

Fig.6.4.3

The echo is shown with 0.5% frequency detuning, again with Q_C = 30. The steady-state phase shift of the echo-signal is now increased to 33°.

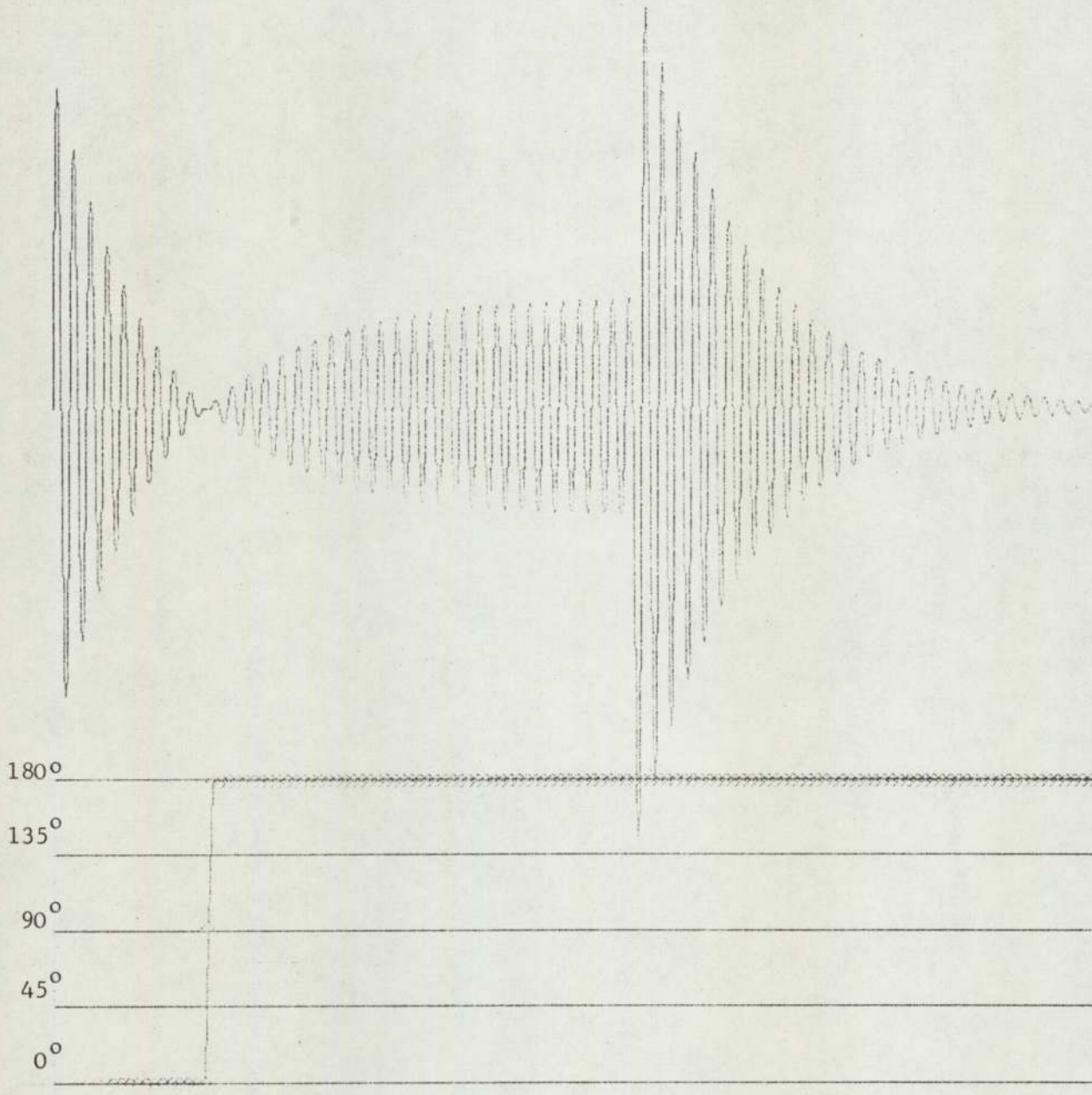

Fig.6.4.4

Material losses have now been introduced such that $Q_C = 30$, $Q_M = 60$. The transmitted signal is tuned to resonance, and the phase reversal is maintained.

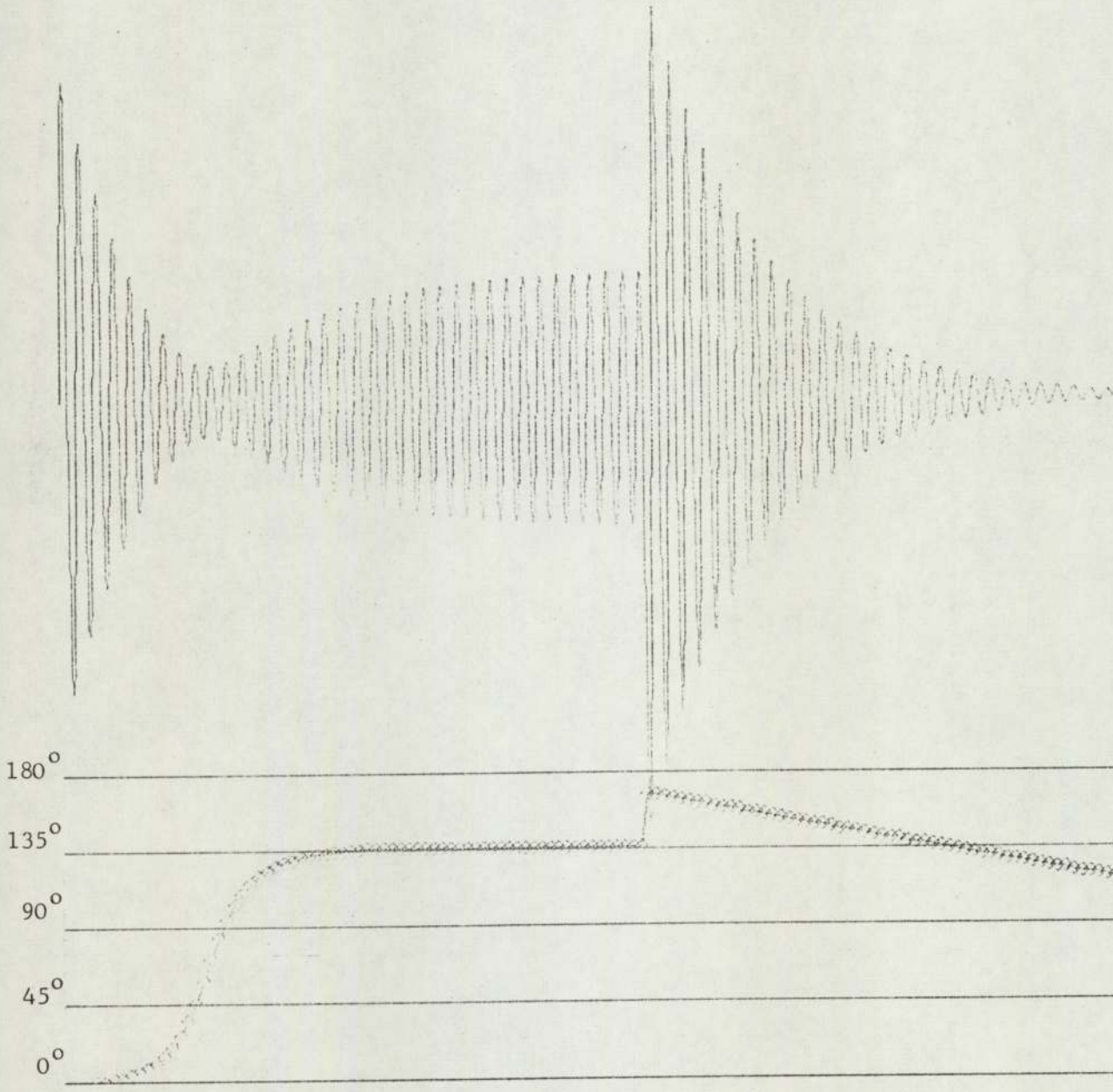

Fig.6.4.5

The echo is shown with Q_C = 30, Q_M = 60, and 0.5% frequency detuning. The steady-state phase shift of the echo-signal is 45°. The effect of material losses is to increase the sensitivity of phase as an indication of detuning.

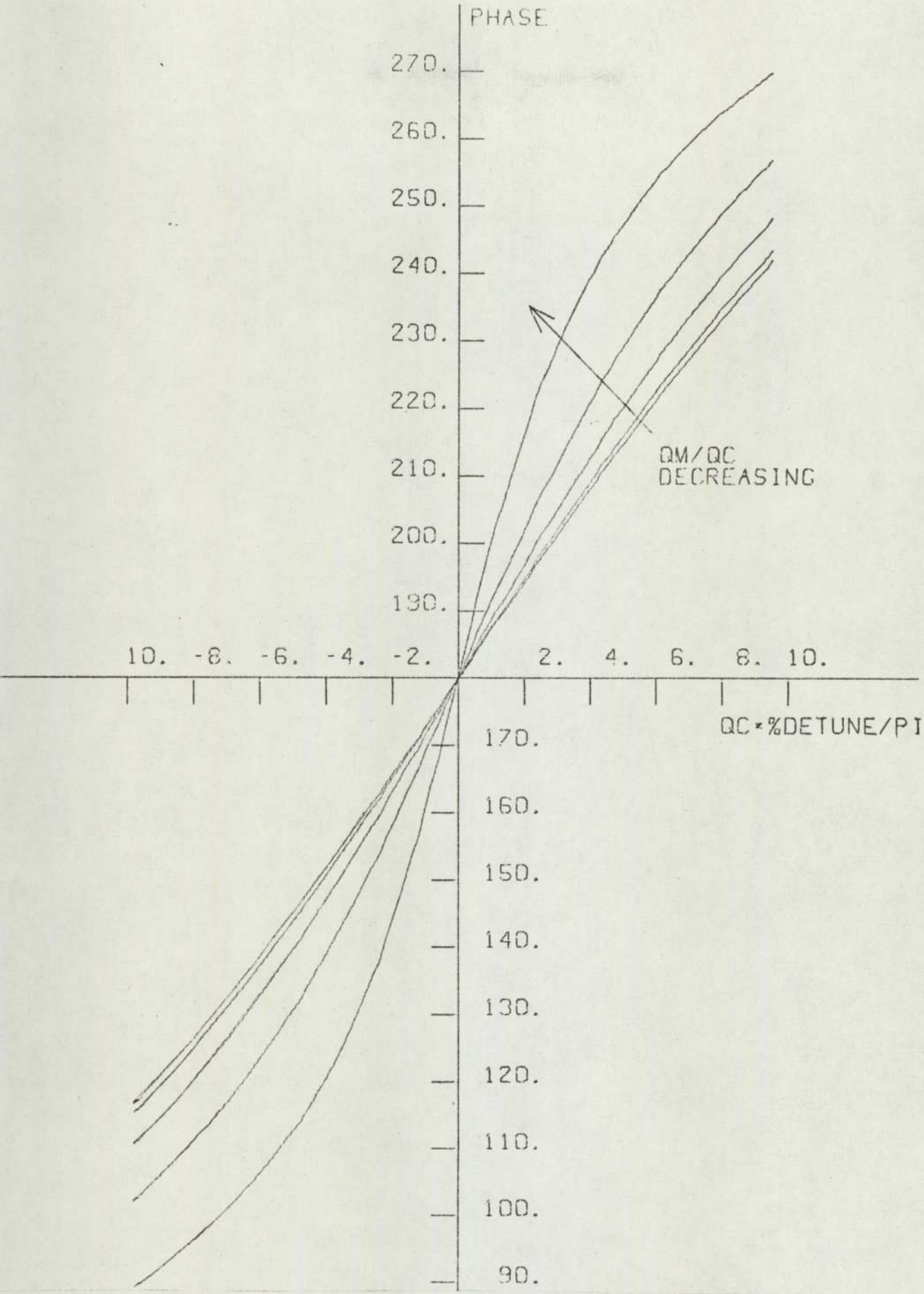

Fig.6.4.6

The steady-state phase of the echo-signal is shown as a function of frequency detuning for $Q_M/Q_C = \infty$, 5.00, 2.50, 1.65, and 1.25.

LIST OF SYMBOLS

Subscripts may be used with these symbols to refer to a particular solution or region. A bar over a symbol indicates that its Laplace Transformation has been taken.

a	amplitude of transmitted oscillations
a	outside radius
a_1	mean radius
A	cross-sectional area
A	arbitrary constant
A(p),B(p)	general functions of p
B	arbitrary constant
b	inside radius
C	velocity of propagation
E	dynamic Young's Modulus
E	echo return
F	force
f	frequency
H	material loss coefficient
h	dilatational wave number
h	heavyside step function
h_m	$(= Q_{Cm}/Q_{Mm})$
k	$(= 1_n(1/r))$
k	shear wave number
K	radius of gyration
K	frequency parameter
L	frequency parameter
l	length
M_n, N_n	combinations of Bessel functions as defined in the text
P_N	number of oscillations in transmitted burst
P_m	number of oscillations to the crossover point

p	Laplacean operator for τ
Q_C	coupling Q factor
Q_M	material Q factor
Q_T	total Q factor
R	reflected signal
R'	modified reflected signal
r	reflection coefficient from boundary of transmission and resonator
r	radius direction (polar co-ordinates)
S	strain
s	Laplacean operator for t
T	duration of oscillation burst
T	stress
t	time
U	velocity
V	amplitude component
V_L	($= \sqrt{(E/\rho)}$) longitudinal rod velocity
x	direction (Cartesian co-ordinates)
z	acoustic impedance
α , β	defined in chapter 2
γ	transmission constant
θ	angle
Θ	ratio of shear and dilatational wave numbers
ρ	density
σ	dynamic Poissons Ratio
τ	time
ξ	displacement
ω_s	transmitted angular frequency
ω_m	resonant angular frequency
Δ	dilatation
$\bar{\omega}$	rotation

REFERENCES

Ambati, G. : Experimental and Numerical Studies of Radial and Contour Extensional modes in elastic Disks. M.Sc. Thesis. University of Aston, 1973.

Bell, J.F.W. : The velocity of sound in metals at high temperatures. Phil.Mag. Vol.2, p.1113-1120 (1957).

Bell, J.F.W. : A solid acoustic thermometer. Ultrasonics, Vol.6, p.11-14 (1968).

Bell, J.F.W., Noble, A.E., Seth, T.N. : Graphical displays of acoustic properties of solids. Ultrasonics, p.178-181 (1973).

Bell, J.F.W., Sharp, J.C.K., Wong, Y. : Digital Oscillators. Int.J. Electronics, (accepted January 1973).

Bishop, R.E.D., Gladwell, G.M.L., Michaelson, S. : The matrix analysis of vibration. Camb. U.P., (1965).

Bordoni, P.G. : Nuovo Cimento, Vol.4, p.177 (1947).

Bozorth, R.M. : Ferromagnetism. Van Nostrand (1951).

Buckens, F. : Influence of the relative radial thickness of a ring on its natural frequencies. J.A.S.A., Vol.22, p.437-443 (1950).

Chladni, E.E.F. : Entdeckungen uber der theorie des klanges. Leipzig (1787).

Granato, A., Lucke, K. : Theory of mechanical damping due to dislocations. J. Appl.Phys., Vol.27, p.583-593. (1956).

Granato, A., Lucke, K. : Application of dislocation theory to Internal Friction Phenomena at high frequencies. J. Appl. Phys. Vol.27, p.789 - 805 (1956).

Hawgood, J. : Numerical methods in Algol. Mc Graw-Hill (1965).

Hearmon, R.F.S.: The elastic constants of anisotropic materials. Rev. Mod. Phys. Vol.18, (1946).

Holland, R. : Numerical studies of elastic disk contour modes lacking axial symmetry. J.A.S.A. Vol.40, p.1051 - 1057 (1966).

Johnson, A.C.J. : An apparatus for ultrasonic measurement. M.Sc. Thesis, University of Aston (1971).

Kaye, G.W.C., Laby, T.H. : Tables of physical and chemical constants. Longmans (1958).

Ke, T.S. : Experimental evidence of the viscous behaviour of grain boundaries in metals. Phys. Rev., Vol.71, p.533 - 546 (1947).

Kolsky, H. : Stress waves in solids. Dover (1963).

Love, A.E.H. : The Mathematical theory of elasticity. Cambridge (1927).

Lynworth, L.C. : N.A.S.A. report No. CR-72395 (1967).

Meitzler, A.H., O'Bryan, H.M., Tiersten, H.F. : Definition and measurement of radial mode coupling factors in piezoelectric ceramic materials with large variations in Poissons Ratio. IEEE Trans. on Sonics and Ultrasonics, Vol. SU-20, p.233 - 239 (1973).

Mc Mahon, G.W. : Measurement of Poissons Ratio in poled ferroelectric ceramic Disks. IEEE Trans. Ultrasonic Engineering, p.102 - 103 (1963).

Onoe, M. : Contour vibrations of isotropic circular plates, J.A.S.A.,Vol. 28 , p.1158 - 1162 (1956).

Pelmore, J.M. : An instrument to measure Young's Modulus at high temperatures. M.Sc. Thesis, University of Aston (1971).

Pelmore, J.M. : Internal Friction and high temperature measurement of refractory materials. Ph.D. Thesis, University of Aston (1974).

Powers, R.W., Doyle, M.V.. : Diffusion of interstitial solutes in group V transition metals. J.Appl. Phys.,Vol.30, p.514 - 524 (1959).

Ravenhall, F.W. : Some recent observations on Chladni's figures. Acoustica, Vol.29, p.14 - 21, (1973).

Salvadori, M.G., Baron, M.L. : Numerical methods in Engineering. Longmans (1955).

Seth, T.N. : Ultrasonic pyrometer for industrial applications. Ph.D. Thesis, University of Aston (1974).

Snoek, J.L. : Effect of small quantities of carbon and nitrogen on the elastic and plastic properties of iron. Physica, Vol.8, p.711 - 733 (1941).

Stephens, R.W.B., Bate, A.E. : Acoustics and vibrational physics. Edward Arnold (1966).

Stokes, Sir George : Cambridge Mathematical Transactions (1845)

Timoshenko, S.P. : Theory of plates and shells. Mc Graw-Hill (1959).

Timoshenko, S.P. : Theory of Elasticity. Mc Graw-Hill (1970).

Tzannes, N.S. : Joule and Wiedermann effects - The simultaneous generation of Longitudinal and Torsional stress pulses in magnetostrictive materials. IEEE Trans.

Sonics and Ultrasonics, Vol.SU-13, p.33 - 41 (1966)

Wegel, R.L., : Internal dissipation in solids for small cyclic
Walther, H. strains. Physics, Vol.6, p.141 - 157 (1935).

Zepler, E.E., : Transients in electronic engineering. Chapman
Nichols, K.G. and Hall (1971).

APPENDIX A.2.2

MATHEMATICAL ANALYSIS OF TRANSMISSION LINE AND LINE RESONATOR

Fig.2.2.1 shows the line and resonator in diagrammatic form. The solution obtained here is for the first reflection (echo) only. (For a similar electrical case see Zepler 1971, page 287).

It is convenient to define,

Impedance (Z) = Fore (F)/Displacement Velocity (U)

where

$$U = \frac{\partial \xi_x}{\partial x}$$

The one dimensional general equation of Stokes 1845 can be written in the form

$$\frac{\partial^2 U}{\partial \tau^2} = c^2 \frac{\partial^2 U}{\partial x^2} + H \frac{\partial^3 U}{\partial x^2 \partial \tau} \qquad \text{A.2.2.1}$$

where $U = U(x, \tau)$

See also Stephens 1966.

It is also convenient to write equation A.2.2.1 in the form of two coupled partial differential equations. They are written here in their Laplace transformation.

$$\overline{F}(x,p) = \rho A \frac{(H_p + c^2)}{p} \frac{\partial U(x,p)}{\partial x} \qquad \text{A.2.2.2}$$

$$\overline{U}(x,p) = -\frac{1}{\rho A} \frac{1}{p} \frac{\partial F(x,p)}{\partial x} \qquad \text{A.2.2.3}$$

The general solution of equation A.2.2.1 is,

$$\overline{U}(x,p) = A(p) \exp(-\gamma x) + B(p) \exp(\gamma x) \qquad \text{A.2.2.4}$$

where

$$\gamma^2 = p^2/(Hp + c^2)$$

From equations A.2.2.2, A.2.2.3, A.2.2.4 the characteristic impedance of an infinite line can be found,

$$Z(p) = \rho A(Hp + c^2)^{1/2} \qquad \text{A.2.2.5}$$

A suffix will be used to refer the general equations A.2.2.1/2/3/4 to either the transmission line region (1) or the resonator region (2).

Region (2) will be considered first in order to determine the impedance presented as the termination of the transmission line (i.e. $F_2(1_1,p)/U_2(1_1,p)$). The boundary conditions for region (2) where $(1_1 < x < 1_1 + 1_2)$ are,

$$\bar{F}_2(1_1 + 1_2, p) = 0 \qquad \text{A.2.2.6}$$

$$\bar{F}_2(1_1, p) = \bar{F}_1(1_1,p) \qquad \text{A.2.2.7}$$

$$\bar{U}_2(1_1,p) = \bar{U}_1(1_1,p) \qquad \text{A.2.2.8}$$

Substituting equation A.2.2.4 into A.2.2.2 and A.2.2.3 gives the general solution for region(2),

$$\bar{U}_2(x,p) = A_2(p) \exp(-\gamma_2 x) + B_2(p) \exp(\gamma_2 x) \qquad \text{A.2.2.9}$$

$$\bar{F}_2(x,p) = Z_2(p) \left[A_2(p) \exp(-\gamma_2 x) - B_2(p) \exp(\gamma_2 x)\right] \qquad \text{A.2.2.10}$$

where $Z_2(p) = \rho_2 A_2 (H_2 p + c_2^2)^{1/2}$

and $\gamma_2^2 = p^2/(H_2 p + c_2^2)$

Using boundary condition A.2.2.6 in equation A.2.2.10 gives,

$$B_2(p)/A_2(p) = \exp(-2\gamma_2(1_1 + 1_2)) \qquad \text{A.2.2.11}$$

Using boundary condition A.2.2.7 in equation A.2.2.10 gives,

$$\bar{F}_1(1_1,p) = Z_2(p) \left[A_2(p) \exp(-\gamma_2 1_1) - B_2(p) \exp(\gamma_2 1_1)\right] \qquad \text{A.2.2.12}$$

and using A.2.2.8 in equation A.2.2.9 gives,

$$\bar{U}_1(1_1,p) = A_2(p) \exp(-\gamma_2 1_1) + B_2(p) \exp(\gamma_2 1_1) \qquad \text{A.2.2.13}$$

Combining equations A.2.2.11/12/13 yields,

$$\bar{Z}_1(l_1,p) = \bar{F}_1(l_1,p)/\bar{U}_1(l_1,p) = Z_2(p) \tanh(\gamma_2 l_2) \qquad \text{A.2.2.14}$$

Now there is enough information to obtain a solution for region (1) where $(0 \leq x < l_1)$. Suppose that at time $\tau = 0$ a forcing function $U_1(0,\tau) = a \sin(\omega_s \tau)$ is applied at the end of the line, $x = 0$ and so a boundary condition is,

$$\bar{U}_1(0,p) = a\omega_s/(p^2 + \omega_s^2) \qquad \text{A.2.2.15}$$

The general solutions for region (1) are,

$$\bar{U}_1(x,p) = A_1(p) \exp(-\gamma_1 x) + B_1(p) \exp(\gamma_1 x) \qquad \text{A.2.2.16}$$

$$\bar{F}_1(x,p) = Z_1(P)\left[A_1(p) \exp(-\gamma_1 x) - B_1(p) \exp(\gamma_1 x)\right] \qquad \text{A.2.2.17}$$

$\bar{U}_1(x,p)$ consists of two components, a forward travelling wave, U_{1+} and a reverse travelling wave, U_{1-}.

$$U_{1+}(x,p) = A_1(p) \exp(-\gamma_1 x); \quad U_{1-}(x,p) = B_1(p) \exp(\gamma_1 x)$$

So at the junction $(x = l_1)$,

$$\bar{U}_1(l_1,p) = \bar{F}_1(l_1,p)/\bar{Z}_1(l_1,p) \qquad \text{A.2.2.18}$$

and by substituting with equations A.2.2.16/17

$$U_{1+}(l_1,p) + U_{1-}(l_1,p) = \frac{Z_1(p)}{\bar{Z}_1(l_1,p)}\left[U_{1+}(l_1,p) - U_{1-}(l_1,p)\right] \qquad \text{A.2.2.19}$$

therefore,

$$\frac{U_{1-}(l_1,p)}{U_{1+}(l_1,p)} = \frac{Z_1(p) - \bar{Z}_1(l_1,p)}{Z_1(p) + \bar{Z}_1(l_1,p)} \qquad \text{A.2.2.20}$$

So the first reflection $\bar{R}(x,p)$ will have initial magnitude $U_{1-}(l_1,p)$. So substituting with equation A.2.2.14 for $\bar{Z}_1(l_1,p)$,

$$\bar{R}(x,p) = \frac{Z_1(p) - Z_2(p) \tanh(\gamma_2 l_2)}{Z_1(p) + Z_2(p) \tanh(\gamma_2 l_2)} \; U_{1+}(l_1,p) \exp \gamma_1 (x - 2\,l_1)$$

A.2.2.21

and now using boundary condition A.2.2.15 gives,

$$\bar{R}(x,p) = \frac{Z_1(p) - Z_2(p) \tanh(\gamma_2 l_2)}{Z_1(p) + Z_2(p) \tanh(\gamma_2 l_2)} \; \frac{a\omega_s}{(p^2 + \omega_s^2)} \exp \gamma_1 (x - 2l_1)$$

A.2.2.22

γ_1 and Z_1 have similar expressions to those for γ_2 and Z_2.

By splitting the forward and reverse waves as has been done here, a solution (A.2.2.22) for the first reflection only is formed and hence it is of simpler form than a complete solution.

Integrating around the contour shown in Fig.A.2.2.1 gives

$$\int_{AB} + \int_{BC} + \int_{CD} + \int_{DE} + \int_{EF} + \int_{FA} = (\text{sum of residues}).$$

The positive square root is taken in the definition of γ_1 and so Jordon's Lemma holds (i.e. $\bar{R}(x,p) \to 0$ as $p \to \infty$ on the boundaries BC and FA). Therefore $\int_{BC} = \int_{FA} = 0$

Now,

$$\int_{CD} = \int_{p=-\infty}^{P=-C_1^2/H_1} \bar{R}(x,p) \exp(p\tau) dp \qquad \text{A.2.2.23}$$

Typically however $C_1^2/H_1 >> 10^6$ and so the term $\exp(p\tau)$ is extremely small over the range of the integral and so $\int_{CD} \simeq 0$.

Similarly $\int_{DE} \simeq 0$ and $\int_{EF} \simeq 0$.

The Laplacean Inversion of $\bar{R}(x,p)$ can now be written,

$$R(x,\tau) = \int_{AB} = (\text{sum of residues}) \qquad \text{A.2.2.24}$$

The attenuation and time delay effects of the term $\exp \gamma_1(x-2l_1)$ on these residues will be shown later. As these effects are not important in the practical case a new function $\bar{R}(o,s)$ is defined

$$\bar{R}(o,s) = \frac{Z_1(s) - Z_2(s) \tanh(\gamma_2 l_2)}{Z_1(s) + Z_2(s) \tanh(\gamma_2 l_2)} \quad \frac{a\omega_s}{(s^2 + \omega_s^2)} \qquad \text{A.2.2.25}$$

s is the Laplacean operator for t, where $\tau - t = 2l_1/c_1$. $t = o$ defines the start of the echo signal.

The expression A.2.2.25 splits into two parts; the transfer function of the system, and the forcing function applied to it. The poles of the transfer function are given when,

$$Z_1(s) + Z_2(s) \tanh(\gamma_2 l_2) = 0 \qquad \text{A.2.2.26}$$

Replacing $\tanh(\gamma_2 l_2)$ by its exponential form $(\exp(\gamma_2 l_2) - \exp(-\gamma_2 l_2)/(\exp(\gamma_2 l_2) + \exp(-\gamma_2 l_2))$ gives,

$$\exp(2\gamma_2 l_2) = (Z_2(s) - Z_1(s))/(Z_2(s) + Z_1(s)) \qquad \text{A.2.2.27}$$

However, $H_1 << c_1^2$; $H_2 << c_2^2$, and H_1 and H_2 can be neglected in the right-hand side of equation A.2.2.27. This is because the effect of H_1 and H_2 on these vectors in the s-plane is extremely small. (See Section 2.2 on limits of practical applications). Equation A.2.2.27 becomes

$$2\gamma_2 l_2 = \ln(r) \qquad \text{A.2.2.28}$$

where $r = (\rho_2 c_2 A_2 - \rho_1 c_1 A_1)/(\rho_2 c_2 A_2 + \rho_1 c_1 A_1)$.

Letting $\ln(r) = - k + j\theta$ gives $\theta = 0, \pm 2\pi, \pm 4\pi$ etc. and k is in general a small positive real number. Equation A.2.2.28 now becomes

$$4l_2^2 \frac{s^2}{H_2 s + c_2^2} = (- k + j\theta)^2$$

so

$$s^2 - \left[\frac{- k + j\theta}{2l_2}\right]^2 H_2 s - \left[\frac{-k + j\theta}{2l_2}\right]^2 c_2^2 = 0 \qquad \text{A.2.2.29}$$

This quadratic equation can be solved for s.

$$s = \left[\frac{- k + j\theta}{2l_2}\right]^2 \frac{H_2}{2} + \frac{1}{2}\sqrt{\left[\frac{- k + j\theta}{2l_2}\right]^4 H_2^2 + \left[\frac{- k + j\theta}{l_2}\right]^2 c_2^2}$$

A.2.2.30

But $H_2 << c_2$ so,

$$s = \left[\frac{- k + j\theta}{2l_2}\right]^2 \frac{H_2}{2} + \frac{1}{2} \frac{- k + j\theta}{l_2} c_2 \qquad \text{A.2.2.31}$$

On expanding this expression further approximations can be made because $k << c_2$ and $H_2 << c_2$. Thus equation A.2.2.31 becomes,

$$s = - \frac{\theta^2 H_2}{8l_2^2} - \frac{kc_2}{2l_2} + j \frac{c_2}{2l_2}\theta \qquad \text{A.2.2.32}$$

The approximations involved in obtaining equation A.2.2.32 from equation A.2.2.29 can be simply evaluated for a particular case. However, the practical applications give extremely small errors as stated in Section 2.2.

Let $\alpha = (H_2\pi^2)/(2l_2^2)$; $\beta = (kc_2)/(2l_2)$; $\omega_1 = (c_2\pi)/l_2$, then equation A.2.2.32 becomes,

$$s = -n^2 \alpha - \beta + jn\omega_1 \qquad \text{A.2.2.33}$$

where n = 0, $\pm$ 1, $\pm$ 2 etc.

In an exactly similar way the zeros of the transfer function can be shown to occur at points where,

$$s = -n^2 \alpha + \beta + jn\omega_1 \qquad \text{A.2.2.34}$$

The poles of the forcing function are at $s = \pm j\omega_s$. These can be moved along the imaginary axis of the s-plane by altering the transmitted frequency. A typical s-plane diagram is shown in Fig.2.2.2 of Section 2.2, and the subsequent derivation of the echo is clearly explained in that section.

The effect on the residues of considering the term $\exp \gamma_1(x-2l_1)$ will be determined for the simple dominant pole case (See Fig.2.3.1 of section 2.3). Now,

$$\exp\left[\frac{-(2l_1-x)p}{(H_1p + C_1^2)^{\frac{1}{2}}}\right] = \exp\left[\frac{-(2l_1-x)p}{C_1}\left(1- \frac{H_1p}{2C_1^2} + \frac{3}{4}\frac{H_1^2p^2}{C_1^4} :.....\right)\right]$$

A.2.2.35

But $C_1^2 / H_1 >> 10^6$ so,

$$\exp\left[\frac{-(2l_1-x)p}{(H_1p+C_1^2)^{\frac{1}{2}}}\right] \simeq \exp\left[\frac{-(2l_1-x)p}{C_1}\right] \exp\left[\frac{(2l_1-x)H_1p^2}{2C_1^3}\right]$$

A.2.2.36

The term $\exp(-(2l_1-x)p/C_1)$ produces the well known time delay of the whole function by an amount $(2l_1-x)/C_1$. The term $\exp\left[(2l_1-x)H_1p^2/(2C_1^3)\right]$ must be taken into the residues. For example the residue from pole $p = -\beta - m^2\alpha + j\omega_m$ becomes,

$$\frac{2a\,\beta\omega_s}{j\,\omega_m}\,\frac{V_1V_8}{V_2V_3}\,\exp j(\omega_m\tau + \theta_7 - \theta_8)\,\exp(-\beta - m^2\alpha)\,\tau$$

A.2.2.37

where $V_8 = \exp\left[-(2l_1-x)H_1\,\omega_m^2/(2C_1^3)\right]$

and $\theta_8 = (2l_1-x)(\beta + m^2\alpha)\,\omega_m\,H_1/C_1^3$

and the other symbols were defined in section 2.3. Summing the four residues the complete solution becomes,

$$R(x,\tau) = a\left[\frac{V_4V_5V_9}{V_2V_3}\sin(\omega_s\tau + \theta_6) + 2\frac{\omega_s}{\omega_m}\frac{2\beta V_1V_8}{V_2V_3}\right.$$

$$\left.\sin(\omega_m\tau + \theta_7 - \theta_8)\exp(-\beta - m^2\alpha)\tau\right] \qquad \text{A.2.2.38}$$

where $V_9 = \exp\left[-(2l_1-x)H_1\,\omega_s^2/(2C_1^3)\right]$

Near resonance $\omega_m \simeq \omega_s$ and so $V_8 \simeq V_9$ producing an attenuation of the whole echo. Typically θ_8 is much less than one degree of arc for normally used line materials, giving a negligable effect on the echo. However if a particularly lossy line material is used, its effect should be investigated.

The effect of the branch point for more general cases than the dominant pole case, gives a similar attenuation.

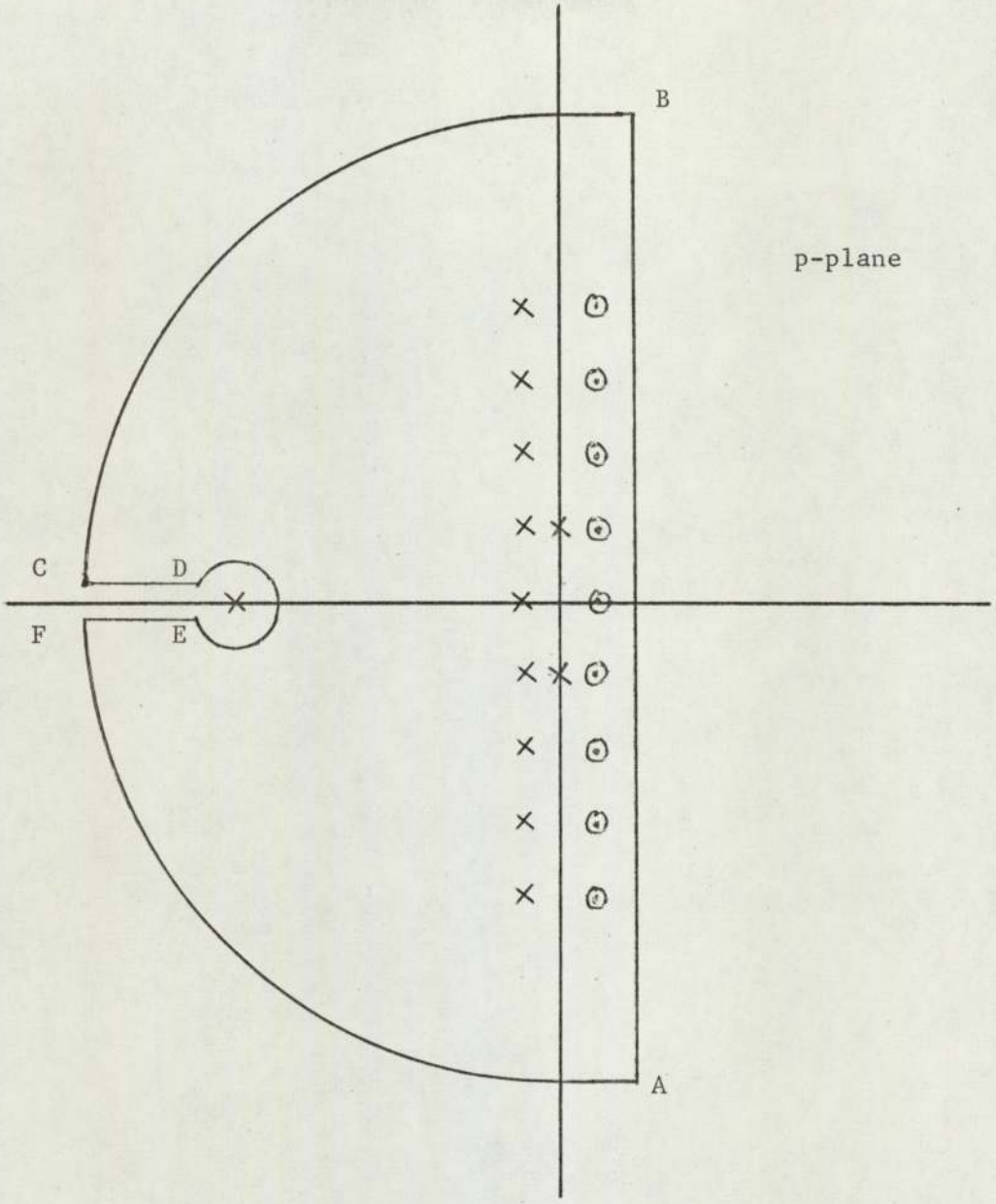

Fig.A.2.2.1 Diagram showing the branch point and some poles of $\bar{R}(x,p)$. See equation A.2.2.22.

APPENDIX A.3.1

DERIVATION OF FREQUENCY EQUATIONS FOR DISK

In general at any point in an elastic medium, the matrix equation

$$S = sT \qquad \text{A.3.1}$$

relates the strain vector S_i and the stress vector T_i.

In cartesian co-ordinates it becomes,

$$\begin{bmatrix} S_1 \\ S_2 \\ S_3 \\ S_4 \\ S_5 \\ S_6 \end{bmatrix} = \begin{bmatrix} s_{11} & s_{12} & s_{13} & s_{14} & s_{15} & s_{16} \\ s_{21} & s_{22} & s_{23} & s_{24} & s_{25} & s_{26} \\ s_{31} & s_{32} & s_{33} & s_{34} & s_{35} & s_{36} \\ s_{41} & s_{42} & s_{43} & s_{44} & s_{45} & s_{46} \\ s_{51} & s_{52} & s_{53} & s_{54} & s_{55} & s_{56} \\ s_{61} & s_{62} & s_{63} & s_{64} & s_{65} & s_{66} \end{bmatrix} \begin{bmatrix} T_1 \\ T_2 \\ T_3 \\ T_4 \\ T_5 \\ T_6 \end{bmatrix} \qquad \text{A.3.1.2}$$

S_i are engineering strains. S_1, S_2 and S_3 are longitudinal strains in the x, y, and z directions. S_4, S_5 and S_6 are shear strains about the x, y, and z directions. Similarly, for the engineering stresses T_i. s_{ij} are the 26 elastic constants of the material. By a consideration of the Strain-Energy-Function Love 1927 shows that,

$$s_{ij} = s_{ji}$$

Further for an isotropic medium the elastic constants must be unaltered by a change to a new cartesian co-ordinate system. A consideration of this reduces the number of independent elastic constants to only two, and so

$$\begin{bmatrix} S_1 \\ S_2 \\ S_3 \\ S_4 \\ S_5 \\ S_6 \end{bmatrix} = \begin{bmatrix} s_{11} & s_{12} & s_{12} & 0 & 0 & 0 \\ s_{12} & s_{11} & s_{12} & 0 & 0 & 0 \\ s_{12} & s_{12} & s_{11} & 0 & 0 & 0 \\ 0 & 0 & 0 & s_1 & 0 & 0 \\ 0 & 0 & 0 & 0 & s_1 & 0 \\ 0 & 0 & 0 & 0 & 0 & s_1 \end{bmatrix} \begin{bmatrix} T_1 \\ T_2 \\ T_3 \\ T_4 \\ T_5 \\ T_6 \end{bmatrix} \qquad \text{A.3.1.3}$$

where $s_1 = 2\ (s_{11} - s_{12})$

For a consideration of thin disks, any interaction with the thickness direction (z-direction) can be neglected so,

$$\begin{bmatrix} S_1 \\ S_2 \\ S_6 \end{bmatrix} = \begin{bmatrix} s_{11} & s_{12} & 0 \\ s_{12} & s_{11} & 0 \\ 0 & 0 & s_{66} \end{bmatrix} \begin{bmatrix} T_1 \\ T_2 \\ T_6 \end{bmatrix} \qquad \text{A.3.1.4}$$

Love's result for interchangeability of axes in this case leads to,

$$s_{66} = 2(s_{11} - s_{12}) \qquad \text{A.3.1.5}$$

Equation A.3.1.5 holds because an isotropic material is being considered. A cubic material would have had three elastic constants; in that case $s_{44} = s_{55} = s_{66}$ is the third elastic constant, and equation A.3.1.5 becomes $As_{66} = 2(s_{11} - s_{12})$, where A is the elastic anistropy of the material. A good account of the equations relating to crystal structures is given by Hearmon 1946.

Poisson's ratio is defined as,

$$\sigma = -\frac{S_2}{S_1} \quad \text{when } T_2 = T_6 = 0$$

Therefore

$$\sigma = -s_{12}/s_{11} \qquad \text{A.3.1.6}$$

Young's Modulus is defined,

$$E = \frac{T_1}{S_1} \quad \text{when } T_2 = T_6 = 0$$

Therefore

$$E = 1/s_{11} \qquad \text{A.3.1.7}$$

By Kramer's Rule from equations A.3.1.4

$$T_1 = \frac{\begin{vmatrix} S_1 & s_{12} & 0 \\ S_2 & s_{11} & 0 \\ S_6 & 0 & s_{66} \end{vmatrix}}{\begin{vmatrix} s_{11} & s_{12} & 0 \\ s_{12} & s_{11} & 0 \\ 0 & 0 & s_{66} \end{vmatrix}} = \frac{\begin{vmatrix} S_1 & s_{12} \\ S_2 & s_{11} \end{vmatrix}}{\begin{vmatrix} s_{11} & s_{12} \\ s_{12} & s_{11} \end{vmatrix}} = \frac{E\,(S_1 + \sigma S_2)}{1 - \sigma^2}$$

Therefore

$$T_1 = \frac{E}{(1 - \sigma^2)} \left[\frac{\partial \xi_x}{\partial x} + \sigma \frac{\partial \xi_y}{\partial y} \right] \qquad \text{A.3.1.8}$$

Similarly

$$T_2 = \frac{E}{(1 - \sigma^2)} \left[\frac{\partial \xi_y}{\partial y} + \sigma \frac{\partial \xi_x}{\partial x} \right] \qquad \text{A.3.1.9}$$

and

$$T_6 = \frac{S_6}{2(s_{11} - s_{12})} = \frac{E}{2(1+\sigma)} \left[\frac{\partial \xi_x}{\partial y} + \frac{\partial \xi_y}{\partial x} \right] \qquad \text{A.3.1.10}$$

Now to derive the equations of motion consider the incremental element of the plate in Fig. A.3.1.1.

In x direction,

$$\left(\frac{\partial T_1}{\partial x}\,\delta x\right)\,\delta y\,\delta z + \left(\frac{\partial T_6}{\partial y}\,\delta y\right)\,\delta x\,\delta z = \delta x\,\delta y\,\delta z \rho \frac{\partial^2 \xi_x}{\partial t^2}$$

Therefore

$$\frac{\partial T_1}{\partial x} + \frac{\partial T_6}{\partial y} = \rho \frac{\partial^2 \xi_x}{\partial t^2} \qquad \text{A.3.1.11}$$

Similarly in y direction.

$$\frac{\partial T_6}{\partial x} + \frac{\partial T_2}{\partial y} = \rho \frac{\partial^2 \xi_y}{\partial t^2} \qquad \text{A.3.1.12}$$

Equations A.3.1.8 to A.3.1.12 are those with which Love 1927 commences. (page 497).

Substituting into equation A.3.1.11 for T_1 and T_6 from equations A.3.1.8 and A.3.1.10 yields,

$$\frac{\partial^2 \xi_x}{\partial x^2} + \frac{1}{2}(1-\sigma)\frac{\partial^2 \xi_x}{\partial y^2} + \frac{1}{2}(1+\sigma)\frac{\partial^2 \xi_y}{\partial x\,\partial y} = \rho\frac{(1-\sigma^2)}{E}\frac{\partial^2 \xi_x}{\partial t^2} \qquad \text{A.3.1.13}$$

Similarly equation A.3.1.12 becomes,

$$\frac{1}{2}(1-\sigma)\frac{\partial^2 \xi_y}{\partial x^2} + \frac{\partial^2 \xi_y}{\partial y^2} + \frac{1}{2}(1+\sigma)\frac{\partial^2 \xi_x}{\partial x\,\partial y} = \rho\frac{(1-\sigma^2)}{E}\frac{\partial^2 \xi_y}{\partial t^2} \qquad \text{A.3.1.14}$$

If $\Delta = \frac{\partial \xi_x}{\partial x} + \frac{\partial \xi_y}{\partial y}$ and $\bar{\omega} = \frac{1}{2}\left(\frac{\partial \xi_y}{\partial x} - \frac{\partial \xi_x}{\partial y}\right)$,

then equations A.3.1.13 and A.3.1.14 can be rewritten,

$$\frac{\partial \Delta}{\partial x} - (1-\sigma)\frac{\partial \bar{\omega}}{\partial y} = \rho\frac{(1-\sigma^2)}{E}\frac{\partial^2 \xi_x}{\partial t^2} \qquad \text{A.3.1.15}$$

$$\frac{\partial \Delta}{\partial y} + (1-\sigma)\frac{\partial \bar{\omega}}{\partial x} = \rho\frac{(1-\sigma^2)}{E}\frac{\partial^2 \xi_y}{\partial t^2} \qquad \text{A.3.1.16}$$

In polar co-ordinates,

$$\Delta = \frac{\partial \xi_r}{\partial r} + \frac{\xi_r}{r} + \frac{1}{r}\frac{\partial \xi_\theta}{\partial \theta}\,; \quad \bar{\omega} = \frac{1}{2}\left[\frac{\partial \xi_\theta}{\partial r} + \frac{\xi_\theta}{r} - \frac{1}{r}\frac{\partial \xi_r}{\partial \theta}\right] \qquad \text{A.3.1.17}$$

and the stress resultants become,

$$T_{rr} = \frac{E}{(1-\sigma^2)}\left[\frac{\partial \xi_r}{\partial r} + \sigma\left(\frac{\xi_r}{r} + \frac{1}{r}\frac{\partial \xi_\theta}{\partial \theta}\right)\right] \qquad \text{A.3.1.18}$$

$$T_{r\theta} = \frac{E}{(1+\sigma)2}\left[\frac{\partial \xi_\theta}{\partial r} - \frac{\xi_\theta}{r} + \frac{1}{r}\frac{\partial \xi_r}{\partial \theta}\right] \qquad \text{A.3.1.19}$$

If equation A.3.1.15 is differentiated with respect to x and A.3.1.16 with respect to y, the resultant equations can be summed to give,

$$\nabla^2 \Delta = \rho\frac{(1-\sigma^2)}{E}\frac{\partial^2 \Delta}{\partial t^2} \qquad \text{A.3.1.20}$$

Similarly,

$$\nabla^2 \bar{\omega} = 2\rho\frac{(1+\sigma)}{E}\frac{\partial^2 \bar{\omega}}{\partial t^2} \qquad \text{A.3.1.21}$$

In general for a normal mode a solution $\Delta = F(r)\,G(\theta)\cos\omega t$ can be assumed. Putting this solution into equation A.3.1.20

gives cosωt as a common factor, and then the variables r and θ can be separated. The general solution resulting from this is,

$$\Delta = \left[A_1 J_n(hr) + A_2 Y_n(hr)\right]\left[A_3 \cos n\theta + A_4 \sin n\theta\right]\cos\omega t \qquad \text{A.3.1.22}$$

where $h^2 = \rho (1 - \sigma^2)\omega^2/E$.

It is convenient here to state the boundary conditions for the disk of radius a.

$$T_{rr} = 0 \quad \text{at } r = a \qquad \text{A.3.1.23}$$

$$T_{r\theta} = 0 \quad \text{at } r = a \qquad \text{A.3.1.24}$$

$$\Delta,\ \bar{\omega},\ \xi_r \text{ and } \xi_\theta \text{ are finite for all } r < a \qquad \text{A.3.1.25}$$

Concentrating on the θ ordinate first, it will be shown that ξ_θ and ξ_r are orthogonal as assumed by Love 1927. ξ_r, ξ_θ, Δ and $\bar{\omega}$ will all be of the form $f(r)\cos\omega t\,(A_c \cos n\theta + A_s \sin n\theta)$. The θ ordinate is chosen such that,

$$\xi_r = U_n(r) \cos n\theta \cos\omega t \qquad \text{A.3.1.26}$$

$$\xi_\theta = V_n(r)\,(A_5 \cos n\theta + A_6 \sin n\theta)\cos\omega t \qquad \text{A.3.1.27}$$

Equation A.3.1.26 and A.3.1.27 are used to substitute for ξ_r and ξ_θ in equation A.3.1.18. Then applying boundary condition A.3.1.23 gives,

$$\cos n\theta \left[\frac{\partial U_n(r)}{\partial r} + \frac{\sigma}{r} U_n(r) + A_6 \frac{\sigma n}{r} V_n(r)\right]$$

$$- \sin n\theta \left[A_5 \frac{\sigma n}{r} V_n(r)\right] = 0 \text{ at } r = a.$$

Hence,

$$\frac{\partial U_n(r)}{\partial r} + \frac{\sigma}{r} U_n(r) + A_6 \frac{\sigma n}{r} V_n(r) = 0$$

and

$$A_5 \frac{\sigma n}{r} V_n(r) = 0 \quad \text{at } r = a.$$

So $A_5 = 0$, and the solutions for ξ_r and ξ_θ are orthogonal. Substituting these solutions into equation A.3.1.17 will show that Δ and $\bar{\omega}$ are also orthogonal in θ. So using the solutions,

$$\Delta = F_1(r) \cos n\theta \cos\omega t$$

$$\bar{\omega} = F_2(r) \sin n\theta \cos\omega t$$

in equations A.3.1.20 and A.3.1.21 yields,

$$\Delta = \left[A_7 J_n(hr) + A_8 Y_n(hr)\right] \cos n\theta \cos\omega t \qquad \text{A.3.1.28}$$

$$\bar{\omega} = \left[A_9 J_n(kr) + A_{10} Y_n(kr)\right] \sin n\theta \cos\omega t \qquad \text{A.3.1.29}$$

where

$$h^2 = \rho (1 - \sigma^2)\, \omega^2/E, \quad k^2 = 2\rho (1 + \sigma)\, \omega^2/E$$

Boundary condition A.3.1.25 requires that $A_8 = A_{10} = 0$.

Equations A.3.1.15 and A.3.1.16 when converted to their polar forms become

$$\frac{\partial \Delta}{\partial r} - (1 - \sigma)\frac{1}{r}\frac{\partial \bar{\omega}}{\partial \theta} = -\rho\omega^2 \frac{(1 - \sigma^2)}{E} \xi_r \qquad \text{A.3.1.30}$$

$$(1 - \sigma)\frac{\partial \bar{\omega}}{\partial r} + \frac{1}{r}\frac{\partial \Delta}{\partial \theta} = -\rho\omega^2 \frac{(1 - \sigma^2)}{E} \xi_\theta \qquad \text{A.3.1.31}$$

Substituting into A.3.1.30 and A.3.1.31 with the general solutions A.3.1.28 and A.3.1.29 gives the form for the solutions of ξ_r and ξ_θ.

$$\xi_r = \left[A_{11} \frac{dJ_n(hr)}{dr} + nA_{12} \frac{J_n(kr)}{r}\right] \cos n\theta \cos\omega t \qquad \text{A.3.1.32}$$

$$\xi_\theta = -\left[nA_{11} \frac{J_n(hr)}{r} + A_{12} \frac{dJ_n(kr)}{dr}\right] \sin n\theta \cos\omega t \qquad \text{A.3.1.33}$$

For radial modes ξ_θ vanishes and ξ_r is independent of θ. This occurs when $n = 0$. Equation A.3.1.18 and boundary condition A.3.1.23 give,

$$\left[\frac{d\xi_r}{dr} + \sigma\left(\frac{\xi_r}{r} + \frac{1}{r}\frac{d\xi_\theta}{d\theta}\right)\right]_{r = a} = 0 \qquad \text{A.3.1.34}$$

So using solution A.3.1.32 in A.3.1.34 yields,

$$\frac{dJ_1(ha)}{da} + \frac{\sigma}{a} J_1(ha) = 0 \qquad \text{A.3.1.35}$$

as the radial modes frequency equation.

The choice of the θ ordinate is arbitary so rotating $\theta = o$ by $\pi/2$ and putting $n = 0$ yields tangential modes in which ξ_r vanishes and ξ_θ is independent of θ. The general solution A.3.1.33 is put into equation A.3.1.19 and applying boundary condition A.3.1.24 gives the frequency equation for tangential modes.

$$\frac{dJ_1(ka)}{da} = \frac{J_1(ka)}{a} \qquad \text{A.3.1.36}$$

The remaining solutions are those for which $n > 0$. Two equations are obtained by substituting A.3.1.32 and A.3.1.33 into A.3.1.18 and A.3.1.19 with their appropriate boundary conditions.

$$\frac{A_{11}}{A_{12}} = \frac{\left[\frac{1}{a}\frac{dJ_n(ka)}{da} - \frac{1}{a^2} J_n(ka)\right] n(1-\sigma)}{\left[\frac{(1-\sigma)}{a}\frac{dJ_n(ha)}{da} + (h^2 - \frac{(1-\sigma)}{a^2} n^2) J_n(ha)\right]} \qquad \text{A.3.1.37}$$

$$\frac{A_{11}}{A_{12}} = \frac{\left[\frac{2}{a}\frac{dJ_n(ka)}{da} + (k^2 - \frac{2n^2}{a^2}) J_n(ka)\right]}{\left[\frac{1}{a}\frac{dJ_n(ha)}{da} - \frac{1}{a^2} J_n(ha)\right] 2n} \qquad \text{A.3.1.38}$$

The frequency equation for these compound modes is formed by eliminating A_{11}/A_{12} between A.3.1.37 and A.3.1.38.

Equations A.3.1.35 to A.3.1.38 are the frequency equations as given by Love 1927. The notation of Holland 1966 lends itself readily to numerical analysis.

$$K = ha = \omega a \left(\rho (1 - \sigma^2)/E \right)^{1/2} \qquad \text{A.3.1.39}$$

$$\Theta = k/h = \left[2/(1 - \sigma)\right]^{1/2} \qquad \text{A.3.1.40}$$

Also the expressions are simplified by introducing a modified Bessel function

$$M_n(\Lambda) = \Lambda J_{n-1}(\Lambda)/J_n(\Lambda)$$

Using the relations A.3.1.39 and A.3.1.40 the frequency equations are converted to the following forms.

Radial modes frequency equation,

$$M_1(K_{mR}) = 1 - \sigma \qquad \text{A.3.1.41}$$

Tangential modes frequency equation,

$$M_1(K_{mT}\ \Theta) = 2 \qquad \text{A.3.1.42}$$

Compound modes frequency equation; formed by eliminating A_{11}/A_{12} in,

$$\frac{A_{11}}{A_{12}} = \frac{J_n(\Theta K_{m,n})}{J_n(K_{m,n})} \cdot \frac{n(M_n(\Theta K_{m,n}) - (n+1))}{\frac{1}{2}(\Theta K_{m,n})^2 - n(n+1) + M_n(K_{m,n})} \qquad \text{A.3.1.43}$$

$$\frac{A_{11}}{A_{12}} = \frac{J_n(\Theta K_{m,n})}{J_n(K_{m,n})} \cdot \frac{2M_n(\Theta K_{m,n}) + (\Theta K_{m,n})^2 - 2n(n+1)}{2n(M_n(K_{m,n}) - (n+1))} \qquad \text{A.3.1.44}$$

The subscripts of K refer to particular solutions.

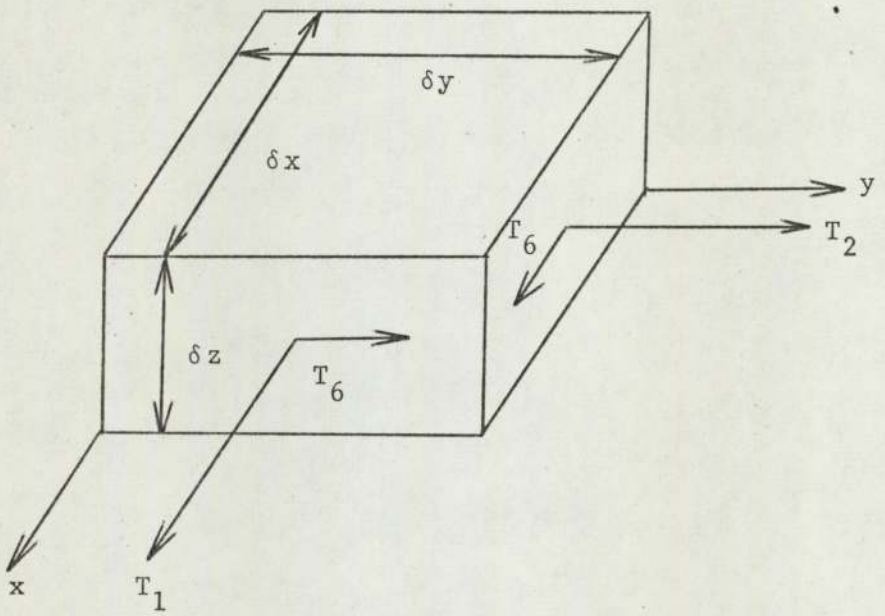

Fig.A.3.1.1

An incremental element of a thin plate is shown. Notice the directions of T_6 on faces y = constant, and x = constant. These directions are verified by taking moments about the centre of the element. See Love 1927 (page 77).

APPENDIX A.3.4

CURVE FITTING

A curve fitting program was available at the University computer centre. This used the method of least squares via orthogonal polynomials. The output gave coefficients of polynomials of degree up to and including the limit given. For each result the sum of the squared deviations was also given.

The method is outlined very well in Hawgood 1965. A good reference for Cholesky's Scheme for solving determinants is Salvadori 1952.

The sum of the mean squares is printed out permitting the selection of a polynomial with sufficiently high degree.

APPENDIX A.4.3

TABLES OF K VALUES FOR RINGS

$K_{1,R}$ Values

σ \ Φ	0.0	0.1	0.2	0.3	0.4	0.5	0.6	0.7	0.8	0.9
0.00	1.8412	1.8035	1.7051	1.5821	1.4618	1.3547	1.2621	1.1824	1.1134	1.0531
0.05	1.8789	1.8372	1.7291	1.5964	1.4695	1.3582	1.2632	1.1821	1.1124	1.0519
0.10	1.9154	1.8689	1.7501	1.6074	1.4736	1.3584	1.2612	1.1789	1.1087	1.0480
0.15	1.9506	1.8988	1.7681	1.6147	1.4741	1.3551	1.2559	1.1727	1.1021	1.0415
0.20	1.9845	1.9268	1.7828	1.6182	1.4709	1.3482	1.2473	1.1634	1.0927	1.0322
0.25	2.0172	1.9528	1.7941	1.6176	1.4636	1.3377	1.2353	1.1509	1.0802	1.0202
0.30	2.0490	1.9766	1.8015	1.6126	1.4521	1.3233	1.2197	1.1351	1.0647	1.0052
0.35	2.0796	1.9981	1.8046	1.6028	1.4362	1.3047	1.2003	1.1158	1.0460	0.9872
0.40	2.1091	2.0171	1.8028	1.5878	1.4153	1.2818	1.1770	1.0929	1.0238	0.9659
0.45	2.1379	2.0331	1.7954	1.5669	1.3891	1.2541	1.1494	1.0660	0.9980	0.9412
0.50	2.1659	2.0456	1.7815	1.5395	1.3571	1.2212	1.1171	1.0349	0.9682	0.9129
0.55	2.1930	2.0539	1.7598	1.5045	1.3186	1.1826	1.0797	0.9991	0.9341	0.8804
0.60	2.2192	2.0566	1.7286	1.4608	1.2726	1.1376	1.0365	0.9580	0.8952	0.8434
0.65	2.2448	2.0518	1.6857	1.4070	1.2181	1.0851	0.9868	0.9110	0.8507	0.8013
0.70	2.2696	2.0367	1.6281	1.3410	1.1535	1.0241	0.9294	0.8571	0.7998	0.7531
0.75	2.2937	2.0060	1.5514	1.2598	1.0767	0.9525	0.8628	0.7947	0.7410	0.6975
0.80	2,3171	1.9505	1.4493	1.1595	0.9843	0.8677	0.7844	0.7216	0.6725	0.6328
0.85	2.3399	1.8524	1.3114	1.0329	0.8709	0.7651	0.6902	0.6343	0.5907	0.5556
0.90	2.3621	1.6734	1.1190	0.8673	0.7263	0.6358	0.5724	0.5254	0.4890	0.4598
0.95	2.3838	1.3177	0.8268	0.6305	0.5244	0.4574	0.4110	0.3768	0.3504	0.3294

$K_{1,1}$ Values

σ \ φ	0.0	0.1	0.2	0.3	0.4	0.5	0.6	0.7	0.8	0.9
0.00	1.7497	1.7555	1.7683	1.7770	1.7701	1.7411	1.6917	1.6285	1.5583	1.4859
0.05	1.7402	1.7469	1.7616	1.7727	1.7678	1.7398	1.6906	1.6271	1.5566	1.4841
0.10	1.7258	1.7331	1.7497	1.7633	1.7606	1.7339	1.6851	1.6216	1.5510	1.4786
0.15	1.7061	1.7142	1.7327	1.7489	1.7486	1.7234	1.6751	1.6118	1.5414	1.4693
0.20	1.6816	1.6903	1.7107	1.7294	1.7316	1.7081	1.6607	1.5979	1.5278	1.4561
0.25	1.6520	1.6614	1.6835	1.7048	1.7096	1.6880	1.6417	1.5795	1.5100	1.4390
0.30	1.6176	1.6275	1.6512	1.6749	1.6824	1.6629	1.6178	1.5565	1.4879	1.4178
0.35	1.5781	1.5885	1.6136	1.6396	1.6498	1.6325	1.5890	1.5288	1.4613	1.3923
0.40	1.5336	1.5444	1.5707	1.5988	1.6116	1.5966	1.5549	1.4961	1.4299	1.3622
0.45	1.4838	1.4949	1.5222	1.5521	1.5674	1.5549	1.5151	1.4580	1.3934	1.3274
0.50	1.4285	1.4398	1.4678	1.4993	1.5169	1.5069	1.4693	1.4141	1.3513	1.2872
0.55	1.3675	1.3789	1.4072	1.4399	1.4596	1.4521	1.4168	1.3638	1.3033	1.2414
0.60	1.3001	1.3114	1.3399	1.3733	1.3948	1.3897	1.3570	1.3065	1.2485	1.1892
0.65	1.2256	1.2367	1.2649	1.2986	1.3215	1.3188	1.2888	1.2411	1.1860	1.1296
0.70	1.1429	1.1537	1.1811	1.2145	1.2384	1.2379	1.2108	1.1664	1.1146	1.0616
0.75	1.0504	1.0606	1.0868	1.1194	1.1436	1.1451	1.1211	1.0802	1.0324	0.9832
0.80	0.9454	0.9549	0.9794	1.0103	1.0341	1.0373	1.0165	0.9799	0.9365	0.8919
0.85	0.8235	0.8320	0.8542	0.8824	0.9050	0.9093	0.8921	0.8602	0.8222	0.7831
0.90	0.6761	0.6833	0.7020	0.7263	0.7463	0.7512	0.7378	0.7117	0.6804	0.6480
0.95	0.4806	0.4858	0.4995	0.5175	0.5327	0.5372	0.5282	0.5098	0.4874	0.4642

$K_{1,2}$ Values

σ \ Φ	0.0	0.1	0.2	0.3	0.4	0.5	0.6	0.7	0.8	0.9
0.00	1.6518	1.5250	1.2520	0.9942	0.7806	0.6003	0.4439	0.3068	0.1875	0.0851
0.05	1.6115	1.4933	1.2345	0.9848	0.7754	0.5974	0.4424	0.3061	0.1872	0.0851
0.10	1.5697	1.4596	1.2145	0.9732	0.7684	0.5931	0.4398	0.3046	0.1864	0.0844
0.15	1.5267	1.4240	1.1920	0.9593	0.7595	0.5873	0.4361	0.3023	0.1851	0.0841
0.20	1.4819	1.3863	1.1671	0.9432	0.7487	0.5801	0.4313	0.2993	0.1834	0.0840
0.25	1.4356	1.3466	1.1398	0.9248	0.7360	0.5713	0.4253	0.2954	0.1812	0.0826
0.30	1.3877	1.3048	1.1100	0.9041	0.7214	0.5609	0.4181	0.2907	0.1784	0.0811
0.35	1.3377	1.2607	1.0776	0.8810	0.7047	0.5489	0.4097	0.2852	0.1751	0.0792
0.40	1.2858	1.2143	1.0426	0.8555	0.6860	0.5353	0.4001	0.2787	0.1712	0.0773
0.45	1.2314	1.1653	1.0048	0.8274	0.6650	0.5198	0.3890	0.2712	0.1668	0.0761
0.50	1.1745	1.1135	0.9640	0.7964	0.6417	0.5024	0.3765	0.2628	0.1616	0.0741
0.55	1.1145	1.0585	0.9198	0.7625	0.6157	0.4829	0.3623	0.2531	0.1558	0.0711
0.60	1.0510	0.9999	0.8720	0.7251	0.5869	0.4610	0.3463	0.2422	0.1492	0.0680
0.65	0.9834	0.9369	0.8199	0.6839	0.5547	0.4365	0.3283	0.2298	0.1416	0.0642
0.70	0.9106	0.8689	0.7628	0.6382	0.5188	0.4089	0.3079	0.2157	0.1330	0.0606
0.75	0.8315	0.7944	0.6996	0.5869	0.4782	0.3774	0.2846	0.1996	0.1232	0.0564
0.80	0.7438	0.7116	0.6285	0.5288	0.4316	0.3413	0.2576	0.1808	0.1117	0.0510
0.85	0.6443	0.6171	0.5466	0.4611	0.3772	0.2987	0.2257	0.1586	0.0980	0.0451
0.90	0.5261	0.5045	0.4481	0.3790	0.3106	0.2463	0.1864	0.1311	0.0810	0.0373
0.95	0.3721	0.3572	0.3180	0.2696	0.2215	0.1759	0.1333	0.0938	0.0580	0.0262

$K_{1,3}$ Values

σ \ Φ	0.0	0.1	0.2	0.3	0.4	0.5	0.6	0.7	0.8	0.9
0.00	2.5069	2.5009	2.4162	2.1557	1.8028	1.4537	1.1251	0.8122	0.5145	
0.05	2.4523	2.4468	2.3676	2.1215	1.7818	1.4414	1.1182	0.8088	0.5132	
0.10	2.3944	2.3892	2.3152	2.0831	1.7569	1.4257	1.1087	0.8035	0.5106	
0.15	2.3332	2.3283	2.2593	2.0407	1.7282	1.4066	1.0964	0.7962	0.5068	
0.20	2.2688	2.2642	2.2000	1.9944	1.6955	1.3841	1.0814	0.7868	0.5015	
0.25	2.2012	2.1970	2.1370	1.9441	1.6590	1.3582	1.0636	0.7753	0.4950	
0.30	2.1304	2.1264	2.0707	1.8899	1.6185	1.3288	1.0430	0.7617	0.4870	
0.35	2.0562	2.0525	2.0008	1.8316	1.5741	1.2959	1.0194	0.7459	0.4776	
0.40	1.9783	1.9749	1.9270	1.7691	1.5255	1.2593	0.9928	0.7278	0.4667	
0.45	1.8965	1.8933	1.8490	1.7022	1.4725	1.2188	0.9629	0.7071	0.4542	
0.50	1.8103	1.8074	1.7666	1.6304	1.4148	1.1740	0.9295	0.6839	0.4398	
0.55	1.7191	1.7165	1.6790	1.5534	1.3519	1.1247	0.8923	0.6577	0.4237	
0.60	1.6223	1.6200	1.5858	1.4704	1.2833	1.0703	0.8509	0.6283	0.4053	
0.65	1.5189	1.5167	1.4857	1.3806	1.2083	1.0100	0.8046	0.5952	0.3845	
0.70	1.4073	1.4054	1.3776	1.2827	1.1255	0.9431	0.7528	0.5578	0.3609	
0.75	1.2856	1.2839	1.2593	1.1748	1.0335	0.8679	0.6941	0.5152	0.3338	
0.80	1.1507	1.1492	1.1278	1.0540	0.9295	0.7823	0.6269	0.4661	0.3024	
0.85	0.9971	0.9959	0.9778	0.9155	0.8092	0.6826	0.5480	0.4081	0.2651	
0.90	0.8146	0.8136	0.7993	0.7496	0.6640	0.5613	0.4515	0.3368	0.2190	
0.95	0.5763	0.5757	0.5658	0.5314	0.4718	0.3996	0.3220	0.2406	0.1569	

$K_{1,4}$ Values

σ \ ϕ	0.0	0.1	0.2	0.3	0.4	0.5	0.6	0.7	0.8	0.9
0.00	3.2321	3.2318	3.2210	3.1225	2.8191	2.3821	1.9163	1.4397	0.9484	
0.05	3.1689	3.1688	3.1585	3.0655	2.7769	2.3550	1.9001	1.4313	0.9450	
0.10	3.1001	3.1000	3.0903	3.0028	2.7290	2.3225	1.8794	1.4193	0.9393	
0.15	3.0261	3.0259	3.0168	2.9346	2.6755	2.2848	1.8543	1.4039	0.9312	
0.20	2.9470	2.9468	2.9382	2.8613	2.6165	2.2420	1.8247	1.3850	0.9207	
0.25	2.8629	2.8628	2.8547	2.7828	2.5521	2.1940	1.7906	1.3624	0.9077	
0.30	2.7740	2.7739	2.7664	2.6993	2.4824	2.1409	1.7520	1.3364	0.8923	
0.35	2.6801	2.6800	2.6730	2.6105	2.4070	2.0823	1.7086	1.3064	0.8742	
0.40	2.5809	2.5808	2.5743	2.5164	2.3260	2.0181	1.6603	1.2725	0.8533	
0.45	2.4763	2.4762	2.4701	2.4164	2.2390	1.9482	1.6068	1.2344	0.8296	
0.50	2.3655	2.3654	2.3598	2.3103	2.1454	1.8720	1.5478	1.1918	0.8028	
0.55	2.2480	2.2478	2.2427	2.1972	2.0448	1.7889	1.4828	1.1444	0.7724	
0.60	2.1227	2.1226	2.1179	2.0764	1.9362	1.6983	1.4110	1.0914	0.7382	
0.65	1.9885	1.9883	1.9841	1.9464	1.8185	1.5990	1.3317	1.0323	0.6996	
0.70	1.8434	1.8432	1.8394	1.8055	1.6900	1.4896	1.2434	0.9660	0.6561	
0.75	1.6848	1.6847	1.6813	1.6512	1.5482	1.3678	1.1443	0.8909	0.6063	
0.80	1.5086	1.5045	1.5056	1.4794	1.3894	1.2302	1.0314	0.8047	0.5490	
0.85	1.3077	1.3077	1.3053	1.2833	1.2070	1.0710	0.8999	0.7036	0.4800	
0.90	1.0688	1.0688	1.0668	1.0493	0.9884	0.8789	0.7400	0.5797	0.3978	
0.95	0.7564	0.7564	0.7551	0.7430	0.7009	0.6245	0.5268	0.4136	0.2819	

$K_{1,5}$ Values

σ \ φ	0.0	0.1	0.2	0.3	0.4	0.5	0.6	0.7	0.8	0.9
0.00	3.9094	3.9094	3.9084	3.8847	3.7240	3.3107	2.7569	2.1431	1.4654	
0.05	3.8387	3.8386	3.8376	3.8150	3.6622	3.2660	2.7283	2.1271	1.4581	
0.10	3.7601	3.7601	3.7591	3.7376	3.5928	3.2141	2.6934	2.1061	1.4482	
0.15	3.6744	3.6744	3.6734	3.6531	3.5164	3.1553	2.6524	2.0799	1.4344	
0.20	3.5819	3.5819	3.5810	3.5619	3.4332	3.0897	2.6052	2.0487	1.4166	
0.25	3.4828	3.4828	3.4820	3.4640	3.3432	3.0174	2.5518	2.0123	1.3952	
0.30	3.3774	3.3774	3.3766	3.3598	3.2466	2.9384	2.4922	1.9707	1.3701	
0.35	3.2654	3.2654	3.2646	3.2489	3.1432	2.8524	2.4262	1.9237	1.3410	
0.40	3.1466	3.1466	3.1459	3.1313	2.0328	2.7593	2.3535	1.8710	1.3078	
0.45	3.0208	3.0208	3.0201	3.0066	2.9151	2.6587	2.2738	1.8124	1.2701	
0.50	2.8872	2.8871	2.8865	2.8740	2.7894	2.5501	2.1867	1.7474	1.2279	
0.55	2.7451	2.7450	2.7444	2.7329	2.6550	2.4327	2.0913	1.6754	1.1801	
0.60	2.5932	2.5932	2.5927	2.5821	2.5108	2.3055	1.9869	1.5956	1.1269	
0.65	2.4302	2.4301	2.4297	2.4201	2.3553	2.1672	1.8721	1.5071	1.0680	
0.70	2.2537	2.2536	2.2532	2.2446	2.1863	2.0156	1.7453	1.4083	0.9998	
0.75	2.0605	2.0604	2.0601	2.0524	2.0006	1.8480	1.6037	1.2971	0.9237	
0.80	1.8456	1.8456	1.8452	1.8386	1.7935	1.6596	1.4434	1.1701	0.8349	
0.85	1.6004	1.6004	1.6001	1.5945	1.5565	1.4427	1.2575	1.0217	0.7308	
0.90	1.3084	1.3083	1.3081	1.3037	1.2734	1.1823	1.0326	0.8408	0.6107	
0.95	0.9263	0.9262	0.9260	0.9228	0.9021	0.8389	0.7341	0.5998		

$K_{1,6}$ Values

σ \ Φ	0.0	0.1	0.2	0.3	0.4	0.5	0.6	0.7	0.8	0.9
0.00	4.5657	4.5656	4.5655	4.5608	4.4981	4.1954	3.6143	2.8930	2.0464	
0.05	4.4870	4.4870	4.4869	4.4823	4.4223	4.1326	3.5713	2.8675	2.0348	
0.10	4.3988	4.3988	4.3987	4.3942	4.3371	4.0610	3.5202	2.8351	2.0182	
0.15	4.3016	4.3016	4.3015	4.2973	4.2431	3.9809	3.4613	2.7961	1.9966	
0.20	4.1961	4.1961	4.1960	4.1920	4.1408	3.8925	3.3946	2.7504	1.9701	
0.25	4.0826	4.0826	4.0825	4.0787	4.0305	3.7960	3.3201	2.6980	1.9385	
0.30	3.9611	3.9611	3.9610	3.9574	3.9122	3.6914	3.2378	2.6387	1.9017	
0.35	3.8316	3.8316	3.8315	3.8283	3.7859	3.5786	3.1475	2.5724	1.8596	
0.40	3.6939	3.6939	3.6938	3.6907	3.6513	3.4573	3.0490	2.4988	1.8115	
0.45	3.5476	3.5476	3.5475	3.5446	3.5079	3.3270	2.9417	2.4175	1.7577	
0.50	3.3919	3.3919	3.3918	3.3892	3.3552	3.1871	2.8252	2.3279	1.6971	
0.55	3.2260	3.2260	3.2259	3.2235	3.1922	3.0368	2.6984	2.2293	1.6298	
0.60	3.0486	3.0485	3.0485	3.0462	3.0176	2.8747	2.5604	2.1206	1.5544	
0.65	2.8577	2.8577	2.8576	2.8556	2.8296	2.6992	2.4095	2.0006	1.4701	
0.70	2.6509	2.6508	2.6508	2.6489	2.6255	2.5077	2.2435	1.8673	1.3779	
0.75	2.4242	2.4242	2.4241	2.4225	2.4017	2.2968	2.0591	1.7179	1.2693	
0.80	2.1719	2.1718	2.1718	2.1703	2.1523	2.0606	1.8511	1.5480	1.1491	
0.85	1.8838	1.8837	1.8837	1.8825	1.8672	1.7897	1.6109	1.3501	1.0290	
0.90	1.5403	1.5402	1.5402	1.5392	1.5271	1.4652	1.3214	1.1110	0.8426	
0.95	1.0905	1.0904	1.0904	1.0899	1.0815	1.0383	0.9369	0.8109		

$K_{1,7}$ Values

σ \ φ	0.0	0.1	0.2	0.3	0.4	0.5	0.6	0.7	0.8	0.9
0.00	5.2106	5.2107	5.2107	5.2098	5.1889	5.0095	4.4677	3.6706	2.6755	
0.05	5.1240	5.1240	5.1239	5.1231	5.1029	4.9308	4.4091	3.6338	2.6578	
0.10	5.0259	5.0259	5.0259	5.0251	5.0057	4.8414	4.3407	3.5886	2.6337	
0.15	4.9174	4.9174	4.9174	4.9166	4.8981	4.7420	4.2628	3.5350	2.6030	
0.20	4.7990	4.7990	4.7990	4.7982	4.7806	4.6328	4.1756	3.4732	2.5659	
0.25	4.6710	4.6710	4.6710	4.6703	4.6537	4.5142	4.0791	3.4031	2.5225	
0.30	4.5337	4.5337	4.5337	4.5330	4.5174	4.3862	3.9734	3.3246	2.4722	
0.35	4.3870	4.3870	4.3870	4.3864	4.3717	4.2487	3.8582	3.2375	2.4152	
0.40	4.2308	4.2307	4.2307	4.2301	4.2163	4.1014	3.7332	3.1414	2.3509	
0.45	4.0643	4.0642	4.0642	4.0637	4.0509	3.9438	3.5980	3.0359	2.2788	
0.50	3.8870	3.8869	3.8869	3.8864	3.8745	3.7753	3.4517	2.9203	2.1987	
0.55	3.6977	3.6977	3.6977	3.6972	3.6862	3.5947	3.2935	2.7937	2.1100	
0.60	3.4951	3.4950	3.4950	3.4946	3.4845	3.4005	3.1219	2.6549	2.0110	
0.65	3.2769	3.2769	3.2769	3.2765	3.2673	3.1908	2.9350	2.5021	1.9018	
0.70	3.0403	3.0403	3.0403	3.0399	3.0316	2.9627	2.7302	2.3332	1.7800	
0.75	2.7809	2.7808	2.7808	2.7805	2.7732	2.7118	2.5035	2.1444	1.6427	
0.80	2.4917	2.4918	2.4918	2.4915	2.4851	2.4316	2.2486	1.9304	1.4909	
0.85	2.1615	2.1615	2.1615	2.1613	2.1559	2.1107	1.9551	1.6820		
0.90	1.7676	1.7676	1.7676	1.7676	1.7633	1.7271	1.6029	1.3908		

$K_{1,8}$ Values

σ \ Φ	0.0	0.1	0.2	0.3	0.4	0.5	0.6	0.7	0.8	0.9
0.00	5.8491	5.8491	5.8491	5.8489	5.8425	5.7512	5.3016	4.4632	3.3411	
0.05	5.7541	5.7541	5.7541	5.7539	5.7478	5.6596	5.2272	4.4140	3.3159	
0.10	5.6461	5.6461	5.6461	5.6460	5.6399	5.5554	5.1412	4.3546	3.2827	
0.15	5.5261	5.5261	5.5261	5.5260	5.5202	5.4396	5.0441	4.2854	3.2418	
0.20	5.3948	5.3948	5.3948	5.3946	5.3891	5.3126	4.9362	4.2062	3.1928	
0.25	5.2525	5.2525	5.2525	5.2524	5.2471	5.1747	4.8176	4.1173	3.1357	
0.30	5.0995	5.0995	5.0995	5.0993	5.0943	5.0262	4.6884	4.0184	3.0708	
0.35	4.9357	4.9357	4.9357	4.9356	4.9308	4.8668	4.5484	3.9094	2.9972	
0.40	4.7609	4.7609	4.7609	4.7608	4.7563	4.6965	4.3972	3.7898	2.9146	
0.45	4.5745	4.5745	4.5745	4.5744	4.5703	4.5145	4.2342	3.6592	2.8233	
0.50	4.3758	4.3758	4.3758	4.3757	4.3718	4.3201	4.0587	3.5167	2.7221	

$K_{1,9}$ Values

σ \ Φ	0.0	0.1	0.2	0.3	0.4	0.5	0.6	0.7	0.8	0.9
0.00	6.4832	6.4832	6.4832	6.4831	6.4812	6.4390	6.1041	5.2623	4.0338	
0.05	6.3798	6.3798	6.3798	6.3797	6.3780	6.3368	6.0143	5.1997	4.0000	
0.10	6.2618	6.2618	6.2618	6.2618	6.2600	6.2204	5.9113	5.1253	3.9568	
0.15	6.1303	6.1303	6.1303	6.1302	6.1285	6.0905	5.7956	5.0394	3.9041	
0.20	5.9860	5.9860	5.9860	5.9859	5.9842	5.9840	5.6676	4.9421	3.8421	
0.25	5.8293	5.8293	5.8293	5.8293	5.8277	5.7933	5.5276	4.8335	3.7707	
0.30	5.6606	5.6606	5.6606	5.6606	5.6591	5.6266	5.3756	4.7135	3.6893	
0.35	5.4798	5.4798	5.4798	5.4798	5.4784	5.4478	5.2115	4.5819	3.5981	
0.40	5.2866	5.2866	5.2866	5.2866	5.2852	5.2566	5.0349	4.4382	3.4966	
0.45	5.0805	5.0805	5.0805	5.0804	5.0792	5.0524	4.8452	4.2818	3.3843	
0.50	4.8604	4.8604	4.8604	4.8604	4.8592	4.8344	4.6415	4.1119	3.2590	

Due to the limited volume of computer time available, certain K values have been omitted from the tables. These have been restricted to what is considered the less useful extremes of the parameters σ and Φ . However the programs for obtaining these values do exist.